Title
Mechanisms underlying spontaneous glutamatergic activity in developing mouse retina

Author
Firl, Alana

Publication Date
2014

Peer reviewed|Thesis/dissertation

Mechanisms underlying spontaneous glutamatergic activity in developing mouse retina

by

Alana Julia Firl

A dissertation submitted in partial satisfaction of the

requirements for the degree of

Doctor of Philosophy

in

Vision Science

in the

Graduate Division

of the

University of California, Berkeley

Committee in charge:

Professor Marla Feller, Chair
Professor Richard Kramer
Professor Christopher Chang

Spring 2014

Mechanisms underlying spontaneous glutamatergic activity in developing mouse retina

Abstract

Mechanisms underlying spontaneous glutamatergic activity in developing mouse retina

by

Alana Julia Firl

Doctor of Philosophy in Vision Science

University of California, Berkeley

Professor Marla Feller, Chair

Throughout the developing nervous system, spontaneous oscillatory patterns of activity has been observed. The developing murine retina is no exception, where spontaneous activity manifests as spatially correlated waves of depolarizations. These retinal waves propagate between neighboring neurons within retinal layers during the two postnatal weeks just prior to eye-opening and development of the light response. Waves are necessary for the normal patterning of connections of the retinal projections to their primary targets in the brain, indicating they contribute to a general self-organizing principal of neural development.

There are three distinct circuits that mediate these waves at different developmental stages: gap junction mediated waves that occur around birth, acetylcholine-receptor mediated that occur during the first postnatal week, and glutamate-receptor mediated that occur between postnatal day 10 (P10) and P13. At this age, retinal circuitry appears adult-like such that excitatory synapses connect neurons across layers but inhibitory synapses connect neurons within layers. Thus it remains a mystery as to how depolarization propagates between neighboring within-layer neurons during waves.

This dissertation addresses the cellular and synaptic basis underlying the initiation and propagation of glutamatergic retinal waves. Using a combination of multielectrode array recording and two-photon calcium imaging, I identified a role for electrical coupling, diffuse release of glutamate, and inhibitory circuits in the retinal wave generation. In addition, I studied the role of endogenous copper in modulating retinal waves. This research represents a near-complete description of the intraretinal circuits that underlie the spatial and temporal properties of glutamatergic retinal waves.

Contents

List of Figures

Acknowledgments

First and foremost, I would like to thank my advisor Marla Feller for giving me the chance to work in her lab, and for providing scientific guidance, advice and inspiration; I learned immeasurably from her methodical way of pursuing questions. Science is interactive; reading the retina literature provides a biased view of its scientific progress. Gaining insight into the full scope of which experiments have been attempted in the field requires talking to people who have worked in the field. Marla prepares her students for this, encouraging us to ask questions and defend our ideas, and supporting conference attendance. This generosity has not gone unnoticed. I am extremely grateful for the experience of working in her lab and could not have asked for a more complete graduate-level training.

I would also like to thank my committee members Christopher Chang and Richard Kramer, for their time and guidance throughout my graduate studies. Thanks to my undergraduate advisor Bill Warren who introduced me to neuroscience research. I would like to thank all members of the Feller lab for their companionship, making my graduate experience fun and motivating; also, thanks to Justin Elstrott and Aaron Blankenship for their guidance while I was getting started. I want to thank the administrative staff in the Vision Science Graduate Group, Inez Bailey and Olga Lepilina, for their energy, help, and support over the years.

Chapter 1

Introduction

1.1 Vision and retina

The visual system is the part of the brain that underlies vision. Many organisms rely on vision for making sense of the environment, using light as a proxy for the world. The first neural structure that light encounters is the retina. Retinal photoreceptors transduce photons into graded electrical signals, and downstream retinal circuits transform these graded signals into features of the visual scene such as movement, contrast, brightness, and color information. These features are encoded in the form of patterns of discrete action potentials that transmit information about the visual scene to the brain along the optic nerve. These downstream retinal circuits consist of several cell types: retinal ganglion cells (RGCs), amacrine cells, bipolar cells, and horizontal cells, of which there are multiple subtypes within these cell types [Masland, 2012].

In order to encode visual information, the retina develops highly structured circuitry between distinct cell types. This structure emerges slowly over development: cells differentiate, migrate to their correct cell layer, and send their processes to distinct lamina where they form synaptic connections according to genetically determined chemoaffinity cues. In addition, neural activity plays a role in the refinement of these synaptic conenctions (for review see [Kerschensteiner, 2013]). In mice, this period of activity-dependence occurs before eye-opening, during the first two weeks of postnatal development. Neural activity during development is termed spontaneous because it is not elicited by light; during development, photoreceptors are not light-sensitive, so activity patterns from postnatal day (P0) - P13 are intrinsically generated by the developing retina and are not driven by the brain or external environmental cues. This spontaneous activity, termed retinal waves, occurs at a frequency of roughly once per minute, and the spread of depolarization propagates between neighboring neurons. Retinal waves are conserved across species and occur at equivalent periods of development [Blankenship and Feller, 2010].

Waves are key to establishing retinofugal projections to LGN and SC [Ackman et al., 2012, Colonnese and Khazipov, 2010, Weliky and Katz, 1999]; for review, see [Kirkby et al., 2013].

These projections are responsible for preserving topographic mappings from the outside world, and for maintaining distinct inputs from each eye. It is currently shown empirically and with computational models that while RGC axons coarsely find their targets in appropriate brain regions based on chemoaffinity cues [Feldheim and O'Leary, 2010, Triplett and Feldheim, 2012], there follows a period of activity-dependent refinement, where the axons of nearest-neighbor RGCs grow to become nearest-neighbor projections in downstream targets [Cline, 2003, Goodman and Shatz, 1993, Huberman et al., 2008]. This activity-dependence is driven by retinal waves, and is postulated to be the result of Hebbian principles of plasticity, which states that repeated sequential activity between presynaptic neuron A and postsynaptic neuron B strengthens synaptic coupling between the two [Hebb, 1949]; conversely, uncorrelated activity between two neurons results in weakened synaptic coupling [Katz and Shatz, 1996]. The fact that waves propagate smoothly between neighboring cells would ensure that only connections between neighboring target projections were strengthened, thus preserving topographic maps from retina to downstream projections, and discarding spatially erroneous connections [Eglen et al., 2003].

1.2 Stages of waves

From birth until eye-opening, the mouse retina generates waves. The mechanism of wave initiation and propagation changes according to the retinal circuitry during development. From embryonic development until birth, waves are gap junction mediated, and are referred to as stage I waves. Following birth until P10, waves are mediated by acetylcholine (ACh) release from starburst amacrine cells (SACs), and are referred to as Stage II waves (for review, see [Ford and Feller, 2012]). During stage II waves, bipolar cells have yet to mature, and the retina does not have glutamatergic connectivity between outer retina and inner retina. SACs are highly connected to neighboring retinal neurons, providing a testable mechanism by which a cholinergic wave initiates and propagates. Ford et al have shown that depolarization of a single SAC is sufficient to start a wave, and these waves have been characterized by many models consisting of a cellular lattice with intrinsic pacemaking dynamics and variable coupling between neighboring cells [Butts et al., 1999, Hennig et al., 2009, Godfrey et al., 2009].

Glutamatergic waves, or stage III waves, occur from P10 until eye opening. Stage III waves cease in the presence of ionotropic glutamate receptor blockers, indicating that depolarization via glutamate is necessary for waves [Blankenship et al., 2009]. By P10 the major cell types of the retina are differentiated and bipolar cells have become the major excitatory glutamatergic connection between the outer and inner layers of the retina, with glycinergic and GABAergic amacrine cells serving as inhibitory interneurons. Stage III waves coincide with and require the maturation of the bipolar cell vesicular glutamate transporters (VGLUT1) [Blankenship et al., 2009].

In contrast to stage II waves, the mechanism by which a stage III wave initiates and propagates is unknown. The initiation rate of stage III waves can be increased or decreased

without changing properties of wave propagation such as velocity, wavefront direction, and spatial coverage, suggesting that the wave-initiating mechanism functions independently of the propagation mechanism. The mechanism of wave propagation is not straightforward because glutamatergic circuitry is organized vertically while waves are seen to propagate horizontally across neighboring cells. As a result there is no obvious glutamatergic cell type that would be responsible for the horizontal spread of depolarizations seen during waves. Inhibitory amacrine cells are horizontally connected, but their release of glycine and GABA hyperpolarizes neurons. There is a small population of VGLUT3-expressing amacrine cells; however, VGLUT3 ko mice had normal waves, indicating this population is unimportant for stage III waves [Blankenship et al., 2009]. Therefore one must investigate collective dynamics of this complicated system instead of looking for a single neural subtype as the sole mediator. This dissertation attempts to elucidate the collective dynamics allowing for the emergence of horizontally propagating waves from the vertical glutamatergic circuitry.

1.3 Factors contributing to stage III waves

The role of neuronal connexins in stage III waves

Gap junctions are potential facilitators of wave propagation because they are responsible for electrical coupling between neighboring neurons. There is some evidence of gap junction coupling between bipolar cells [Arai et al., 2010]. Since they are the only substrate by which neighboring bipolar cells could directly share excitation, we attempted to assess their role in stage III waves. Previous studies have shown that connexin(Cx) 36ko retinas exhibit increased spontaneous activity between waves [Torborg et al., 2005] and that Cx36 is responsible for On-cone bipolar cell and AII amacrine cell coupling [Veruki and Hartveit, 2009], as well as AII-AII amacrine cell coupling. While many connexin proteins are expressed in retina, Cx36 and Cx45 are the connexin proteins expressed by bipolar cells [Güldenagel et al., 2000, Söhl et al., 2000, Feigenspan et al., 2001, 2004, Han and Massey, 2005, Lin et al., 2005, Maxeiner et al., 2005, Dedek et al., 2006, Pan et al., 2010]. Given that glutamate release from bipolar cells is a requirement for stage III waves, Cx36 and Cx45 were chosen for deletion in the double knockout mouse. Chapter 2 describes the effect on wave phenotype of genetic deletion of gap junction proteins in Cx36ko and Cx36/45dko mice.

Summarized briefly, Cx36 and Cx45 deletion both resulted in increased spontaneous activity between waves. There was a slight additive effect in the Cx36/45dko phenotype. Waves, when detectable against elevated activity levels, occurred as often as WT waves, and displayed normal propagation properties when assayed by epifluorescent Ca^{2+} imaging. Waves measured by multielectrode array (MEA) recordings showed decreased nearest-neighbor correlations, meaning that spatially distant cells were likely to be as correlated in their firing as spatially adjacent cells. While correlation measures were normalized by baseline firing rates, this lack of spatial correlation during waves could be a byproduct of elevated background firing rather than the result of mechanistic changes in wave propagation patterns. Regardless, the undisputed finding is that Cx36 and Cx45 ko increased

uncorrelated firing between waves. This was surprising because the initial hypothesis was that connexins would facilitate propagation of excitation. However, the study still points to a role for connexins in driving correlated retinal firing between retinal neurons. That role appears to be to correlate hyperpolarization across multiple neurons, instead of propagation of depolarization, since their absence results in a loss of quiescence.

The role of glutamate spillover and inhibition in stage III waves

A second hypothesis of wave initiation and propagation is that of glutamate spillover. A similar mechanism was implicated in stage II waves, where volume release of ACh played a critical role in wave propagation [Zhou, 1998]. According to the glutamate spillover hypothesis, a bipolar cell initiates a wave by spontaneously depolarizing, and releasing enough glutamate to spill out of the synaptic cleft onto neighboring bipolar cells, thus propagating the wave. Blankenship et al. demonstrated using outside-out patches that levels of extrasynaptic glutamate increase during waves, indicating that excess glutamate is present during waves despite active neuronal and glial transport of glutamate. In Chapter 3, we used a FRET-based glutamate sensor to image wave-related glutamate release, and verified that volume release of glutamate occurs with the same periodicity that Ca^{2+} waves were observed. We also used 2-photon Ca^{2+} imaging and found that less than half of the neurons in any given field of view in the INL or GCL were depolarized during waves. Because every retinal neuron should be depolarized by glutamate, with the exception of mGluR-expressing neurons (for review see [Gerber, 2003]), this finding suggested that there is a more complex circuit mechanism underlying wave propagation than glutamate release alone.

There are important and distinct differences between the effect of elevated extrasynaptic glutamate and blockade of inhibition on stage III waves. Blockade of glycine and $GABA_A$ receptors dramatically increased wave frequency, to a point where the retina appeared to wave constantly. However, the temporal correlations of waves remained, suggesting that inhibition is actively involved in wave initiation but not propagation. In addition, a larger fraction of neurons within the ganglion cell layer (GCL) depolarized during waves while inner nuclear layer (INL) cell participation did not increase. These data are consistent with findings that cell participation of RGCs is set by the balance of inhibition and excitation they receive during waves. In contrast, elevated glutamate levels did not dramatically increase wave frequency, but resulted in a larger fraction of neurons within the INL that were depolarized during waves, and a small increase in the GCL. These findings inverted the problem from seeking to identify what excitatory event triggers depolarization in an otherwise quiescent retina, to a question about what causes inhibition to periodically shut off, thus enabling waves.

The findings in Chapter 3 suggest stage III waves are contingent on coordinated glutamate release that occurs as the result of a transient relief of inhibition. The fact that inhibition blockade leads to constant waves, and that gap junction deletion results in increased activity, both implicate inhibition as being important for maintaining the relatively long quiescent periods between waves. Interestingly, a number of network models of spiking neurons require a greater proportion of inhibitory neurons than excitatory neurons in order to maintain network stability. The modeler's problem often comes down to finding a balance of excitation

and inhibition where the system can exhibit stable oscillations, instead of exploding to constantly increasing activity, or decaying to zero (for review see [Izhikevich, 2004]).

The role of AII-mediated intrinsic oscillations in stage III waves

The pharmacological manipulations described above led to a model in which wave initiation is triggered by transient relief of inhibition. In Chapter 4 we sought to identify the cellular and synpatic basis of these periodic changes in inhibition. We found that blockade of hyperpolarization-activated cyclic nucelotide-gated (HCN) channels resulted in such uncorrelated retinal activity that wave structure was no longer identifiable by eye or algorithm. HCN channels, which are found in several pacemakers throughout excitable tissue, open a nonselective cation channel in response to membrane hyperpolarization, effectively setting the amount of time it takes for a hyperpolarized neuron to return to an excitable state, which is the mechanism by which they set the pace of a network [Wahl-Schott and Biel, 2009]. They are expressed in four isoforms throughout the retina in several cell types [Della Santina et al., 2012]. The model of wave initiation and propagation involves On-cone bipolar cells which function as ±5mV intrinsic oscillators, which are electrically coupled to a set of amacrine cells. Amacrine cells will receive higher and lower levels of excitation from the bipolar cell oscillators. The periodicity of these higher and lower levels of bipolar cell input would be determined by the phase precession of their summed intrinsic oscillation frequencies. A model for wave initiation is that these oscillating levels of depolarization are sufficient to activate voltage-gated channels in amacrine cells.

Interestingly, spontaneous retinal oscillations are seen in photoreceptor degenerated (rd) mice. A number of studies have characterized the ways in which rd retinas can generate oscillations (for example [Stasheff, 2008, Cuenca et al., 1993, Margolis et al., 2014]). Because oscillations have been found to originate from the electrically coupled network of On cone bipolar and AII amacrine cells [Borowska et al., 2011], we looked for ways to characterize the relationship between AII amacrine activity and retinal waves. For this study to answer the question of whether AII amacrine cells are activated by electrical coupling with bipolar cells and subsequently propagate waves, a method of targeted AII stimulation with minimal retinal damage is needed.

The role of endogenous copper in stage III waves

This dissertation primarily focuses on the role of fast neurotransmitters, glutamate, glycine, and GABA, in the generation of retinal waves. In addition to these classic fast neurotransmitters, there are several chemicals that serve as modulators of circuit function. Copper, for example, is found in neural tissue and requires an oxygen-rich environment to become water-soluble through oxidation [Camakaris et al., 1999, Crichton and Pierre, 2001]. Copper misregulation has been implicated in Alzheimer's and more generally with amyloid-β plaque deposits [Nguyen et al., 2014, Squitti et al., 2013]. Mutations in copper transporters result in developmental disorders such as Wilson's and Menkes, which is fatal (for review see [Gaier et al., 2013]). Reasoning that spontaneous activity occurs throughout developing neural systems, we investigated the effect of copper on retinal waves to gain insight into how copper affects neural development. In Chapter 5 we applied copper chelators to the retina to record the effect of copper deficiency on spontaneous activity, and compared the effect to a

mutant mouse with decreased expression of the copper transporter (CTR1) ion channel. We observed that decreased levels of copper led to higher rates of waves and a larger proportion of depolarized cells. This represents the first demonstration of how copper affects neural activity during development.

Chapter 2

The role of neuronal connexins 36 and 45 in shaping spontaneous firing patterns in the developing retina

Preface: This chapter has been published in the journal, *Journal of Neuroscience:* Aaron Blankenship, Alana Firl, Aaron Hamby, Shri Vyas, Stephan Maxeiner, Klaus Willecke, and Marla B. Feller (2011), and is included with permission from all authors. The dissertation author was the co-second author of this paper. The work presented in this chapter is the author's contribution to this paper.

2.1 Abstract

Given that retinal waves propagate across neighboring ganglion cells in absence of glutamatergic synapses between RGCs, gap junctions could provide the mechanism by which depolarization is spread. Gap junction coupling synchronizes activity among neurons in adult neural circuits, and two connexin isoforms, connexin 36 (Cx36) and Cx45 are expressed in bipolar cells and RGCs. Using calcium imaging and multielectrode array recording, we compared spatiotemporal properties of retinal waves in control (WT), single knockout (ko) mice lacking Cx45, and double knockout (dko) mice lacking both Cx45 and Cx36. We found that wave frequency, propagation speed, and bias in propagation direction was unaffected by the absence of Cx45ko, Cx36ko, or Cx36/45 dko. However, spontaneous RGC firing rate was elevated in Cx45ko and Cx36ko, and even more elevated in dko retinas. This elevated firing rate significantly altered the functional connectivity maps as defined by nearest neighbor correlations between cells. Together, these findings suggest that gap junctions dictate spatial structure of wave propagation but not wave initiation.

2.2 Introduction

Gap junction coupling is found throughout the developing nervous system, where it has been postulated to play a number of roles [Cook and Becker, 2009], including regulation of spontaneous firing patterns [Roerig and Feller, 2000, Personius et al., 2007]. Here, we explore the role of gap junction coupling in retinal waves, the spontaneous propagating activity generated in the retina prior to the maturation of vision. Pharmacological blockade of gap junctions produces different effects on waves depending on the species, age and particular antagonist used (for review, see [Blankenship and Feller, 2010]) , and therefore the role of gap junction coupling in mediating retinal waves remains unresolved.

The role of gap junction coupling in the propagation of retinal waves during the second postnatal week is of particular interest. During this time, waves are mediated by glutamate release from bipolar cells [Blankenship and Feller, 2010]. However, bipolar cells have narrow axonal arborizations and are not known to form synapses with one another, so it remains a mystery how retinal waves propagate laterally among them. Gap junctions present a potential source of coupling among neighboring retinal neurons. Since pharmacological blockers of gap junctions have several non-specific effects, knockout mice lacking specific connexins have proven to be a powerful tool for elucidating the role of gap junction coupling in circuit function [Connors and Long, 2004]. Bipolar cells express connexin isoforms that could couple bipolar cells directly [Arai et al., 2010] or indirectly via interneurons (for reviews, see [Söhl et al., 2005, Bloomfield and Völgyi, 2009]). In the mouse retina, bipolar cells express two different connexin proteins, Cx45 and Cx36, which form homologous and heterologous gap junctions with interneurons [Güldenagel et al., 2000, Söhl et al., 2000, Feigenspan et al., 2001, 2004, Han and Massey, 2005, Lin et al., 2005, Maxeiner et al., 2005, Dedek et al., 2006, Pan et al., 2010]. In addition, Cx36 and Cx45 are required for gap junction coupling in

multiple but not all retinal ganglion cell subtypes [Schubert et al., 2005, Völgyi et al., 2005, Dedek et al., 2006, Bloomfield and Völgyi, 2009, Müller et al., 2010, Pan et al., 2010]. Both Cx36 [Belluardo et al., 2000, Hansen et al., 2005, Torborg et al., 2005] and Cx45 [Kihara et al., 2006] are expressed during development and are therefore in a position to influence spontaneous firing patterns. Previously, it was found that in contrast to WT mice, in which RGCs fire correlated bursts of spikes separated by silence [Meister et al., 1991, Wong et al., 1993, McLaughlin et al., 2003], Cx36ko mice [Deans and Paul, 2001, Deans et al., 2002] exhibit an increase in the number of tonically firing RGCs [Hansen et al., 2005, Torborg et al., 2005]. The role of Cx45 in retinal waves is unknown.

Here we use knockout mice lacking Cx45 or both Cx36 and Cx45 to determine whether these connexins are required to coordinate the depolarization of RGCs during waves. Specifically, we use MEA recordings to characterize firing patterns of individual RGCs, Ca^{2+} imaging to characterize propagation properties of waves, and whole cell recording to compare the synaptic circuits that mediate spontaneous activity.

2.3 Results & Discussion

Cx45ko and Cx36/45dko mice have altered spontaneous firing patterns
To characterize the firing patterns of connexin knockout retinas, we used a multielectrode array to record extracellularly from many RGCs simultaneously. In control mice, RGCs fire bursts of action potentials during waves that are correlated with action potentials from neighboring cells and are followed by long periods of silence (Figure 2.1A), [Meister et al., 1991, Wong et al., 1993]). In contrast, Cx45ko RGCs exhibit an increase in asynchronous firing in between the correlated bursts associated with waves (Figure 2.1A, middle), a pattern reminiscent of that observed in Cx36ko mice [Hansen et al., 2005, Torborg and Feller, 2005]. This increase in asynchronous firing was even more dramatic in the Cx36/45dko (Figure 2.1A, bottom).

We quantified the temporal properties of spontaneous firing patterns by monitoring the percentage of time individual RGCs spend firing above 1 Hz and 10 Hz (Figure 2.1C). In control mice, RGCs fire primarily in correlated high frequency bursts during waves with very few asynchronous action potentials in between waves. In contrast, Cx45ko RGCs had a significant increase in the percentage of time firing above 1 Hz between waves (Kruskal-Wallis test $p < 0.001$; Ctr: 1.2±0.3 %, n = 214 wave intervals / 4 mice; Cx45ko 4.1±0.2 %, n = 324 / 4; Cx36/45dko 25.4±1 %, n = 567 / 6; differences found between all groups (Tukey-Kramer post hoc tests)), consistent with our findings of increased asynchronous firing in Cx36ko mice [Hansen et al., 2005, Torborg and Feller, 2005]. Cx36/45dko RGCs also had a significant increase in percent of time firing above 10 Hz and, in contrast to either Cx36ko [Torborg and Feller, 2005] or Cx45ko (Figure 2.1C), there was also a significant increase in the amount of time spent bursting above 10 Hz between waves (Kruskal-Wallis test $p < 0.001$; Ctr 0.39±0.05 %, n = 214 wave intervals / 4 mice; Cx45ko 0.55±0.07 %, n = 324 / 4 ; Cx36/45dko 3.87±0.3 %, n = 567 / 6; difference found only between Cx36/45dko and other

groups, Tukey-Kramer post hoc test).

To quantify the effects of increased asynchronous action potential firing on the spatial correlations of waves, we computed the correlation index as a function of distance between cells (Figure 2.1B). Nearest-neighbor correlations are higher for nearby cells than distant cells, an indicator of propagating waves, though asynchronous action potentials reduce the sensitivity of this measure in Cx36ko mice by reducing the correlation index at all distances [Torborg and Feller, 2005]. For Cx45ko and Cx36/45dko mice, in general, the magnitude of the correlation index was lower at all distances than in control retinas. However, similar to control and Cx36Ko mice, the correlation index was highest for nearby neurons, and then decreased as a function of distance for all genotypes, consistent with the persistence of propagating waves (Figure 2.1B, inset). However, for Cx36/45dko mice, the correlation index dropped off more slowly. If we restricted the analysis only to action potentials fired during waves, the values of the correlation indices increased overall, but the fall off with distance remained more gradual for Cx36/45dko (data not shown).

The finding that Cx36/45dko mice are more correlated over longer distances suggests that the absence of these connexins has altered the underlying network that determines the firing pattern of RGCs. To further explore the spatial properties of correlated neurons, we computed functional connectivity maps for the pairs of neurons with the highest correlation indices [Bonifazi et al., 2009, Bullmore and Sporns, 2009, Feldt et al., 2011]. Functional connectivity maps are a means to quantitatively describe complex network organization, and they have recently been applied to developing neural circuits [Bonifazi et al., 2009].

To establish functional connectivity maps, we first computed correlation matrices to determine the strength of correlations across all RGCs in a given recording (Figure 2.1D). After selecting the most strongly correlated units, we then determined which were most highly connected, i.e. the RGCs that are correlated with the firing of the most other RGCs (Figure 2.1E, red units, see Methods). For both control and Cx45ko retinas, RGCs had the highest connectivity to nearby RGCs, whereas in Cx36/45dko retinas RGCs had the highest connectivity with RGCs that were more dispersed (Figure 2.1E, blue lines; Figure 2.1F). Again, if we restricted the analysis only to action potentials that fired during waves, we found an increase in correlation index but no change to the distribution of distances between highly connected cell pairs. Hence, as indicated both by the correlation index (Figure 2.1B) as a function of distance and by the functional connectivity maps (Figure 2.1F), gap junctions serve to ensure that RGCs are most strongly correlated with nearby RGCs.

Propagation properties of retinal waves are normal in Cx36ko, Cx45ko and Cx36/45dko mice

The high level of asynchronous firing detected in MEA recordings from connexin knockouts blurs the distinction between bursts of activity correlated with and independent of waves. Thus, to determine whether Cx45- or Cx36-containing gap junctions in the inner retina play a role in shaping glutamatergic retinal waves, we performed Ca^{2+} imaging. Ca^{2+} transients in RGCs during waves are driven by depolarization and therefore can be used to monitor depo-

larization in many cells simultaneously. In addition, Ca^{2+} imaging functions as a spatial and temporal filter on spiking patterns, making it easier to detect correlated increases in firing rate. This method has been used extensively to monitor the spatial and temporal properties of retinal waves [Wong et al., 1995, Sernagor et al., 2000, Syed et al., 2004b, Blankenship et al., 2009].

Whole-mount retinas from Cx36ko, Cx45ko and Cx36/45dko mice were bolus-loaded with OGB-1 AM and fluorescence was monitored over time across large areas of the ganglion cell layer. P10P13 retinas displayed waves in all genotypes (Cx36ko: n=17 retina pieces / 6 mice; Cx45ko n = 20/7; Cx36/45dko: n = 22 of 23 retina pieces / 8 mice). Although waves were visible in all but one retina, the magnitude of the change in fluorescence during waves was very small in some Cx36/45dko retinas (n = 12 retinas from 5 mice), precluding analysis of propagation properties on these retinas. We postulate that the source of this low signal to noise in Ca^{2+} imaging was the high baseline firing between waves.

Waves were blocked in most P10-P13 retinas by ionotropic glutamate receptor antagonists (10 μM DNQX and 50 μM AP5; 9/10 Cx36ko retinas, 8 of 10 Cx45ko retinas, 7 of 12 Cx36/45dko retinas), and not blocked by nicotinic acetylcholine receptor antagonists (8 μM DHßE; n = 3 Cx36ko retinas, n = 5 Cx36/45dko retinas). A combination of DHßE, DNQX and AP5 (after either DNQX/AP5 alone or DHßE alone) blocked waves in all cases (n = 3 retinas in Cx36ko; n = 1 Cx45ko; n = 7 Cx36/45dko).

We also compared the propagation speed and initiation frequency of waves [Blankenship et al., 2009] across genotypes. There was no difference in propagation speed among genotypes (One way ANOVA, p = 0.17; Control, n = 9 retinas / 5 mice; Cx36ko, n = 17/6; Cx45ko, n = 15/6; Cx36/45dko, n = 10/6). The distribution of wave initiations was shifted slightly to the left (shorter inter-wave intervals) in Cx36/45dko retinas compared to Cx36ko, Cx45ko and control retinas. These findings suggest that Cx36- and Cx45-containing gap junctions modulate wave initiation, but are not required for glutamatergic wave propagation.

Retinal waves exhibit a propagation bias in that there are more waves propagating in the temporal-to-nasal direction [Stafford et al., 2009, Elstrott and Feller, 2010]. The mechanisms underlying this bias are not understood. To test whether Cx36 or Cx45 contribute to this propagation bias, we compared the propagation bias in waves recorded with Ca^{2+} imaging in Ctr, Cx45ko and Cx36/45dko mice. Using binarized images of retinal waves, the direction of propagation of the wave front was determined for each imaging frame. These individual vectors were summed and a single vector was computed to represent the bias for each retina. The magnitude of the bias in wave propagation was variable from retina to retina but there was no difference in distribution across genotypes (Kruskal-Wallis test, p = 0.35; Control, n = 9 retinas / 5 mice; Cx36ko, n = 17/6; Cx45ko, n = 15/6; Cx36/45dko, n = 10/6). Hence, the correlations that are mediated by gap junctions do not influence the bias in propagation direction.

2.4 Concluding remarks

Role of connexins in shaping spontaneous firing patterns

Our results indicate that the two known neuronal connexins expressed in bipolar cells are not required for wave generation. However, these connexins do act to suppress action potential firing between waves. Our finding that ionotropic glutamate receptor antagonists dramatically decrease the average firing rate of RGCs in Cx36/45dko mice demonstrates that glutamate receptor activation is largely responsible for action potential firing in Cx36/45dko RGCs. This increase in asynchronous firing could be due to several changes in the circuit induced by the absence of Cx45 and Cx36. First, there could be an increase in excitability in bipolar cell terminals. In mammals, ON bipolar cells form strong gap junctions with AII amacrine cells, and the bipolar cell-to-AII amacrine cell gap junction is perturbed in Cx45ko retinas [Maxeiner et al., 2005]. A lack of coupling in bipolar cell terminals could cause an increase in input resistance, making the terminals more excitable [Deans et al., 2001, Long et al., 2002]. In this scenario, spontaneous depolarization in bipolar cells may lead to glutamate release between waves, causing the action potential firing in RGCs. Alternatively, an absence of neuronal connexins in RGCs may increase the input resistance of RGCs, causing them to be more excitable. The absence of gap junctions throughout development in constitutive knockout mice could also cause long-term changes in cell excitability due to differential expression of a variety of ion channels [Iacobas et al., 2003, 2007].

Comparison to results of pharmacological manipulations of gap junctions

In this study, we used knockout mice to determine a role for specific connexin isoforms in modulating spontaneous firing patterns in the developing retina. In the absence of both Cx45 and Cx36, there was an increase in the frequency of retinal waves and asynchronous action potentials between waves, while wave propagation remained unaffected. These effects are distinct from those described by application of gap junction blockers. Carbenoxolone blocked waves measured by Ca^{2+} imaging in chick [Wong et al., 1998]. However, carbenoxolone had no effect on cholinergic or glutamatergic waves as measured by multielectrode array recordings in mice [Stacy et al., 2005, Kerschensteiner and Wong, 2008], whereas it slightly reduced cholinergic wave frequency [Stacy et al., 2005]. In rabbit, carbenoxolone had no effect on waves measured by Ca^{2+} imaging [Syed et al., 2004b]. Similarly mixed results have been seen with related compounds 18-α- and 18-β-glycyrrhetinic acid in rabbit [Syed et al., 2004b], mouse [Singer et al., 2001] and chick [Wong et al., 1998]. Octanol blocked cholinergic waves measured by Ca^{2+} imaging in rabbit [Syed et al., 2004b] and dramatically reduced wave frequency in E9E10 chick [Catsicas et al., 1998]. Finally, meclofenamic acid [Harks et al., 2001, Connors and Long, 2004, Pan et al., 2007] increased glutamatergic wave frequency in mice as measured with multielectrode array recordings [Kerschensteiner and Wong, 2008].

One interpretation of the finding that gap junction antagonists suppress activity while knockout mice have enhanced activity is that gap junction blockers have non-specific effects, as described in several studies [Wu et al., 2001, Connors and Long, 2004, Cruikshank et al., 2004, Vessey et al., 2004, Takeda et al., 2005, Sheu et al., 2008, Tovar et al., 2009, Veruki and Hartveit, 2009]. A second interpretation is that there is a role for non-Cx36 or Cx45-

containing gap junctions in wave generation [Dermietzel et al., 2000, Willecke et al., 2002, Massey et al., 2003]. Our data argue against a role for coupling of bipolar cells in wave generation since thus far Cx36 and Cx45 are the only connexins identified in bipolar cells. However, other neuronal connexins are expressed in other cell types of the retina during development [Güldenagel et al., 2000, Söhl et al., 2000, Kihara et al., 2008]. For example, Cx50 and Cx57 are expressed exclusively in horizontal cells [Deans and Paul, 2001, Hombach et al., 2004, Huang et al., 2005, O'Brien et al., 2006], an interneuron in the outer retina that has not yet been implicated in retinal waves [Firth et al., 2005]. There is some evidence that BCs are coupled via gap junctions [Cuenca et al., 1993, Jacoby and Marshak, 2000, Arai et al., 2010], though the connexins mediating this coupling are not yet defined. Another intriguing possibility is release of an excitatory agent from hemichannels composed of pannexins [Scemes et al., 2007], which are transiently expressed in the retina during development [Ray et al., 2005, Dvoriantchikova et al., 2006].

A third possible explanation for our finding that Cx36/45dko retinas exhibit normal retinal waves is that constitutive deletion of Cx36 and Cx45 caused compensatory expression of other circuit components. Recent studies have showed that knockdown or knockout of some connexins leads to increased expression of mRNA for other connexins [Iacobas et al., 2003, 2007, Spray and Iacobas, 2007]. However, available data suggest that compensatory expression of other gap junctions does not take place in Cx36ko or Cx45ko retinal neurons. Deletion of Cx36 causes most classes of ganglion cells to lose gap junction coupling [Pan et al., 2010], arguing that compensation does not take place in RGCs after deletion of Cx36. Similarly, deficits in gap junction coupling have been observed in retinas lacking Cx45 protein in specific cell classes [Maxeiner et al., 2005, Dedek et al., 2009]. Because these studies were done in single knockout mice, we cannot rule out the possibility that expression of other gap junction proteins is increased when both Cx36 and Cx45 are absent. Furthermore, gap junction protein knockout has also been shown to cause upregulation of a number of ion channels [Iacobas et al., 2003, 2007], which could provide an alternative means for waves to propagate in the absence of Cx36 and Cx45. However, waves in Cx36/45dko mice were nearly indistinguishable from waves in control retinas, indicating that if compensation has occurred, it enabled a circuit to mediate waves that is remarkably similar to the endogenous circuit.

2.5 Experimental methods

Retinal preparation

P10-P12 C57BL/6 mice of either sex were deeply anesthetized with isoflurane and decapitated. Eyes were removed, and retinas were isolated in oxygenated artificial cerebrospinal fluid [ACSF; containing (in mM) 119.0 NaCl, 26.2 $NaHCO_3$, 11 glucose, 2.5 KCl, 1.0 K_2HPO_4, 2.5 $CaCl_2$, and 1.3 $MgCl_2$]. For Ca^{2+} and fluorescence resonance energy transfer (FRET) imaging, retinas were mounted GCL-up on filter paper (Millipore) and perfused continuously with oxygenated ACSF.

Calcium imaging Retinas were loaded with Oregon green 488 BAPTA-1 AM (OGB) using the multicell bolus loading technique [Stosiek et al., 2003, Blankenship et al., 2009]. Two-photon Ca^{2+} imaging of neurons in the INL and GCL was performed using a custom-modified two-photon microscope (Fluoview 300, Olympus America). XYZ scans were used to localize neurons in the GCL and INL. Time series images were acquired at 1 Hz using a ×60 objective (Olympus LUMPlanFl/IR ×60/0.90W) with the excitation laser tuned to 790 nm. Images were corrected for motion artifacts using the Turboreg ImageJ plugin. Ten × ten-pixel regions (12 × 12 μm) of interest were manually selected within all cells in the field of view. Fluorescence signals were averaged within these regions over time. Cell events were identified when change in fluorescence exceeded 15% of the cell's baseline fluorescence within 1 s. Cells were categorized as participating in a retinal wave if cell events correlated with neighboring cells.

Multielectrode recordings and analysis The retina was placed ganglion cell side-down onto a 60-electrode array (Multi-channel systems). The electrodes are each 10 μm in diameter, arranged in an 8×8 grid (minus four corners) with 100 μm inter-electrode spacing. The retina was held in place on the array with a weighted piece of dialysis membrane and superfused continuously with oxygenated ACSF (3ml/min, pH 7.4, gassed with 95% O_2 and 5% CO_2) maintained at 32 °C.

The voltage trace on each electrode was sampled at 20kHz and stored for offline analysis. The traces were then bandpass filtered between 120 and 2000Hz. Spikes that crossed a threshold of four times the root mean square of the noise were sorted according to the first two principle components of their voltage waveforms. A t-distribution-based expectation-maximization algorithm was then used to sort spike clusters into individual units. To verify that each unit identified by this algorithm corresponded to a single cell, units were inspected manually. Furthermore, those that lacked a refractory period in their autocorrelation function were considered contaminated by other neurons and excluded from the analysis.

The mean spike rate, r, was calculated by dividing the total number of spikes for each unit by the recording duration, and units whose mean spike rate was less than 1/10 of the mean firing rate of all cells were excluded from further analysis to reduce influence from low-spiking cells, which were generally the result of poor contact with the array. This constituted less than 10% of the units identified per retina. After this cut, 5590 units were identified per retina.

Bursts were then identified for each neuron using a modified Poisson Surprise method. In this method, spike trains of minimum three spikes whose inter-spike interval (ISI) was less than half of the mean ISI of that unit were identified. The probability that such a spike train would occur given a Poisson spike distribution was then calculated from

$$P_c = \frac{e^{-rt}(rt)^c}{C!}.$$

where t is the duration of the spike train (time between the first and last spike under investigation), C is the number of spikes in the burst, and r is the units mean spike rate. The spike train was accepted as a burst when its probability of occurrence was $P_c < 10^{-4}$. Upon

identification of bursts, the inter-burst interval (time between end of one burst and start of the next), burst duration (t), firing rate (C/t) and the percent of time firing (sum of t for all bursts/total length of recording) were computed and averaged for each unit. The start of a wave was identified when 8% or more of identified cells were bursting simultaneously, and the end of the wave was identified when 2.5% of cells were still bursting.

The correlation index was calculated for all cell pairs in each retina using a method previously described [Wong et al., 1993, Torborg et al., 2005]. The correlation index is a measure of the likelihood relative to chance that a pair of neurons fire together within a given time window, $\Delta \mathrm{t} = 0.1s$. It is calculated from

$$CI = \frac{N_{AB(-\Delta t,\Delta t)} \cdot T}{N_{A(0,T)} \cdot N_{B(0,T)} \cdot 2\Delta t}$$

where N_{AB} is the number of spike pairs for which cell B fires within a time $\pm\Delta t$ from cell A, N_A and N_B are the total number of spikes fired by cells A and B respectively, during the entire recording, T total time of recording, and Δt is the correlation time window. The distance between cells was approximated to be the distance between the electrodes on which the cells activity was recorded. The cell pairs were grouped according to their inter-cellular distance, and the median and quartile correlation indices computed over all cell pairs in a given distance group, for each age and genotype. The median correlation index was then plotted as a function of increasing intercellular distance.

We determined functional connectivity maps between spontaneously firing units. Here, we used functional connectivity as a quantitative measure to characterize the spatial organization of pairs of RGCs that have a high correlation index. First we computed the correlation index between all pairs of units (Figure 2.1D). We designated a pair connected if its correlation index was in the top 5% of all correlation indices in its retina. Any units that were not connected to at least one other unit were not further analyzed. Each correlation matrix was then binarized into an adjacency matrix (not shown), in which each pair is identified as either connected or not connected. Using the adjacency matrix we determined the connectivity value for each unit, i.e. how many connections each unit made divided by the total number of possible connections for that unit. The distribution of connectivity values obeyed a power-law, indicating that the most highly-connected units (which are located in the tail of the distribution) are most informative [Clauset et al., 2009]. We designated units that were connected to more than 15% of all of the units in the adjacency matrix as highly connected (Figure 2.1E, red units). We then mapped these units back onto the electrodes from which they were recorded and computed the distances between these highly connected units and the units to which they were connected (Figure 2.1E, blue lines).

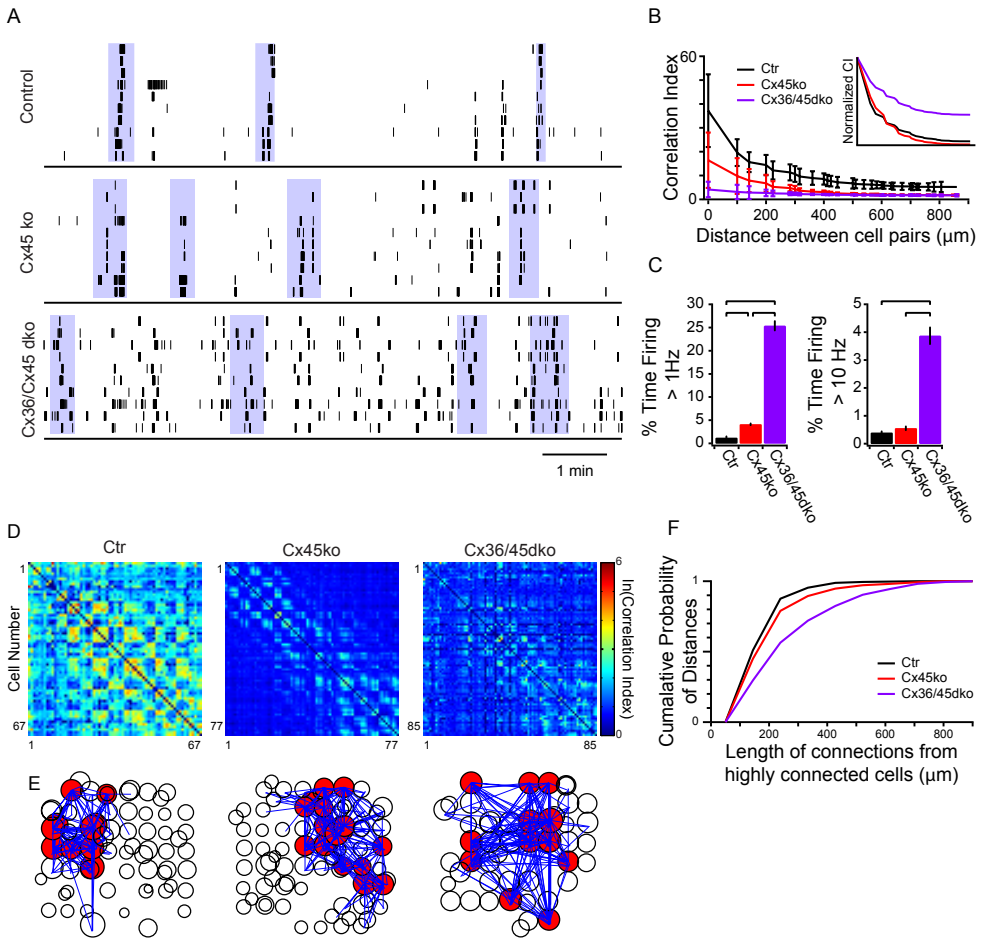

Figure 2.1: Tonic firing between waves is elevated in Cx45ko and Cx36/45dko mice. (A) Raster plots of 10 single-unit spike trains over a 10 min interval, recorded from retinas isolated from P12 control, P11 Cx45ko, and P10 Cx36/45dko retinas. Purple shaded regions indicate waves. (B) Pairwise correlation index as a function of intercellular distance for Ctr (black), Cx45ko (red), and Cx36/45dko (purple). Data points are averages of median values from individual retinas. Error bars are ±SD. Inset shows the same data normalized within each genotype to the maximum correlation index. (C) Percentage of time cells fire above 1 Hz (left) and 10 Hz (right), based on 1 s time bins during inter-wave intervals. Percentages were obtained across all inter-wave intervals pooled within a genotype. Bars are mean ±SD. (D). Correlation matrices for example retinas from each genotype. The correlation coefficient was computed as in *B* for every possible pair of cells in each retina. The x- and y-axes correspond to all single units isolated from that retina. Diagonals (i.e., autocorrelations) were set to zero. Because the distribution of correlation coefficients followed a power-law, they are plotted on a logarithmic scale. (E) Connection matrices for example retinas shown in *D*. Circles correspond to locations of units identified by spike sorting, with the diameter of the circle scaled by the magnitude of the normalized correlation index, such that the largest circles correspond to the largest average correlation index found in the example retina. Units that were localized on the same electrode are slightly displaced. Red circles correspond to units that had connections (i.e., high correlation indices) with at least 15% of the other units (connections shown with blue lines). (F) Cumulative distributions of the distances between the most highly connected RGCs and the units to which they are connected (see Materials and Methods).

Chapter 3

Extrasynaptic glutamate and inhibitory neurotransmission modulate ganglion cell participation during glutamatergic retinal waves.

Preface: This chapter has been published in the journal, *Journal of Neurophysiology:* Alana Firl, Georgeann S. Sack, Zachary Newman, Hiroaki Tani, and Marla B. Feller (2013), and is included with permission from all authors. The dissertation author was the primary author of this paper.

3.1 Abstract

During the first 2 weeks of mouse postnatal development, transient retinal circuits give rise to the spontaneous initiation and lateral propagation of depolarizations across the ganglion cell layer (GCL). Glutamatergic retinal waves occur during the second postnatal week, when GCL depolarizations are mediated by ionotropic glutamate receptors. Bipolar cells are the primary source of glutamate in the inner retina, indicating that the propagation of waves depends on their activation. Using the fluorescence resonance energy transfer-based optical sensor of glutamate FLII^{81}E-1μ, we found that retinal waves are accompanied by a large transient increase in extrasynaptic glutamate throughout the inner plexiform layer. Using two-photon Ca^{2+} imaging to record spontaneous calcium transients in large populations of cells, we found that despite this spatially diffuse source of depolarization, only a subset of neurons in the GCL and inner nuclear layer (INL) are robustly depolarized during retinal waves. Application of the glutamate transporter blocker dl-threo-ß-benzyloxyaspartate (25 μM) led to a significant increase in cell participation in both layers, indicating that the concentration of extrasynaptic glutamate affects cell participation in both the INL and GCL. In contrast, blocking inhibitory transmission with the $GABA_A$ receptor antagonist gabazine and the glycine receptor antagonist strychnine increased cell participation in the GCL without significantly affecting the INL. These data indicate that during development, glutamate spillover provides a spatially diffuse source of depolarization, but that inhibitory circuits dictate which neurons within the GCL participate in retinal waves.

3.2 Introduction

Before the maturation of the light response, the murine retina is spontaneously active, exhibiting laterally propagating depolarizations termed retinal waves. This spontaneous activity is necessary for refinement of retinal ganglion cell (RGC) axons within target regions of the brain (for reviews, see [Guido, 2008, Huberman et al., 2008]). In addition, there is growing evidence that retinal waves may play a role of the stratification of dendrites of a subset of RGCs [Xu et al., 2010] as well as in the synaptic maturation of particular retinal circuits [Kerschensteiner et al., 2009, Soto et al., 2012].

Retinal waves are detected for an extended period perinatally, from 1 week before to 2 weeks after birth in mice. During this time, the retina undergoes a substantial amount of development, and, as a result, the circuits that mediate waves change with age [Blankenship and Feller, 2010]. During the first postnatal week, waves are mediated by a transient cholinergic circuit composed of starburst amacrine cells [Zhou, 2001, Ford and Feller, 2012]. Volume release of acetylcholine provides a diffuse source of depolarization that drives the participation of all nearby starburst amacrine cells and RGCs [Syed et al., 2004a, Ford et al., 2012].

Just before eye opening, from postnatal day (P)10-P13, retinal waves are dependent upon the activation of ionotropic glutamate receptors (iGluRs) [Bansal et al., 2000, Wong

et al., 2000, Zhou and Zhao, 2000] and are modulated by inhibition. Similar to cholinergic waves, glutamatergic waves are accompanied by increases in extrasynaptic glutamate [Blankenship et al., 2009] providing a diffuse source of depolarization. In both ferrets and mice, $GABA_A$ transmission modulates the percentage of retinal waves that recruit On and Off RGCs [Fischer et al., 1998, Kerschensteiner and Wong, 2008]. However, the role of inhibitory transmitters in determining the percentage of cells that are recruited into waves in the inner nuclear layer (INL) and ganglion cell layer (GCL) is unknown. Here, we used an optical indicator of extrasynaptic glutamate and two-photon Ca^{2+} imaging to explore how the balance of diffuse excitation and inhibition influences the participation of retinal neurons in glutamatergic waves.

3.3 Results & Discussion

Glutamate waves are detected using a FRET-based sensor.
We have previously demonstrated that glutamatergic waves are accompanied by increases in extrasynaptic glutamate by probing the IPL with an outside-out patch of RGC membrane [Blankenship et al., 2009]. To visualize the spatial extent of glutamate spillover during retinal waves, we developed a new strategy using the FRET-based optical sensor of glutamate FLII^{81}E-1μ. FLII^{81}E-1μ is a diffusible extracellular sensor that has been previously optimized to detect glutamate spillover in brain slices [Dulla et al., 2008]. It contains the *Escherichia coli* glutamate binding protein YbeJ with internally fused eCFP and COOH-terminally fused Venus, a variant of yellow fluorescent protein [Deuschle et al., 2005]. Upon binding of glutamate, there is a decrease in FRET between the fluorophores, allowing for a ratiometric analysis of glutamate transients by fluorescence.

FLII^{81}E-1μ was bath loaded into P10-P12 whole mount retinas. FRET imaging was then used to detect glutamate in the IPL for a period of 5 min. Periodic increases of glutamate could be visualized as a spatially diffuse band of FRET change that propagated through the IPL (Figure 3.1). The band of FRET changes, which we refer to as glutamate waves, had clearly defined front and back edges (Figure 3.1A) and passed through the field of view at a median frequency of 1.8 waves/min (wave interval median, lower quartile/upper quartile: 33 s, 22/78 s, N = 47 waves; Figure 3.1, B and C). Increases in extrasynaptic glutamate were transient, lasting 24 s in control conditions. The addition of 20 μM 6,7-dinitroquinoxaline-2,3-dione (DNQX) and 50 μM d-2-amino-5 phosphonopentanoic acid (AP5), iGluR antagonists that have previously been shown to block retinal waves [Blankenship et al., 2009], completely abolished glutamate waves (data not shown, n = 4 retinas). These data indicate that glutamatergic retinal waves are accompanied by large increases in extrasynaptic glutamate that propagate throughout the IPL.

Neurons in the INL participate in retinal waves
To investigate whether neuronal populations in the INL participate in retinal waves, we used two-photon Ca^{2+} imaging to record from large numbers of neurons simultaneously. Retinas were acutely isolated from P10-P12 mice and bolus loaded with the Ca^{2+} indicator OGB

as previously described [Stosiek et al., 2003, Blankenship et al., 2009, Ford et al., 2012]. Two-photon imaging enabled us to record Ca^{2+} transients in different neuronal populations with single cell resolution by varying the depth of the imaging plane (Figure 3.2A) without contamination from out-of-focus fluorescence.

Neurons in the INL and GCL exhibited propagating waves of Ca^{2+} transients (Figure 3.2, A-C). The rapid rise time and short time course of the Ca^{2+} transients are consistent with membrane depolarization rather than Ca^{2+} release from internal stores. The frequency of waves detected with Ca^{2+} imaging was similar in the INL and GCL, with a median frequency of 1.6 waves/min (wave interval median, lower quartile/upper quartile: 36 s, 20/82 s, GCL: 89 waves, 10 retinas and INL: 76 waves, 6 retinas; Figure 3.2D), and waves were blocked in both retinal layers by bath application of iGluR antagonists (n = 6 retinas; data not shown). Consistent with a previous study [Blankenship et al., 2009], we found that retinal waves often occur in episodic clusters during which two to five waves occur in rapid succession followed by a much longer interval of inactivity. This pattern was observed in both the INL and GCL (Figure 3.2C). Note that FLII^{81}E-1μ was unable to detect a rapid succession of glutamate waves (Figure 3.2D). We believe this is a limitation in the temporal resolution of the glutamate imaging, because increases in extrasynaptic glutamate were previously shown to occur in clusters by outside-out patch [Blankenship et al., 2009].

There are four general classes of cell types whose somas are roughly stratified within the INL by P10. From the inner to outer plexiform layer, there are amacrine cells, Müller glial cells, bipolar cells, and horizontal cells. We used an antibody against Chx10, a transcription factor expressed in all bipolar cells, to identify bipolar cell somas and determine their location relative to the somas of other cell types in the P10-P13 INL (Figure 3.3A) [Katoh et al., 2010]. Bolus loading of OGB labeled both neurons and glial cells indiscriminately throughout the INL and GCL (Figure 3.3B) [Sullivan et al., 2005]. Müller glial cells have been reported to have both spontaneous and neurally evoked Ca^{2+} transients [Newman, 2001, 2005]. To see if glial Ca^{2+} transients correlated with retinal waves, we performed Ca^{2+} imaging in P11-P13 retinas from GLAST-tdTomato mice, which express tdTomato in Müller glial cells. After bolus loading with OGB, tdTomato was used to identify Müller somas within the INL (Figure 3.3B). We chose a single XY plane that contained both Müller and neuronal somas for 1-Hz two-photon imaging (Figure 3.3C). We found that spontaneous Ca^{2+} transients in Müller somas were infrequent and uncorrelated with wave events seen in OGB-loaded neurons (n = 6 retinas; Figure 3.3, D and E). Hence, the correlated Ca^{2+} transients we observed in the INL originate from neurons and not from glial cells.

Pharmacological manipulation of glutamatergic waves.

To further strengthen our conclusion that glutamate waves and correlated Ca^{2+} transients in the INL and the GCL all originate from the same wave events, we used pharmacology to alter wave frequency. First, we blocked glutamate uptake through transporters by the bath application of 25 μM TBOA, an approach we have previously shown to increase extrasynaptic glutamate levels and the frequency of retinal waves [Blankenship et al., 2009]. TBOA led to a prolonged duration of glutamate waves, consistent with glutamate lingering in the extracellular space longer, whereas block of inhibitory GABA and glycine receptors

with Gbz/Stry did not (Figure 3.4A). As measured by both FLII^{81}E-1μ and Ca^{2+} imaging, TBOA increased the frequency of glutamate waves in the IPL and the frequency of correlated Ca^{2+} transients in neurons of the INL and GCL (Figure 3.4, AC). Previously, we have shown that inhibition shapes cholinergic waves by decreasing wave frequency via increased shunting inhibition to RGCs through potentiated amacrine cells [Wang et al., 2007]. Similarly, we found that Gbz/Stry led to a dramatic increase in event frequency, as assessed by both FLII^{81}E-1μ and Ca^{2+} imaging (Figure 3.4, AC). Consistent with a previous report [Blankenship et al., 2009], we found that inhibition had the most marked effect on wave initiation rate in glutamatergic waves, by shifting the wave interval distribution to lower values, indicating that inhibition is important for the timing of triggering a wave (Figure 3.4C).

As measured by FLII^{81}E-1μ, the spatial properties of glutamate waves in the IPL also showed differential effects of TBOA versus Gbz/Stry (Figure 3.4D). In contrast to the spatially coherent wavefronts of glutamate waves in control conditions, glutamate waves in the presence of Gbz/Stry exhibited a greater range of rotational propagation trajectories. In the presence of TBOA, glutamate waves propagated in multiple directions simultaneously. In addition, there were regions of sustained decreases in FRET, indicative of stationary pools of glutamate. These observations indicate that the excitability of the circuit, set by extrasynaptic glutamate and inhibition, is not only a critical determinant of wave initiation [Blankenship et al., 2009] but also the trajectory of glutamate wave propagation.

Inhibition limits ganglion cell participation in retinal waves.
The single cell resolution of two-photon Ca^{2+} imaging revealed that not all cells participate in waves (Figure 3.2A). This is in sharp contrast to cholinergic retinal waves, where the vast majority of RGCs and displaced starburst amacrine cells are depolarized in each event [Ford et al., 2012]. In the INL we found that, on average, roughly half the identified cells in the field of view participated in at least one wave over the entire recording duration of 8 min (mean: 54 ± 16%, n = 6 retinas; Figure 3.5A control). The GCL had slightly higher percentages of cells that participated in at least one wave (mean: 68 ± 30%, n = 6 retinas; Figure 3.5A control). Cell participation per wave was even lower. In the INL, on average, 25 ± 16% of cells participated per wave (76 waves). The GCL had nearly identical levels of cell participation per wave (25 ± 18% of cells, 89 waves). Of the cells that did not participate in waves, some had detectable Ca^{2+} events between waves (10 1.0% of nonwaving cells in the INL and 15 4.2% of nonwaving cells in the GCL, n = 4 retinas). This indicates that a cell's participation in waves is linked to its circuitry and is not an artifact of dye loading.

The sparse participation of cells in both the INL and GCL suggest that the diffuse excitation provided by glutamate spillover is balanced by specific inhibitory circuits, influencing the strength of depolarization of cells during retinal waves. To test this hypothesis, we assayed the effects of increasing glutamate spillover and blocking inhibitory signaling on the percentage of cells that participate in waves.

Using two-photon Ca^{2+} imaging, the proportion of cells participating in at least one wave was tracked across different drug conditions in both the INL and GCL (Figure 3.5, A and B). This method of quantification revealed changes in the population of cells depolarized by waves. In the INL, TBOA increased cell participation (Table 3.1). In contrast, Gbz/Stry

did not significantly affect an INL neuron's likelihood of participating in a wave. In the GCL, TBOA increased cell participation and Gbz/Stry dramatically increased the proportion of cells participating in waves. Few to no neurons within the GCL failed to participate in any waves when inhibitory neurotransmission was blocked. Interestingly, blockade of inhibition had a significantly greater effect on neuron participation in the GCL compared with the INL ($F(3, 27) = 3.35, P < 0.05$).

We also tracked the proportion of cells participating per wave (Figure 3.5C and Table 3.1). This is a measure of the density of cells participating in waves and how that changes in different drug conditions. Interestingly, the proportion of GCL neurons that exhibited an increase in intracellular Ca^{2+} per wave significantly increased after blockade of inhibition with Gbz/Stry. These results indicate that inhibitory neurons in the INL, and glutamate levels in the IPL, may be responsible for selecting which GCL cells participate in waves. In contrast, cell participation in the INL was primarily reliant on glutamate levels.

A subset of On-bipolar cells participates in retinal waves.
To further determine which inhibitory circuits are responsible for determining cell participation, we manipulated the On-bipolar cell circuit that inhibits Off cells through crossover inhibition [Werblin, 2010, Demb and Singer, 2012]. To directly measure whether bipolar cells participate in retinal waves, we performed Ca^{2+} imaging in retinas from Grm6-eGFP mice, which express eGFP in On-cone bipolar cells and rod bipolar cells (Figure 3.6A, i) [Morgan et al., 2006]. We found that GFP-positive cell somas directly adjacent to the outer plexiform layer, where rod bipolar cell somas are located [Morgan et al., 2006, Morrow et al., 2008], did not exhibit detectable Ca^{2+} transients. However, a subset of GFP-positive cells that were deeper in the INL, closer to the IPL, exhibited correlated spontaneous Ca^{2+} transients that were blocked with 5 μM l-amino-4-phosphonobutyric acid (l-AP4), a group III mGluR agonist that keeps On-bipolar cells in a more hyperpolarized state (Figure 3.6A,ii) [Slaughter and Miller, 1981]. Hence, we concluded that a subset of On-bipolar cells are recruited during retinal waves. We then tracked how INL and GCL cell participation during waves was affected by application of l-AP4. Interestingly, l-AP4 did not significantly affect wave interval but did alter the population of cells that participated in waves (Figure 3.6B). In the presence of l-AP4, some cells that were depolarized during waves in control became inactive and some cells that were inactive during waves in control began to participate in waves. l-AP4 did not affect overall levels of cell participation in the INL but significantly increased levels of cell participation in the GCL (mean increase: 30 ± 10%, n = 4 retinas; Figure 3.6C). These findings suggest that On-bipolar cells play a role in selecting which cells in the GCL participate in waves.

3.4 Concluding remarks

We have presented two-photon Ca^{2+} imaging data demonstrating that neurons within the INL, including a subset of On-bipolar cells, participate in retinal waves. In addition, using an optical sensor for glutamate, we found that glutamatergic retinal waves are accompanied by

significant transient increases in extrasynaptic glutamate throughout the IPL. Prolonging the duration of glutamate waves with TBOA indiscriminately increased the percentage of both INL and GCL neurons that participated in retinal waves, whereas block of inhibition with Gbz/Stry selectively affected the GCL, where it drastically increased the percentage of cells that participated in retinal waves. Taken together, this evidence suggests that glutamatergic waves may activate a specific neural circuit that selects for subsets of neurons within the GCL rather than a gross wavefront of glutamate-based depolarization that activates all cells. This is in contrast to cholinergic waves, where every cell in the GCL is recruited during waves, suggesting that there is a maturation of inhibitory inputs during glutamatergic waves. Additionally, use of l-AP4 to prevent On-bipolar cells from depolarizing changes the pattern of cell activation in the INL and GCL and increases participation in the GCL, indicating that crossover inhibition mediated by specific amacrine cell subtypes may be responsible for activating distinct circuits during development [Kerschensteiner and Wong, 2008].

Previously, we demonstrated that waves led to an increase in extrasynaptic glutamate using outside-out patches [Blankenship et al., 2009]. However, these experiments were limited in that they only assessed extrasynaptic glutamate at one point in space and the electrode may have caused tissue damage that led to increases in glutamate in local regions around the pipette. Here, we used an optical sensor, FLII^{81}E-1μ, to demonstrate that retinal waves lead to a spatially diffuse glutamate wave that propagates throughout the IPL (Figure 3.1). FLII^{81}E-1μ is one of a family of FRET-based indicators that has been used to measure glutamate spillover in brain slices and in vivo [Okumoto et al., 2005, Namiki et al., 2007, Dulla et al., 2008, Matsuo et al., 2009, Okubo et al., 2010, Tani et al., 2010]. This study further demonstrates the applicability of this sensor in measuring glutamate dynamics in response to neuronal activity in intact tissue.

Robust glutamate spillover has been observed in both developing and mature circuits. In the mature retina, glutamate spillover has been detected both at photoreceptor [Szmajda and Devries, 2011] and bipolar cell terminals [Hasegawa et al., 2006, Veruki et al., 2006, Rowan et al., 2010], where it is thought to inhibit glutamate release by the activation of transporters or mGluRs, providing a source of negative feedback [Awatramani and Slaughter, 2001, Higgs et al., 2002]. Extrasynaptic glutamate is also a source of excitation for RGCs [Chen and Diamond, 2002]. During development, extrasynaptic glutamate has been implicated in regulating the early differentiation of neurons in the ventricular zone [Demarque et al., 2002] and might modulate neuronal migration [Manent et al., 2005]. In addition, it is a source of depolarization that is critical for generating spontaneous activity in the cortex and hippocampus [Garaschuk et al., 2000, Allne et al., 2008]. Similarly, volume release of ACh between starburst amacrine cells mediates an earlier stage of spontaneous activity in the retina [Ford et al., 2012].

We posit that glutamate spillover stimulates the propagation of glutamatergic retinal waves through the INL, activating both excitatory and inhibitory neurons. Block of glutamate uptake with TBOA enables an additional population of neurons in the INL to become depolarized during waves. In addition, TBOA leads to prolonged elevations of extrasynaptic glutamate in the IPL. We hypothesize that this, in turn, recruits additional neurons in the

GCL to participate in waves by direct spillover from bipolar cells onto neighboring amacrine and retinal ganglion cells.

Depolarization of neurons in the GCL depends on the balance of excitatory and inhibitory inputs, acting as a readout of the circuits that are activated during retinal waves. Here, we show that blockade of inhibition selectively enabled more neurons in the GCL to participate in waves, with no significant effect on cell participation in the INL. These data suggest that inhibition shapes cell participation in the GCL based on targets from inhibitory INL neurons.

The time around eye opening represents a significant period in retinal development, where a large number of RGC subtypes are undergoing dendritic stratification [Coombs et al., 2007, Kim et al., 2010] and bipolar cell-amacrine and bipolar cell-RGC synapses are forming. Interestingly, recent studies have indicated that the development of some retinal microcircuits may be sensitive to activity, whereas other are not [Kerschensteiner et al., 2009, Elstrott and Feller, 2010, Xu et al., 2010, Soto et al., 2012]. These data suggest that perhaps as subsets of retinal microcircuits emerge, the maturation of inhibitory synapses exerts a more powerful influence on the structure of correlated activity.

3.5 Experimental methods

Mice.
All experiments were performed on acutely isolated mouse retinas. Male and female C57BL/6 mice obtained from Harlan were used for all wild-type recordings. GLAST-tdTomato mice were generated by crossing mice that express Cre recombinase under control of the GLAST promoter [Tg(Slc1a3-cre/ERT)1Nat/J] to mice that ubiquitously express tdTomato preceeded by a loxP-flanked stop cassette [B6;129S6-Gt(ROSA)26Sor$^{tm9(CAG-tdTomato)Hze}$/J, both from The Jackson Laboratory]. Intraperitoneal injection of 0.5 mg of 4-hydroxytamoxifen (50:50 E and Z isomers, Sigma) at P5 reliably induced the expression of tdTomato in Müller glial cells by P10. In Grm6-EFGP mice, enhanced green fluorescent protein (EGFP) is expressed under control of the metabotropic glutamate receptor (mGluR)6 promoter, labeling On bipolar cells [Morgan et al., 2006]. All procedures were approved by the Institutional Animal Care and Use Committees of the University of California (Berkeley, CA) and conformed with guidelines of the National Institutes of Health *Guide for the Care and Use of Laboratory Animals*, the Public Health Service Policy, and the Society for Neuroscience Policy on the Use of Animals in Neuroscience Research.

Retinal preparation.
P10-P12 C57BL/6 mice of either sex were deeply anesthetized with isoflurane and decapitated. Eyes were removed, and retinas were isolated in oxygenated artificial cerebrospinal fluid [ACSF; containing (in mM) 119.0 NaCl, 26.2 $NaHCO_3$, 11 glucose, 2.5 KCl, 1.0 K_2HPO_4, 2.5 $CaCl_2$, and 1.3 $MgCl_2$]. For Ca^{2+} and fluorescence resonance energy transfer (FRET) imaging, retinas were mounted GCL-up on filter paper (Millipore) and perfused continuously with oxygenated ACSF.

Ca^{2+} Imaging.
Retinas were loaded with Oregon green 488 BAPTA-1 AM (OGB) using the multicell bolus loading technique [Stosiek et al., 2003, Blankenship et al., 2009]. Two-photon Ca^{2+} imaging of neurons in the INL and GCL was performed using a custom-modified two-photon microscope (Fluoview 300, Olympus America). XYZ scans were used to localize neurons in the GCL and INL. Time series images were acquired at 1 Hz using a ×60 objective (Olympus LUMPlanFl/IR ×60/0.90W) with the excitation laser tuned to 790 nm. Images were corrected for motion artifacts using the Turboreg ImageJ plugin. Ten × ten-pixel regions (12 × 12 μm) of interest were manually selected within all cells in the field of view. Fluorescence signals were averaged within these regions over time. Cell events were identified when change in fluorescence exceeded 15% of the cell's baseline fluorescence within 1 s. Cells were categorized as participating in a retinal wave if cell events correlated with neighboring cells.

FRET imaging.
The FLII^{81}E-1μ glutamate sensor was purified as previously described [Dulla et al., 2008]. Whole mount retinas were bath loaded with 50 μg/ml of the sensor diluted in aCSF for 20 min at room temperature. Live imaging was performed on an upright Zeiss Axioskop 2 using a ×20 objective (Olympus UMPlanFl N/×20/0.50W). Retinas loaded with the FLII^{81}E-1μ indicator were transferred from the loading solution directly into the microscope perfusion. After retinas had been loaded, the sensor diffused out of the tissue in roughly 58 min, limiting the duration of imaging runs. dl-Threo-ß-benzyloxyaspartate (TBOA; 25 μM), gabazine (Gbz; 5 μM), and strychnine (Stry; 4 μM) were applied by immersing the loaded retina for 5 min before imaging. The imaging plane was located within the inner plexiform layer (IPL).

Individual FRET channel detection was accomplished by using a Dual-View image splitter (DV-FC, Optical Insights) with appropriate yellow (535 nm/30) and cyan (480 nm/40) emission filters. Images were captured on a Photometrics CoolSnap HQ charge-coupled device camera and analyzed in ImageJ. Images were acquired at 2 Hz (200-ms exposures). Background fluorescence (F) was subtracted from both channels, and enhance cyan fluorescent protein (eCFP) bleedthrough into the Venus channel was corrected [Gordon et al., 1998, van Rheenen et al., 2004]:

$$F_{Venus} = F_{FRET} - 0.51 \times F_{eCFP}$$

FRET ratios (R) were calculated as follows:

$$R = \frac{F_{Venus}}{F_{eCFP}}.$$

FRET ratio data were then analyzed with custom MATLAB (Mathworks) scripts to define the spatiotemporal properties of spillover, similar to the process used to define Ca^{2+} waves as described by [Blankenship et al., 2009].

Immunohistochemistry.
Retinas were fixed in 4% paraformaldehyde and then cut into 120-μm sections with a vibratome. Sections were stained using sheep anti-Chx10 primary antibody (1:200, Exalpha Biologicals) and Alexa fluor 647 donkey anti-sheep secondary antibody (1:200, Invitrogen),

collected on slides, and mounted in medium containing 4,6-diamidino-2-phenylindole before being imaged on a Zeiss LSM 780 confocal microscope.

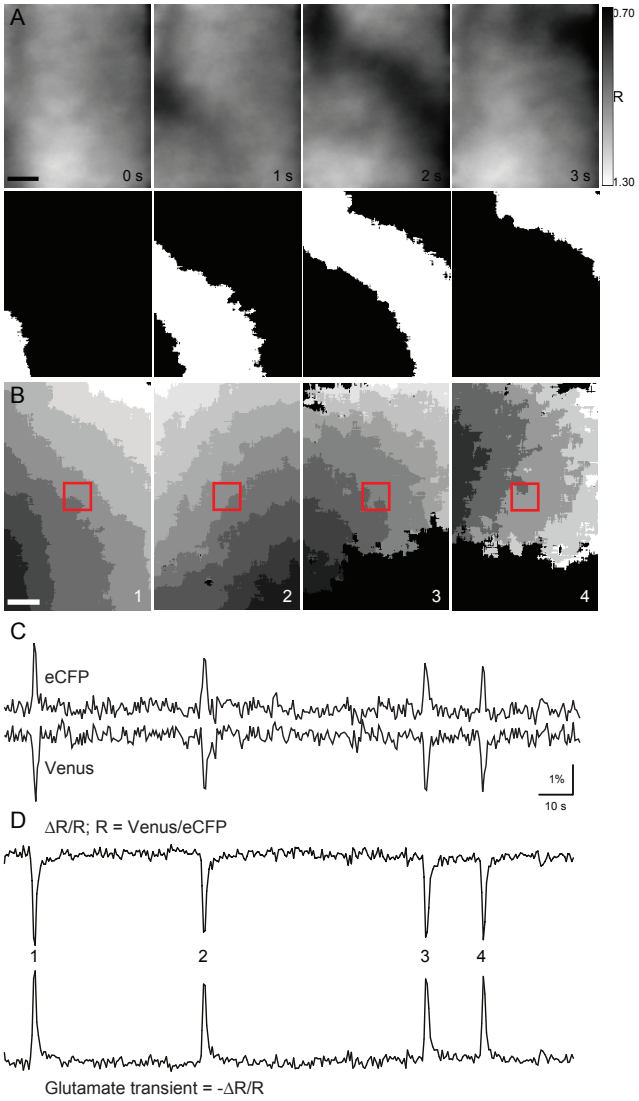

Figure 3.1: The fluorescence resonance energy transfer (FRET)-based glutamate sensor FLII^{81}E-1μ detects coherent wave fronts of glutamate propagating through the inner plexiform layer (IPL) in postnatal day (P)10-P12 retinas. (A) example of a single glutamate wave detected by FRET imaging of FLII^{81}E-1μ in a P11 whole mount retina. The raw ratio data (top) and binarized version used for analysis (bottom) are shown. (B) each image represents the spatial extent and duration of one glutamate transient. Within an image, each grayscale value represents the active area in one frame, with an imaging rate of 2 Hz. Dark gray is the first frame in which glutamate was detected, whereas white is the last. Black is baseline. Red arrows indicate the propagation direction. The red box is the area where ΔR/R was averaged to determine whether an increase in glutamate occurred in that region. (C) example trace of raw fluorescence changes for enhance cyan fluorescent protein (eCFP) and Venus. (D) top: resulting trace when the ratio of Venus to eCFP was taken. The downward peaks indicate the decrease in FRET when glutamate binds. Bottom, reflection of the top trace. The upward peaks indicate increases in glutamate. Numbered peaks correspond to the wave events shown in *B*.

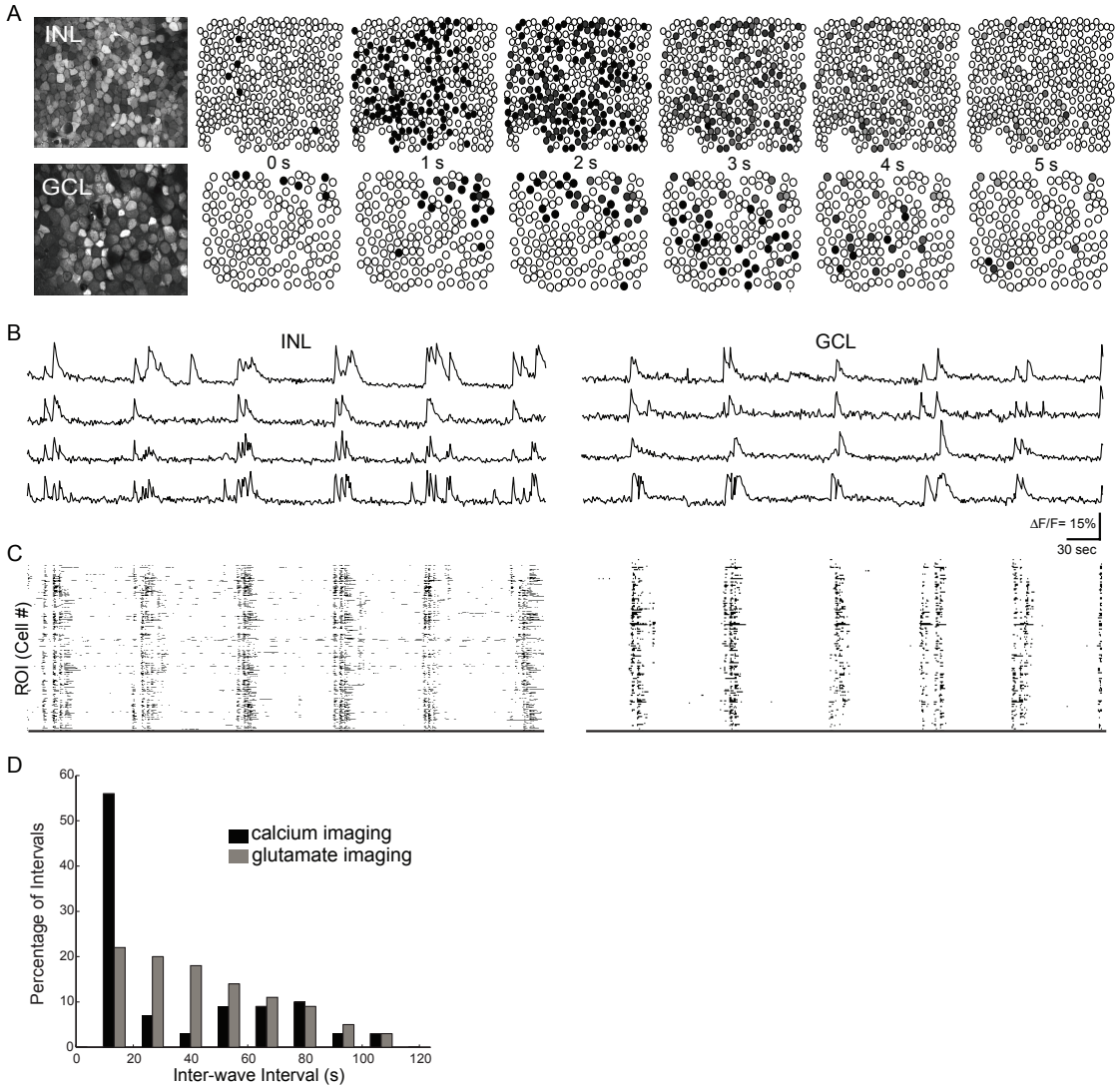

Figure 3.2: Two-photon Ca^{2+} imaging reveals that neurons in the inner nuclear layer (INL) participate in glutamatergic retinal waves. (A) example of wave propagation in the INL (top) and ganglion cell layer (GCL; bottom) observed with two-photon Ca^{2+} imaging at a frame rate of 1 Hz. Leftmost images are the retinal sample loaded with Oregon green BAPTA-1 AM (OGB). Circles are identified cells; black indicates cells with $\Delta F/F$ of >15% for the first time in that frame, and gray indicates cells with persisting $\Delta F/F$ above threshold. (B) sample $\Delta F/F$ traces from averaged regions within cells. Each trace represents a different cell. (C) raster plots of neuronal Ca^{2+} transients of >15% $\Delta F/F$ for all cells in the field of view. The total imaging duration was 5 min. (D) histogram of interwave intervals for glutamate and Ca^{2+} imaging from both the GCL and INL (Ca^{2+} imaging: N = 150 wave intervals and FRET: N = 47 wave intervals).

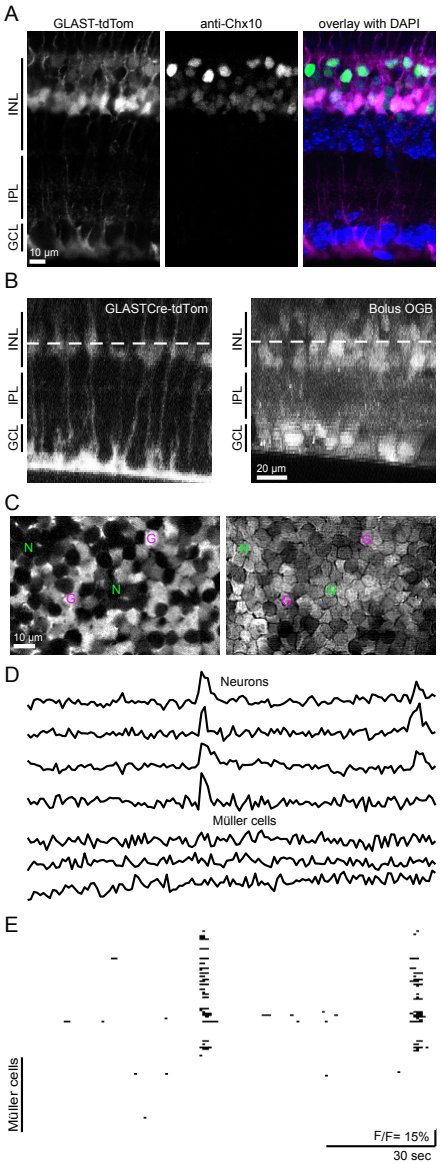

Figure 3.3: Müller glial somas are not depolarized during retinal waves. (A) P11 GLAST-tdTomato retina stained for anti-Chx10 showing the location of Müller glial and bipolar somas within the INL. The confocal image is of a vibratome section. Green is anti-Chx10, magenta is tdTomato, and blue is 4',6-diamidino-2-phenylindole (DAPI). (B) orthogonal projections of two-photon Z-stacks. The dashed line indicates the XY plane chosen for 1-Hz imaging. Left, GLAST-tdTomato labeling of Müller glial cells; right: bolus loading of OGB labeling both neurons and glial cells. (C) XY plane from B, left. G and N indicate examples of Müller glial or neuronal somas, respectively. (D) sample Δ/F traces from averaged regions within identified neuronal or glial somas. E: raster plot of neuronal and glial Ca^{2+} transients of >15% ΔF/F.

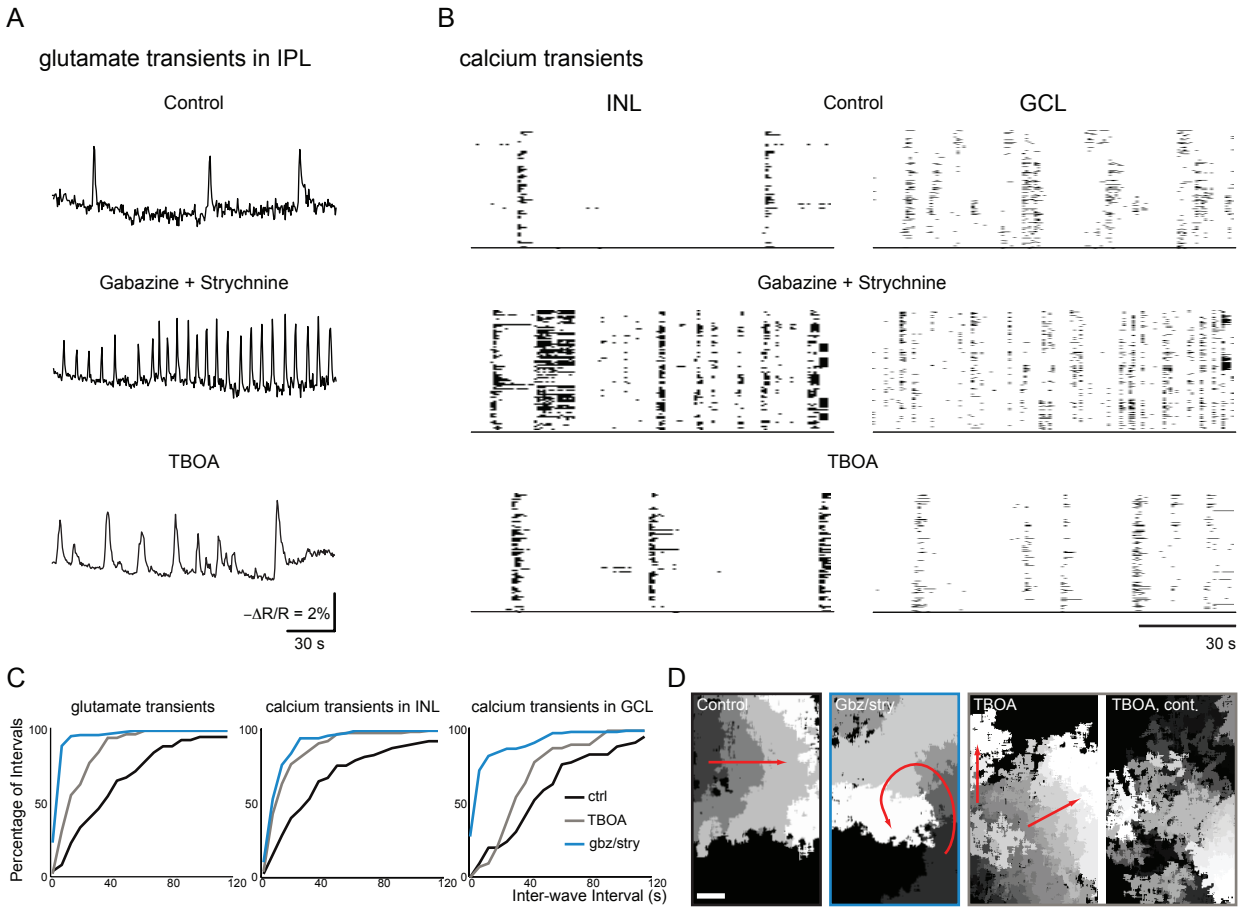

Figure 3.4: dl-Threo-ß-benzyloxyaspartate (TBOA) and gabazine (Gbz)/strychnine (Stry) increase wave frequency as detected by FLII^{81}E-1μ and two-photon Ca^{2+} imaging of neurons in the INL and GCL. (A) representative traces of glutamate transients for control (top), Gbz and Stry (middle) and TBOA (bottom). (B) raster plots of neuronal Ca^{2+} transients detected by two-photon Ca^{2+} imaging as in Figure 3.2C. (C) cumulative distributions of interwave intervals for control (black), TBOA (gray), and Gbz/Str (blue) for FRET imaging in the IPL and Ca^{2+} imaging in the INL and GCL. Binning = 10 s. FRET glutamate transients: control, 47 wave intervals, 8 retinas; Gbz/Stry, 135 intervals, 5 retinas; and TBOA, 42 intervals, 5 retinas; Ca^{2+} INL: control, 84 intervals, 16 retinas; Gbz/Stry, 116 intervals, 8 retinas; and TBOA, 127 intervals, 8 retinas; and Ca^{2+} GCL: control, 156 intervals, 15 retinas; Gbz/Stry, 122 waves, 9 retinas; and TBOA, 42 intervals, 6 retinas. (D) each image represents the spatial extent and duration of one glutamate transient in control (left), Gbz/Stry (middle left), and TBOA (middle right and right). Gray values correspond to the time during which that region of the retina was active, as in Figure 3.1CB. Red arrows indicate the propagation direction.

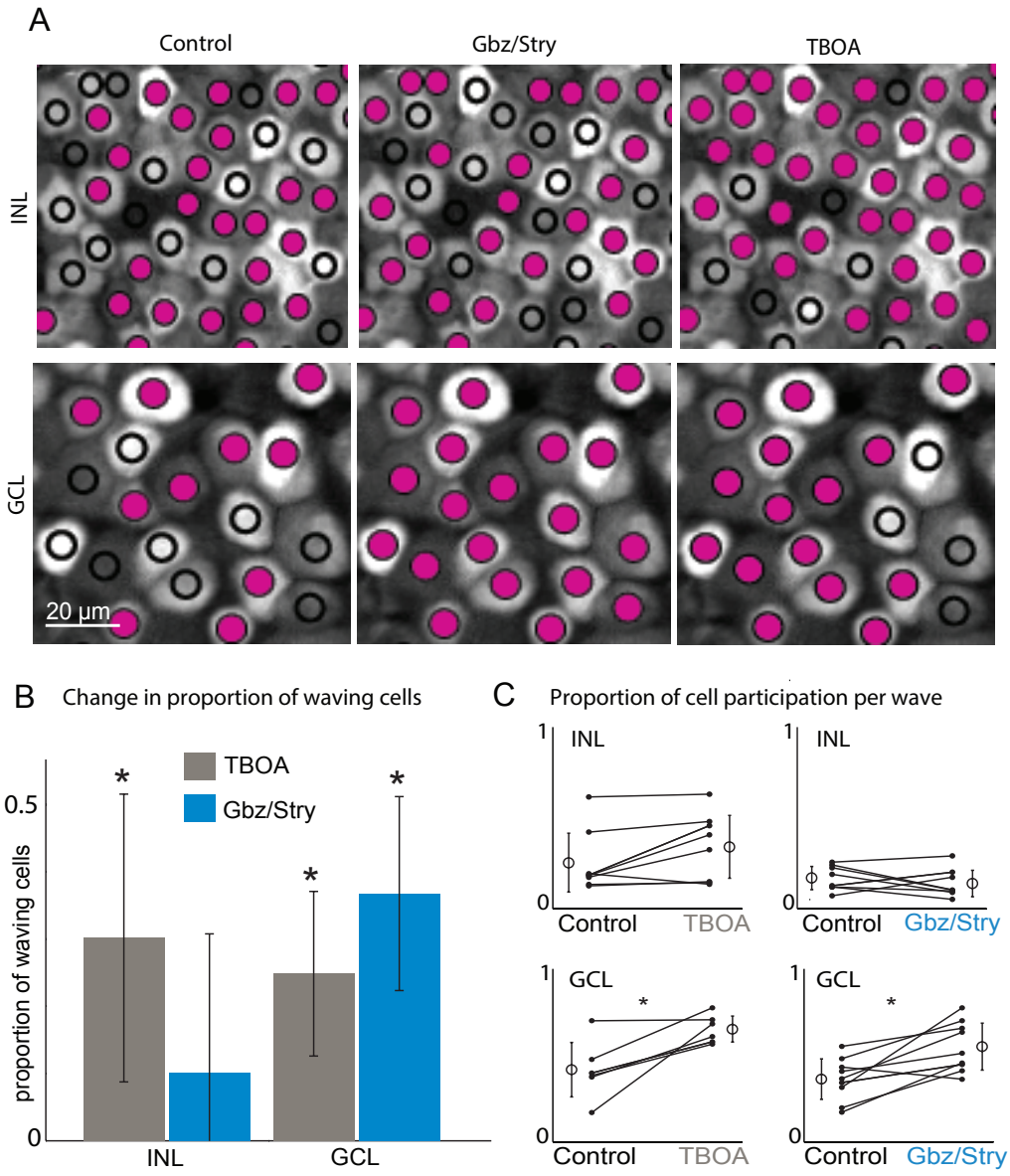

Figure 3.5: TBOA increases cell participation in the INL and GCL, whereas Gbz/Stry only increases GCL participation. (A) cell participation in retinal waves. The INL (top) and GCL (bottom) in a whole mount retina loaded with OGB are shown. Magenta indicates cells that participated in at least one wave during the duration of the recording; open circles indicate cells that did not participate. The same field of view from an example retina was compared in control (left), Gbz/Stry (middle), and TBOA (right). (B) changes in the proportion of waving cells. The change in the proportion of cells participating in at least one wave in the control versus drug condition were quantified for each retina, and these values were then averaged across all retinas (INL: TBOA, N = 8; Gbz/Stry, N = 8 and GCL: TBOA, N = 6; Gbz/Stry, N = 9). (C) summary of effects of TBOA and Gbz/Stry on the average proportion of cells that participated per wave. Lines connect values of average cell participation per wave for one retina in control versus TBOA or Gbz/Stry in the INL and GCL. Open circles are group means and SD. See Table 3.1 for details.

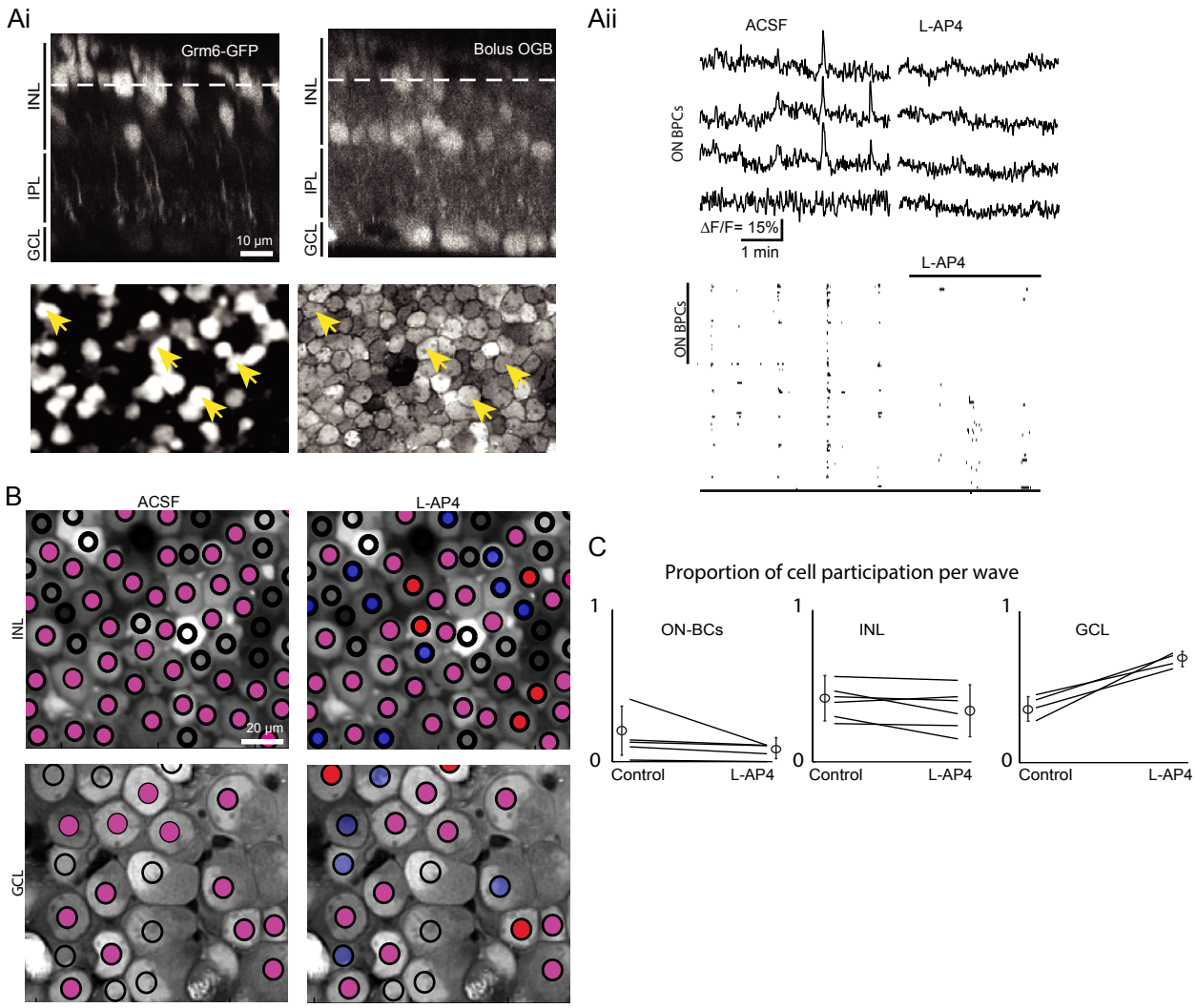

Figure 3.6: The On-bipolar cell (BPC) blocker l-amino-4-phosphonobutyric acid (l-AP4) affects cell participation in glutamatergic waves. (A) (i) Grm6:eGFP-labeled On-BPCs (left) and bolus-loaded INL and GCL neurons (right). Top, orthogonal projections of two-photon Z-stacks. The dashed line indicates the XY plane chosen for 1-Hz imaging. Bottom, XY plane. Yellow arrows indicate On-BPCs. (ii) top: sample $\Delta F/F$ traces from averaged regions within identified On-BPC somas. Bottom, raster plot of neuronal Ca^{2+} transients of >15% $\Delta FF/F$. Regions of interests 130 are identified On-BPCs; the remainder are unidentified neurons within the same imaging plane. On-BPCs stopped participating after the onset of l-AP4 washin (n = 5 retinas). aCSF, artificial cerebrospinal fluid. (B) cell participation in retinal waves. The INL (top) and GCL (bottom) in a whole mount retina loaded with OGB are shown. Magenta indicates cells that participated in at least one wave during the duration of the recording; open circles indicate cells that did not participate. The same field of view from an example retina was compared in control (left) and l-AP4 (right). Red indicates increased activity compared with control; blue indicates decreased activity; magenta cells were unaffected. (C) summary of effects of l-AP4 on the average proportion of cells that participated per wave. Lines connect values of average cell participation per wave for one retina in control versus l-AP4 in the INL and GCL. Open circles are group means and SD. See Table 3.1 for details.

		n	Control	Drug	*P* Value
Percentage of cells that participated in a wave per retina					
GCL					
	Gbz/Stry	6	58±18	95±6	<0.001
	TBOA	6	69±13	94±2	<0.001
INL					
	Gbz/Stry	8	33±15	43±16	0.22
	TBOA	8	41±22	71±18	0.01
Average percentage of cells participating per wave					
GCL					
	Gbz/Stry	9	33±13	53±15	0.0092
	TBOA	6	40±18	65±9	0.013
INL					
	Gbz/Stry	8	15±7	12±8	0.43
	TBOA	8	24±18	33±19	0.35

Table 3.1: Values are means ± SD; n, number of retinas. The percentages of cells that participated in any wave that propagated through an imaged region of the retina as well as the percentages of cells that participated per wave are shown. GCL, ganglion cell layer; Gbz, gabazine; Stry, strychnine; TBOA, dl-threo-β-benzyloxyaspartate; INL, inner nuclear layer.

Chapter 4

The role of AII amacrine cells in shaping the spatiotemporal features of glutamatergic retinal waves.

Preface: This chapter is the dissertation author's original unpublished work.

4.1 Abstract

Immediately prior to eye-opening, the circuits that mediate retinal waves require glutamate release from bipolar cells, excitatory interneurons in the retina. Here we test the hypothesis that in contrast to cholinergic retinal waves, which occur earlier in development and are mediated by a transient network of recurrently connected excitatory interneurons, glutamatergic waves are mediated by the interaction between inhibitory and excitatory circuits. In particular, we used two-photon calcium imaging to characterize the role of AII amacrine cells in setting the initiation and propagation properties of retinal waves. First, we used transgenic mice that express GFP in AII amacrine cells to demonstrate that they are depolarized during retinal waves. Second, we show that the waves in mice lacking the gap junction protein connexin 36, the source of coupling between AII amacrine cells and On cone bipolar cells, have reduced spatial coherence. Third, we find that altering the bursting properties of AII amacrine cells by pharmacological manipulation of the M-type potassium current strongly modulated the frequency of waves but maintained spatial coherence. In contrast, blockade of a pacemaker conductance I_h, presumably localized to cone bipolar cells, caused a dramatic loss of spatial coherence. These data indicate that gap junction coupled networks involving AII amacrine cells play a critical role in coordinating spontaneous activity during retinal development.

4.2 Introduction

Retinal waves are a robust feature of the developing retina, persisting for an extended time during development. As the retina itself matures, the circuits that mediate waves change. The bulk of work on retinal wave circuits has been focused on the cholinergic waves. Cholinergic waves are initiated by spontaneous depolarization in starburst amacrine cells and propagated via recurrent excitatory connections between starburst amacrine cells [Feller et al., 1996, Zhou, 1998].

Though there has been evidence for a role for gap junction coupling [Blankenship et al., 2011], volume release of glutamate and inhibition [Akrouh and Kerschensteiner, 2013, Firl et al., 2013], there is no comprehensive model for glutamatergic wave initiation and propagation. By analogy to the cholinergic circuit, glutamatergic waves would be initiated by spontaneous depolarization of bipolar cells. Cholinergic waves are propagated via excitatory connections between starburst cells and mediated at least in part by volume release of acetylcholine [Ford et al., 2012]. Though bipolar cells are not coupled via chemical synapses (though there is evidence for gap junction coupling between particular subtypes [Arai et al., 2010]), there is robust glutamate spillover during waves [Blankenship et al., 2009, Firl et al., 2013], a potential mechanism for wave propagation. However, the circuit activated by this spillover and how it influences the propagation properties of waves remains to be determined.

The spatial and temporal patterns of glutamatergic waves implicate a role for crossover inhibition. First, inhibition dictates cell participation. While there is evidence for volume

release of glutamate during waves, relatively few cells in both the GCL and INL depolarize during waves [Firl et al., 2013]. The low levels of GCL cell participation is likely the result of inhibitory inputs counterbalancing excitatory inputs they receive during waves [Blankenship et al., 2009, Akrouh and Kerschensteiner, 2013]. For example, under conditions of inhibition blockade, significantly more GCL cells depolarize during waves [Firl et al., 2013]. Second, glutamatergic waves are temporally structured such that On RGCs depolarize roughly 1 second before Off RGCs [Kerschensteiner and Wong, 2008] while wave-related inhibitory inputs are synchronized with no delay, suggesting that inhibition orchestrates waves by providing a common input that suppresses Off RGCs while On RGCs depolarize [Akrouh and Kerschensteiner, 2013, Margolis et al., 2014]. Because of their known role in providing crossover inhibition between On and Off pathways (for review [Werblin, 2010, Oesch and Diamond, 2009]), these data suggest that AII amacrine cells play a role in coordinating the timing of On vs Off during waves.

Recent studies have implicated AII amacrine cells in mediating the oscillatory activity that appears in rd-mice after photoreceptor degeneration. Observed phase relations within 10Hz oscillations between On and Off RGCs are dependent on Na^+ spikes from AII amacrine cells, and persist in the presence of glutamatergic synaptic blockers [Margolis et al., 2014]. Spontaneous oscillations were found to be driven by small intrinsic membrane fluctuations in On-cone bipolar cells and AII amacrine cells, and were blocked by meclofenamic acid (MFA) [Trenholm et al., 2012, Borowska et al., 2011]. AII amacrine cells have been characterized as electrotonically compact, capable of generating TTX-sensitive spikes in their processes [Cembrowski et al., 2012], making them potential candidates for spreading electrical inputs from On cone bipolar cells to downstream retinal neurons.

Here we demonstrate that AII amacrine cells play a critical role in shaping the spatial and temporal properties of glutamatergic retinal waves. To assess the role of interneuronal circuits in shaping the spatiotemporal properties of glutamatergic waves, we used two-photon Ca^{2+} imaging to record with single cell-resolution from large numbers of neurons simultaneously. Though the two-photon Ca^{2+} imaging utilized in this study has a more limited field of view than previous epifluorescent-based studies [Ford et al., 2012, Blankenship et al., 2009], it allows for recording Ca^{2+} transients in different neuronal populations by varying the depth of the imaging plane without contamination from out-of-focus fluorescence, allowing for imaging in the INL and the GCL separately [Firl et al., 2013]. In addition, two-photon imaging allows for the spatial location of cells that participate in waves to be unamibuously identified, an advantage over the known ambiguities introduced by multielectrode array recordings [Marre et al., 2012, Segev et al., 2004, Briggman and Euler, 2011].

4.3 Results & Discussion

Glutamatergic waves are not mediated by a pure glutamatergic circuit.
A critical step for glutamatergic wave generation is the depolarizations in On-cone bipolar cells [Akrouh and Kerschensteiner, 2013, Firl et al., 2013]. However, what provides the

depolarization of On-cone bipolar cells? In the adult retina, On-cone bipolar cells express metabotropic glutamate receptor(mGluRs) which, when activated by glutamate, hyperpolarize the cells. Here we tested whether depolarization via glutamate was sufficient to initiate waves.

Retinas were acutely isolated from P10-P12 WT mice and bolus loaded with the Ca^{2+} indicator OGB as previously described [Stosiek et al., 2003, Blankenship et al., 2009, Ford et al., 2012]. We lowered a pipette filled with 1mM glutamate and 0.1mM Alexa 594 into the INL of a retina loaded with OGB (Figure 4.1A). We then administered 10ms puffs at 5 psi while imaging from the GCL. Though short applications of glutamate reliably depolarized neurons in the GCL (Figure 4.1B), the spatial extent to which GCL cells were depolarized by puffs did not extend past the area of the spread of glutamate (Figure 4.1C, n = 20 puffs, 4 retinas), unlike glutamatergic waves which propagate across the entire field of view in a coherent spatial direction [Blankenship et al., 2009].

Note this is in contrast to cholinergic waves, for which depolarization via activation of nAChRs [Feller et al., 1996] or depolarization of a single starburst amacrine cell was sufficient to start waves [Ford et al., 2012].

AII amacrine cells participate in glutamatergic waves.
The data above suggest that transient increases in extrasynaptic glutamate was not sufficient to initiate waves. Therefore a more complex network must be required to depolarize On-cone bipolar cells. In the absence of mature photoreceptors, the primary inputs to On-cone bipolar cells occurs via an electrical synapse with glycinergic interneurons called the AII amacrine cells [Trenholm et al., 2012, Borowska et al., 2011]. This interaction between AII amacrine cells and On cone bipolars is critical for the generation of rhythmic activity in mice that lack functional photoreceptors, such as the rd-1/rd-1 mouse.

We first verified that AII amacrine cells participate in waves using Ca^{2+} imaging in retinas from Fbxo32-eGFP mice, which express eGFP in AII amacrine cells. We found that GFP-positive cells were uniformly distributed throughout the INL (Figure 4.3A). GFP-expressing cells were also expressed at different depths in the INL (Figure 4.3B), but only GFP-expressing cells nearest to the IPL displayed wave-related Ca^{2+} transients of >15% $\Delta F/F$ in conjunction with other INL neurons (Figure 4.3C, 3D).

Cx36ko and Cx36/45dko lack spatial coherent wave fronts.
The gap junctions between AII amacrine cells and AIIs and On-cone bipolars contain primarily Cx36 [Kolb and Famigilietti, 1974, Veruki and Hartveit, 2002] with a subset presumably hetergeneous electrical synapses with On-cone bipolars expressing Cx45 [Güldenagel et al., 2000, Söhl et al., 2000, Feigenspan et al., 2001, 2004, Han and Massey, 2005, Lin et al., 2005, Maxeiner et al., 2005, Dedek et al., 2006, Pan et al., 2010]. To determine if gap junction coupling between AIIs and AIIs and On cone bipolar cells are critical for generating waves, we looked at spatiotemporal pattern of activity in Cx36 Ko and Cx36/45 ko mice using two-photon Ca^{2+} imaging.

Previous studies based on epifluorescence imaging and MEA recordings have shown that glutamatergic waves cease in the presence of the gap junction blocker meclofenamic acid [Veruki and Hartveit, 2009, Akrouh and Kerschensteiner, 2013]. In contrast, retinas of

connexin knockout mice have increased uncorrelated firing between waves as well as a more spatially uniform distribution of correlated firing during waves, as assayed by microelectrode array recordings [Blankenship et al., 2011]. It is interesting that the dko phenotype has increased inter-wave activity whereas MFA blocks waves entirely. This could be the result of nonspecific effects of MFA, or compensatory effects in the dko. It could also indicate that a different set of connexins besides Cx36 and Cx45 are important for waves. These findings provide evidence that gap junctions play a role in wave initiation and normal propagation.

We used two parameters to assess the spatiotemporal properties of waves that utilize the advantages afforded by two-photon Ca^{2+} imaging. 1) For both the INL and GCL, quantified the interval between spontaneous Ca^{2+} transients, and 2) the percent of cells in the imaging field that participate in waves. We first assessed wave frequency. Neurons in the INL and GCL of WT, Cx36ko and Cx36/45dko retinas exhibited correlated increases in Ca^{2+} The frequency of wave occurrence did not vary significantly across genotypes, indicating that Cx36 and Cx45 do not affect the likelihood of wave initiation. (Figure 4.2B, Kruskal-Wallis test; INL: WT, n = 18 waves; Cx36ko, n = 97 waves; Cx36/45dko, n = 19 waves; GCL: WT, n = 16 waves; Cx36ko, n = 49 waves; Cx36/45dko, n = 17 waves). Cx36ko and Cx36/45dko retina also exhibited an increase in the frequency of uncorrelated inter-wave Ca^{2+} transients in the INL and GCL layers (Figure 4.2A), consistent with previous findings [Blankenship et al., 2011].

We next compared the spatial patterns of the spontaneous firing patterns. In Cx36ko and Cx36/Cx45 dKO mice, the proportion of cells in the GCL that displayed Ca^{2+} transients during waves was higher in compared to WT (Figure 4.2C, Kruskal-Wallis test, $p < 0.05$; INL: WT, n = 9 retinas; Cx36ko, n = 21 retinas; Cx36/45dko, n = 5 retinas; GCL: WT, n = 4 retinas; Cx36ko, n = 6 retinas; Cx36/45dko, n = 4 retinas; differences found between Cx36ko and WT in GCL (Tukey-Kramer post hoc tests)), providing evidence for a gap junction role in cell recruitment during waves. These data point to gap junction facilitation of wave propagation, but not wave initiation.

AII bursting properties critical in determining frequency of retinal waves. If bursting properties in AII amacrine cells play a critical role in the generation of retinal waves, then we would expect that changing the bursting properties of AII amacrine cells would also affect retinal waves. The M-type K conductance regulates to the bursting properties of AII amacrine cells [Cembrowski et al., 2012]. The M-current interacts with the voltage-gated Na^{+} channel that underlies bursting, functioning to limit the duration of the burst. Hence blockade of the M-current increased burst duration while an M-current activator decreased burst duration [Cembrowski et al., 2012]. Interestingly, pharmacological activation of the M-current prevented the spontaneous oscillations observed in rd mice [Choi et al, not yet published] while blockade of the M-current increased the frequency of oscillations.

To determine whether the bursting properties of AII amacrine cells play a role in regulating the frequency of glutamatergic waves we monitored the effects of M-current blocker and activator on cell participation and wave frequency. By monitoring Ca^{2+} transients in GFP-exressing AII amacrine cells, we found that application of the M-channel antagonist

linopirdine (LP, 30μM) induced longer Ca^{2+} transients in AII (Figure 4.4A), consistent with previous reports of prolonged depolarization in adult mice [Cembrowski et al., 2012]. In addition , blockade of the M-current increased the frequency of waves (Figure 4.4B; Wilcoxon signed-rank test p = 0.01; wave interval: control 202.4 ± 90.6 s, N = 21 waves, 5 retinas; LP 92.7 ± 32.8 s, N = 43 waves). Blockade of the M-current did not affect the number of AII amacrine or GCL cells that participated in waves (Figure 4.4C; Students T-test p = 0.19; control 0.84 ± 0.010, LP 0.92 ± 0.071; n = 4 retinas). LP increased wave occurrence but not number of cells depolarized during waves, indicating the effect of LP more strongly affects wave initiation than propagation properties such as the pattern of cell depolarization during waves. AII Ca^{2+} transient widths, pooled across retinas, significantly increased (Figure 4.4D,F, Wilcoxon signed-rank test p < 0.001; control n = 108 transients, 6 retinas; LP n = 416 transients, 6 retinas).

Blockade of I_h disrupts spatial coherence of glutamatergic waves. Thus far we have demonstrated the gap junction coupling helps form coherent wave fronts and suppression of uncorrelated firing between waves. AII burst properties are also critical for normal frequency of waves but not for spatial coherence. We next tested whether the pacemaker conductance I_h was involved. I_h is expressed in On-cone bipolar cells but intrinsic oscillations in rd1 mice were found to be insensitive to Cs^+, an I_h blocker [Trenholm et al., 2012].

We found upon application of I_h blocker ZD7288 (50μM), AIIs and all other INL neurons exhibited increased activity (Figure 4.5A,B). Wave frequency dramatically increased (reported as median, lower quartile/upper quartile; control: 36, 20/82 sec, N = 150 wave intervals; ZD7288: 6, 3/12 sec , N = 62 wave intervals; Figure 4.5C). Cell depolarization during waves increased for cell types in both the INL and GCL, including AIIs (Figure 4.5D GCL: control 0.16 ± 0.12, ZD7288 0.68 ± 0.12; INL: control 0.38 ± 0.11, ZD7288 0.57 ± 0.065; AIIs control 0.50 ± 0.27, ZD7288 0.87 v 0.12). The proportion of cells that never displayed significant Ca^{2+} transients decreased, most notably for AIIs (Figure 4.5E; GCL: control 0.69 ± 0.24, ZD7288 0.089 ± 0.072; INL: control 0.37 ± 0.21, ZD7288 0.059 ± 0.049; AIIs control 0.36 ± 0.27, ZD7288 0 ± 0). These data suggest HCN channels maintained quiescent periods between waves, thus determining the rate at which waves initiate. Assuming I_h is required for maintaining coordinated inhibition, blockade of this coordination abolishes quiescent periods between waves, suggesting that periodicity of coordinated loss of inhibition is the determining factor in how often waves initiate.

4.4 Concluding remarks

We conclude from these findings that volume release of glutamate does not depolarize every cell in the GCL layer or start a wave. Presumably GCL cells are sparsely depolarized in response to glutamate because inhibitory amacrine cells are also depolarized by glutamate, resulting in a mixed response of inhibition and excitation to glutamate puffs. Waves may not propagate in response to a glutamate puff because the circuitry used for wave propagation

requires inhibition of inhibition, not mass excitation caused by volume release of glutamate. If so, glutamate release as assayed by previous FRET-based glutamate imaging and outside-out patches is temporally downstream of wave initiation, a readout of waves rather than a cause.

We also conclude that K^+ conductances are active in AII amacrine cells during stage III waves, and that AII amacrine cells are depolarized during waves. Voltage-clamp recordings will be required to determine the phases of depolarization within a wave, and whether AIIs receive inhibition as well as excitation. Because oscillations have been found to originate from the electrically coupled network of On cone bipolar and AII amacrine cells [Borowska et al., 2011], we looked for ways to characterize the relationship between AII amacrine activity and retinal waves. For this study to fully answer the question of whether AII amacrine cells are activated by electrical coupling with bipolar cells and subsequently propagate waves, a method of targeted AII stimulation with concurrent Ca^{2+} is needed.

Additional controls will be required to verify the ZD7288 effect is specific to I_h and not a nonspecific effect on Na^+ or Ca^{2+} currents. We used ZD7288 at the relatively low concentration of 50μM [Horwitz et al., 2010] to investigate the effects of uncoordinated signaling. However, ZD7288 has been shown in hippocampus to inhibit postsynaptic NMDARs and AMPARs [Chen, 2004] and T-type Ca^{2+} currents in a concentration-dependent manner [Sánchez-Alonso et al., 2008], at comparable concentrations to what we used in this study.

The current proposed model is as follows. Bipolar cells intrinsically oscillate and, by virtue of constructive interference, periodically depolarize AII amacrine cells. Depolarized AII amacrine cells release glycine onto Off bipolar cells, inhibiting glutamate release, allowing for mGluR-expressing On bipolar cells to be further depolarized and release glutamate. When AII amacrine cells repolarize, Off bipolar cells no longer receive inhibition and release glutamate, triggering the Off phase of the wave and hyperpolarizing On bipolar cells. The wave stops when On bipolar cells are hyperpolarized. If I_h is blocked, Off bipolar cells will not intrinsically depolarize after receiving glycinergic input from AIIs, thus leaving the system free to oscillate with no mechanism for stopping a wave.

4.5 Experimental methods

Mice.
All experiments were performed on acutely isolated mouse retinas. Male and female C57BL/6 mice obtained from Harlan were used for all wild-type recordings, and Fbxo32-eGFP mice generated by the GENSAT project [Gong et al., 2003, Siegert et al., 2009]. The mouse strain used for this research project, STOCK Tg(Fbxo32-EGFP)IM138Gsat/Mmucd, identification number 030719-UCD, was obtained from the Mutant Mouse Regional Resource Center, a NCRR-NIH funded strain repository, and was donated to the MMRRC by the NINDS funded GENSAT BAC transgenic project. All procedures were approved by the Institutional Animal Care and Use Committees of the University of California (Berkeley, CA) and conformed with guidelines of the National Institutes of Health *Guide for the Care and Use of Laboratory*

Animals, the Public Health Service Policy, and the Society for Neuroscience Policy on the Use of Animals in Neuroscience Research.

Retinal preparation.

P10-P12 C57BL/6 and Fbxo32-eGFP mice of either sex were deeply anesthetized with isoflurane and decapitated. Eyes were removed, and retinas were isolated in oxygenated artificial cerebrospinal fluid [ACSF; containing (in mM) 119.0 NaCl, 26.2 $NaHCO_3$, 11 glucose, 2.5 KCl, 1.0 K_2HPO_4, 2.5 $CaCl_2$, and 1.3 $MgCl_2$]. For Ca^{2+} and fluorescence resonance energy transfer (FRET) imaging, retinas were mounted GCL-up on filter paper (Millipore) and perfused continuously with oxygenated ACSF.

Ca^{2+} Imaging.

Retinas were loaded with Oregon green 488 BAPTA-1 AM (OGB) using the multicell bolus loading technique ([Stosiek et al., 2003, Blankenship et al., 2009]). Two-photon Ca^{2+} imaging of neurons in the INL and GCL was performed using a custom-modified two-photon microscope (Fluoview 300, Olympus America). XYZ scans were used to localize neurons in the GCL and INL. Time series images were acquired at 1 Hz using a ×60 objective (Olympus LUMPlanFl/IR ×60/0.90W) with the excitation laser tuned to 790 nm. Images were corrected for motion artifacts using the Turboreg ImageJ plugin. Ten × ten-pixel regions (12 × 12 μm) of interest were manually selected within all cells in the field of view. Fluorescence signals were averaged within these regions over time. Cell events were identified when change in fluorescence exceeded 15% of the cell's baseline fluorescence within 1 s. Cells were categorized as participating in a retinal wave if cell events correlated with neighboring cells.

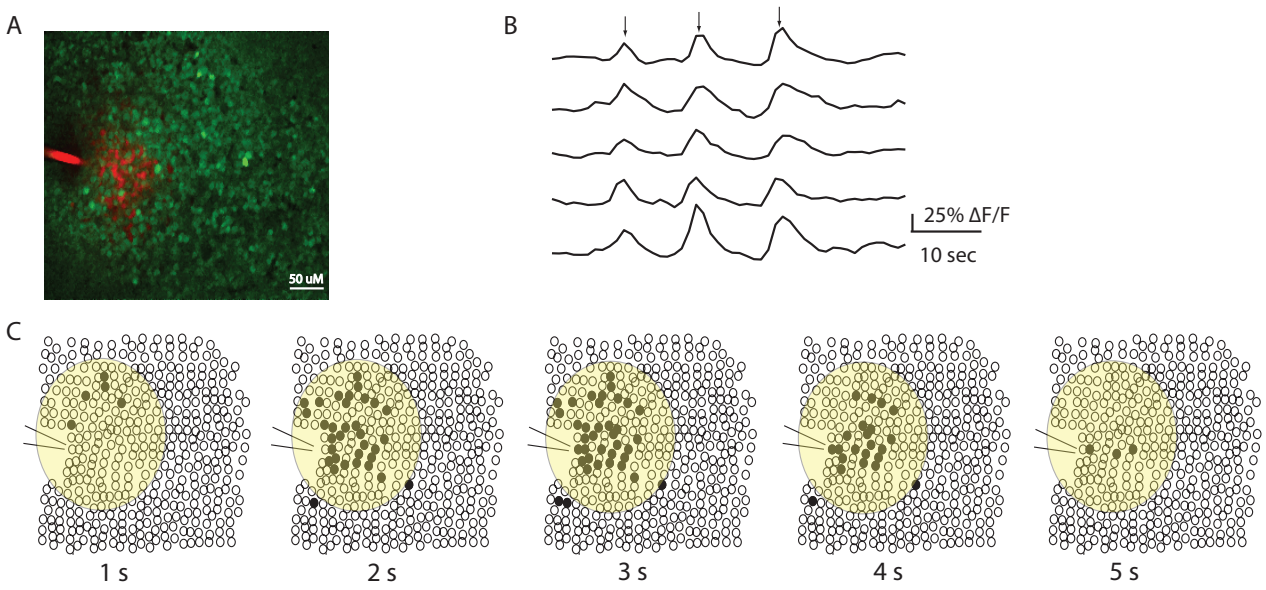

Figure 4.1: Depolarization by exogenous glutamate not sufficient for initiating waves. (A) Fluorescent image of pipette filled with 1mM glutamate and 0.1mM Alexa 594 (red) and retina loaded Oregon green-bapta (green)). Red indicates spatial extent of glutamate after a 10 ms, 5 psi puff into INL. (B) Sample traces from individual GCL cells that were depolarized directly by glutamate puffs. Arrows indicate timing of puffs. (C) Timecourse (5 sec) of GCL depolarization following glutamate puff at 1s. Open circles indicate all cells in field of view, black circles indicate cells that exhibited Ca^{2+} transients at that time point. Yellow region indicates spatial extent to which glutamate and dye spread during puff.

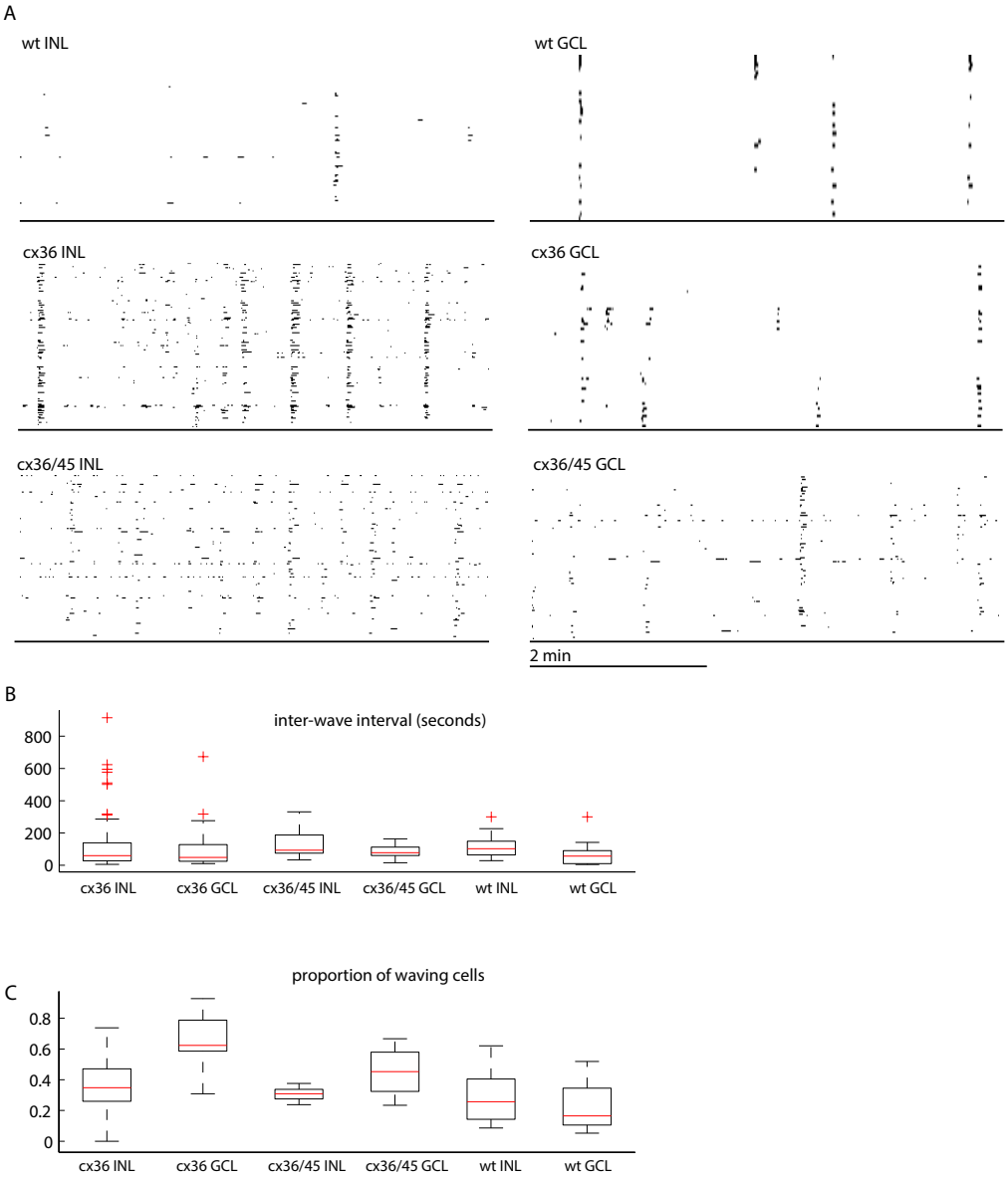

Figure 4.2: Cx36ko and Cx36/45dko exhibited disjointed firing pattern. (A) Raster plots of neuronal Ca^{2+} transients of >15% $\Delta F/F$ for all cells in the field of view, for Cx36 ko, Cx36/45 dKO, and WT. The total imaging duration was 5 min. (B) Boxplot comparisons of interwave intervals across conditions. Box boundaries indicate upper and lower quartiles, with the median plotted in red with whiskers extending to the most extreme values that are still considered not to be outliers. (C) Boxplot comparisons of proportion of cells that displayed transients of >15% $\Delta F/F$ during at least one wave. Cx36 GCL and WT GCL were found to be significantly different (Kruskal-Wallis test, $p = 0.03$).

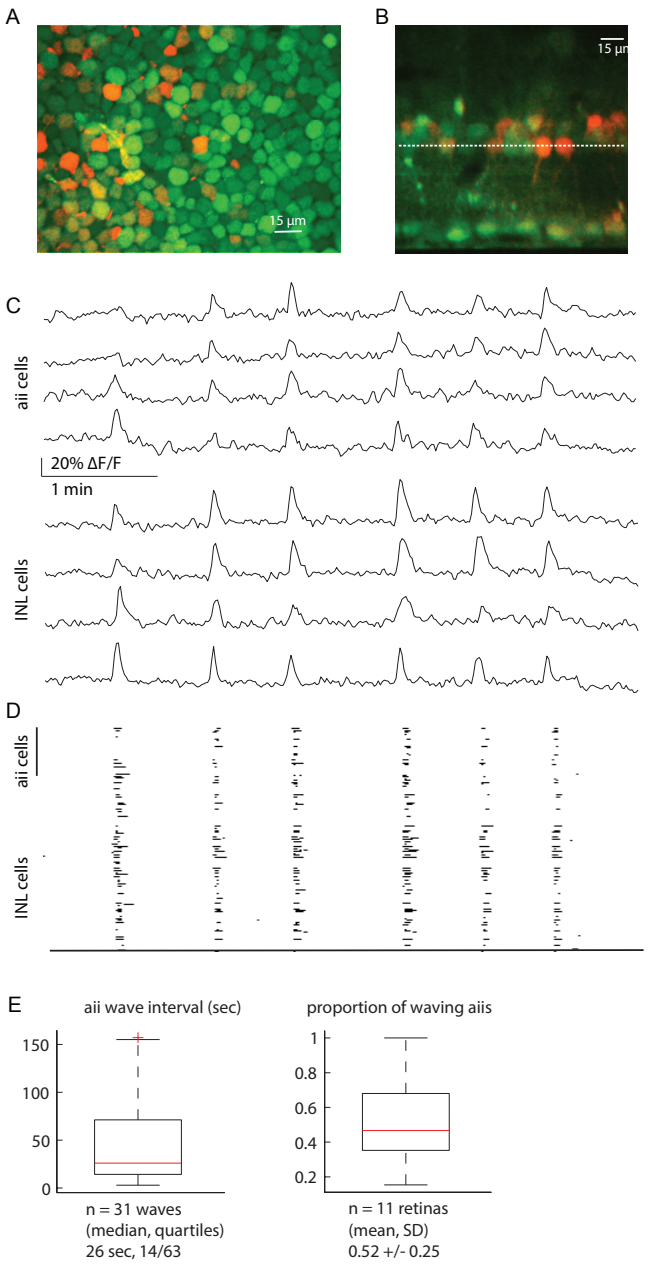

Figure 4.3: AII amacrine cells near the IPL are depolarized during waves. (A) Fluorescence image of INL loaded with OGB (green) overlaid with GFP-expressing aii amacrine cells (red). (B) Orthogonal view of fluorescence image of INL loaded with OGB (green) overlaid with GFP-expressing aii amacrine cells (red). Retina is oriented with GCL on bottom. Dashed white line indicates stratification of AIIs that exhibited Ca^{2+} transients of >15% $\Delta F/F$ during waves. (C) Sample $\Delta F/F$ traces from representative AII amacrine cells (top) and unidentified INL neurons from the same field of view (bottom). (D) Raster plots of neuronal Ca^{2+} transients for all INL cells in the field of view.

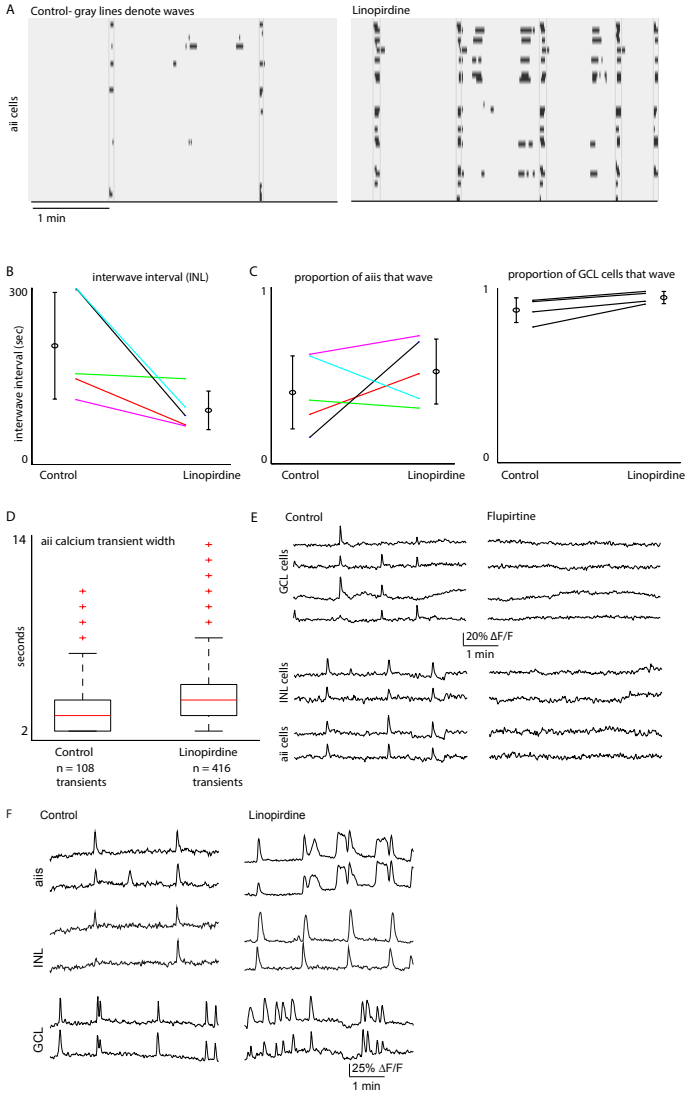

Figure 4.4: Kv7 channel antagonist linopirdine increases wave frequency and the width of Ca^{2+} transients in AII amacrine cells (A) Raster plots of neuronal Ca^{2+} transients for all AII cells in the field of view in control ACSF (right) and 30μM LP (left). The total imaging duration was 4 min. Gray lines denote waves as determined by all INL neurons including AIIs. (B) Summary of effects of LP on the average interwave interval. Lines connect values of average cell interval duration per retina in control versus LP the INL. Open circles are group means and SD. (C) Summary of effects of LP on the average proportion of cells that participated per wave. Lines connect values of average cell participation per wave for one retina in control versus LP amongst aiis (left) and GCL (right). Open circles are group means and SD. (D) Boxplot comparisons of Ca^{2+} transient of >15% $\Delta F/F$ duration in aii cells, in control vs LP conditions. Box boundaries indicate upper and lower quartiles, with the median plotted in red with whiskers extending to the most extreme values that are still considered not to be outliers. (E) Sample $\Delta F/F$ traces from representative GCL cells (top) and AII amacrines and unidentified INL neurons (bottom) in control ACSF (left) which ceased to exhibit waves after application of FL (15μM). (E) Sample $\Delta F/F$ traces from representative GCL cells (bottom) and AII amacrines (top) and unidentified INL neurons (middle) in control ACSF (left). Note increased Ca^{2+} transient length in AIIs after application of LP (30μM).

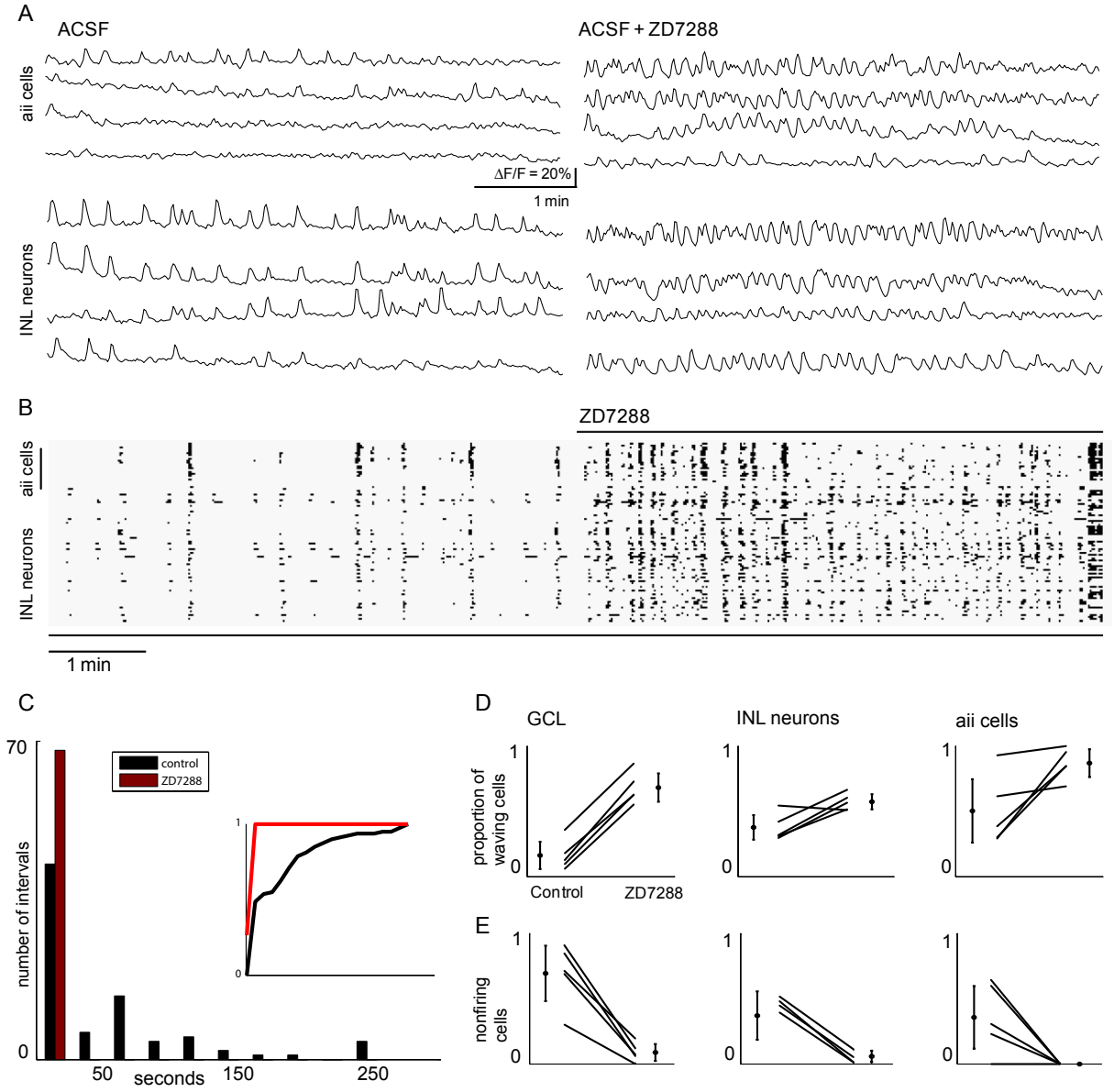

Figure 4.5: Blockade of HCN channels with ZD7288 abolishes wave structure. (A) Sample $\Delta F/F$ traces from representative AII amacrine cells (top) and unidentified INL neurons (bottom) in control ACSF (left) and in the presence of ZD7288, 50μM (right). (B) Raster plots of neuronal Ca^{2+} transients for all INL cells in the field of view in control ACSF (right) and in the presence of ZD7288 (left). The total duration of trace is 10 min. (C) Histogram of interwave intervals as assayed by Ca^{2+} imaging for control ACSF (black) and in the presence of ZD7288 (red). Inset is normalized cumulative distribution for both conditions. (control: N = 150 wave intervals and ZD7288: N = 62 wave intervals). (D) Summary of effects of ZD7288 on the average proportion of cells that participated per wave. Lines connect values of average cell participation per wave for one retina in control versus ZD7288 amongst GCL (left), non-fluroescent neurons in the INL (center) and fluorescently identified AII amacrine cells (right). Open circles are group means and SD. (E) Summary of effects of ZD7288 on the number of cells that never displayed Ca^{2+} transients of >15% $\Delta F/F$. Lines connect values of number of inactive cells per retina in control versus ZD7288 amongst GCL (left), INL neurons other than AII cells (center) and AII cells (right). Open circles are group means and SD.

Chapter 5

Copper is an endogenous modulator of neural circuit spontaneous activity

Preface: This chapter has been written in collaboration with Dr Christopher Chang. The work presented here is the dissertation author's contribution to this collaborative project.

5.1 Abstract

For reasons that remain insufficiently understood, the brain requires among the highest levels of metals in the body for normal function. The traditional paradigm for this organ and others is that fluxes of alkali and alkaline earth metals are required for signaling, but transition metals are maintained in static, tightly-bound reservoirs for metabolism and protection against oxidative stress. Here we show that copper is an endogenous modulator of spontaneous activity, a fundamental property of dynamic neural circuitry. Enabled by Copper Fluor-3 (CF3), a new fluorescent Cu^+ sensor for one- and two-photon imaging, we show that neurons and neural tissue maintain a basal pool of labile copper. Disruption of exchangeable copper stores by acute chelation or genetic knockdown of the CTR1 copper channel alters the spatiotemporal properties of spontaneous activity in developing hippocampal and retinal circuits. The data identify an essential role for copper in a key neural function and suggest broader contributions of this transition metal to cell signaling.

Copper is traditionally regarded as a static, tightly-bound cofactor in enzymes, but emerging data link dynamic, more loosely-bound forms to cell signaling. Here we use molecular imaging to identify a role for copper in the brain as a modulator of spontaneous activity of neural circuits. First, we visualized a labile copper pool in hippocampal neurons and retinal tissue with the newly developed Copper Fluor-3 indicator. We then employed calcium imaging as readout of spontaneous activity to show that disruption of exchangeable copper stores by acute chelation or genetic knockdown of the CTR1 copper channel alters the frequency and spatial propagation of calcium waves. The results establish the requirement for copper in a fundamental, dynamic property of brain circuitry.

5.2 Introduction

The foundation of cellular signal transduction relies on the rapid relay of information, mediated by intricate chemical messenger systems that operate through the dynamic spatial and temporal positioning of elements, ions, and molecules. Nowhere is this concept better illustrated than in the brain, which extensively regulates fluxes of alkali and alkaline earth metals such as sodium, potassium, and Ca^{2+} for a diverse array of signaling processes [Alberts et al., 2002]. For reasons that are insufficiently understood, the brain also accumulates among the highest levels of transition metals in body [Bush, 2000, Burdette and Lippard, 2003, Que et al., 2008], including redox-active copper, despite the fact that this high metal load, in combination with the brain's disproportionately active oxygen metabolism [Götz et al., 1994, Dickinson and Chang, 2011], also makes this organ particularly susceptible to oxidative stress [Dickinson and Chang, 2011, Barnham et al., 2004, Haas and Franz, 2009, Savelieff et al., 2013]. As such, copper has been historically regarded as a tightly-sequestered cofactor that must be buried to protect against reactive oxygen species generation and subsequent free radical damage chemistry. Indeed, elegant work continues to identify molecular players that maintain copper homeostasis in the brain [Lutsenko et al., 2010, Gaier

et al., 2013] and related organs [Kim et al., 2008, Robinson and Winge, 2010, Huffman and O'Halloran, 2001], and loss of this strict regulation is implicated in neurotoxic stress [Schlief et al., 2005, 2006, You et al., 2012] and a variety of neurodegenerative and neurodevelopmental disorders such as Menkes [Kaler, 2011, Camakaris et al., 1999] and Wilson's [Lutsenko et al., 2007] diseases, familial amyotrophic lateral sclerosis [Beckman et al., 2001, Valentine and Hart, 2003], Alzheimer's [Savelieff et al., 2013, You et al., 2012, Bush, 2008, Adlard et al., 2008, Sparks and Schreurs, 2003, Brewer, 2012, Singh et al., 2013, Hureau and Faller, 2009] and Huntington's [Fox et al., 2007, Xiao et al., 2013] diseases, and prion-mediated encephalopathies [You et al., 2012, Brown et al., 1997, Millhauser, 2004, Siggs et al., 2012].

Despite this long-held paradigm, emerging data also link copper in mobile, exchangeable forms to neurophysiology. Included are observations of 64Cu efflux from stimulated neurons [Schlief et al., 2005, Hartter and Barnea, 1988], reversible trafficking of ATP7A from the perinuclear trans-Golgi to neuronal processes by NMDA receptor activation [Schlief et al., 2005], effects of copper chelation on olfactory response to thiol odorants [Duan et al., 2012], and direct imaging of copper translocation in neurons from somatic cell bodies to peripheral processes upon depolarization [Dodani et al., 2011]. Against this backdrop, we have initiated a program aimed at exploring the potential of reactive, redox-active metals like copper in kinetically labile forms for cell signaling purposes. In this report, we identify an essential role for copper in the brain as a mediator of spontaneous activity, a fundamental property of developing neural circuits. The design and synthesis of Copper Fluor-3 (CF3), a fluorescent copper sensor based on a hydrophilic and tunable rhodol scaffold, provides a unique chemical tool for enabling the visualization of endogenous pools of labile Cu^+ in dissociated neurons and neural tissue by one- and two-photon microscopy. Disruption of exchangeable Cu^+ stores by acute application of a copper chelator or genetic knockdown of the copper ion channel CTR1 alters the spatiotemporal properties of spontaneous activity. In dissociated hippocampal cultures, these manipulations increase the correlation of spontaneous Ca^{2+} transients, whereas in retina, both cell participation and frequency of correlated Ca^{2+} transients increase. The data establish a role for copper in a key neural process and suggest broader contributions for this redox-active metal in cell signaling.

5.3 Results & Discussion

Molecular imaging with CF3 reveals basal pools of exchangeable copper in dissociated hippocampal neurons and isolated retinal tissue.

The enhanced sensitivity and hydrophilicity of CF3 enables the study of exchangeable Cu^+ stores in neuronal circuits formed from dissociated hippocampal cultures and retinal tissue models using molecular imaging in one and two-photon mode (Figure 5.5 and Figure 5.1). For example, dissociated hippocampal neurons (DIV 10-13) loaded with CF3 for 20 min followed by washing on a perfusion system and imaging with two-photon confocal microscopy show a diffuse intracellular fluorescent signal (Figure 5.1a). Acute bath application of the cell-impermeable copper chelator bathocuproine disulfonate (BCS) to the same field of neu-

rons shows a patent decrease in intracellular fluorescence intensity. The data indicate that CF3 is capable of detecting basal, endogenous pools of labile copper in neurons and their depletion by on-stage pharmacological treatments within minutes of chelation (Figure 5.1d). Notably, we performed the same experiment with the Ctrl-CF3 dye, which possesses an identical fluorophore but lacks the copper-responsive binding element, and find that there is no change in the fluorescence intensity of Ctrl-CF3, as it does not respond to changes in copper (Figure 5.1b). This control experiment confirms that the observed BCS-induced decreases in CF3 fluorescence are not due to photobleaching and/or dye leakage effects.

Next, isolated retinal tissues from mice (P10-P13) were loaded with CF3 and the fluorescence intensity was imaged from the ganglion cell layer (GCL) in two-photon mode (Figure 5.1c). It is important to note that structurally, the retina is a stratified tissue consisting of photoreceptors, horizontal cells, bipolar cells, amacrine cells, Müller glia, and ganglion cells. CF3 stains the intracellular space of the GCL, and is able to detect a decrease in the labile Cu^+ pool upon perfusion with BCS (Figure 5.1c). Similarly, we find that loading retina with Ctrl-CF3 followed by extracellular copper chelation does not result in a change in fluorescence, indicating that CF3 can be used in a two-photon mode to report on endogenous stores of exchangeable Cu^+ (Figure 5.1d). Taken together, the data show that CF3 enables identification of labile copper stores at basal, endogenous levels in both dissociated neuronal cultures and in brain tissue, and that acute interception using the membrane-impermeable copper chelator BCS alters a kinetically accessible extracellular labile pool, which subsequently depletes the intracellular labile copper pool. As such, we reasoned that dynamic disruptions in these extracellular/intracellular labile copper stores may also result in alterations to spontaneous activity in neural networks.

Modulation of spontaneous activity with acute copper chelation in dissociated hippocampal neurons.

With data in hand showing that labile copper pools at basal levels can be visualized using CF3, we sought to study the contributions of these endogenous, exchangeable copper stores to fundamental properties of neural circuits. As a starting point, we examined the effects of BCS treatment on spontaneous activity of a network of dissociated hippocampal neurons with one-photon Ca^{2+} imaging. Cultures of embryonic neurons (DIV 12-15) were incubated with the Ca2+ indicator Oregon Green BAPTA-1 AM (OGB). These dissociated hippocampal cultures, which consist of neurons and glia, exhibit temporally uncorrelated Ca^{2+} transients (Figure 5.2a). To compare quantitatively the correlated events, we computed cross-correlations based upon the percentage of imaged cells that exhibited spontaneous Ca^{2+} transients surrounding the peak event (see Methods). In control conditions, a lower percentage of cells exhibited correlated Ca^{2+} transients (Figure 5.2b). These data are consistent with the model that disrupting extracellular/intracellular copper pools increases the excitability of the network, leading to an increase in correlated activity [Hennig et al., 2009, Mazzoni et al., 2007], and that acute, reversible modulation of endogenous labile copper pools is sufficient to alter spontaneous activity.

Pharmacological manipulation of endogenous labile copper pools alters spontaneous activity in the developing retina.

The data from dissociated hippocampal cultures prompted us to probe the contributions of copper to spontaneous activity with more native circuit connections. In this context, the developing retina is a canonical model for spontaneous activity during development [Huberman et al., 2008, Blankenship and Feller, 2010]. During postnatal development, before the maturation of the light responses, the retina exhibits spontaneous correlated activity termed retinal waves. To investigate the effects of copper chelation on retinal waves, we used two-photon Ca^{2+} imaging to record from the neurons in the ganglion cell layer (GCL). Importantly, the ganglion cell layer had a pool of exchangeable copper that was altered by acute BCS treatment as determined by imaging CF3 (Figure 5.1). Retinas were acutely isolated from P10-P13 mice and bolus loaded with OGB as previously described [Firl et al., 2013]. Spontaneous Ca^{2+} transients propagate across the GCL in a correlated fashion (Figure 5.3a,b). Acute bath application of 200 μM BCS increases the frequency of waves; the median inter-event interval decreases for BCS treated retina (median, upper/lower quartile; control: 100 sec, 60/130, n = 17 intervals; BCS: 29 sec, 17/58 sec, n = 51 intervals; wash waveinterval: 60 sec, 17/58, n = 6 intervals) (Figure 5.3c,d). In addition, BCS increases the percentage of GCL neurons that depolarize during correlated activity and this effect is reversible upon BCS wash out (median, upper/lower quartile; control: 26%, 8.9/34; BCS: 75%, 56/78; wash: 12%, 1/20, n = 9 retinas; Kruskal-Wallis test, $p < 0.001$) (Figure 5.2e). The collective data suggest that, as was observed in the hippocampal cultures, the disruption of endogenous pools of labile copper by addition of BCS increases excitability of retinal circuits, suggesting a strategic role for copper in regulating spontaneous activity.

Spontaneous activity is altered in CTR1$^{+/-}$ retinal tissue.
Finally, to probe the effects of genetic, long-term disruption of endogenous copper in the developing retina as well as provide a molecular target for dynamic regulation of copper cycling, we turned our attention to studies of retina in the heterozygous mouse model of the CTR1 copper ion channel (CTR1$^{+/-}$), which has approximately 50% less copper in the nervous system compared to wildtype CTR1$^{+/-}$ mice; we note that the homozygous CTR1$^{-/-}$ mice are embryonic lethal and cannot be used for such studies [Lee et al., 2001]. As expected, a patent reduction in CTR1 expression in CTR1$^{+/-}$ mice retina was confirmed by Western blot (Figure 5.4f). Retinas from P11 CTR1$^{+/-}$ mice exhibit spontaneous Ca^{2+} transients as observed in WT mice (Figure 5.4a,b). However, we find that similar to BCS-treated WT retina, waves in CTR1$^{+/-}$ retina were more frequent than littermate controls (median interevent interval upper/lower quartile; WT: 95 sec, 76/149, n = 33 intervals; CTR1$^{+/-}$-: 22 sec, 14/32, n = 129 intervals; Wilcoxon signed-rank test, $p < 0.001$) and the percentage of depolarized cells increased (median, upper/lower quartile; control WT: 27%, 16/51, n = 18 retinas; CTR1$^{+/-}$: 67%, 17/68, n = 16 retinas; Wilcoxon signed-rank test, $p < 0.001$) (Figure 5.4d,e). Taken together, the data establish that disruptions of endogenous copper pools by genetic knockdown of the copper ion channel CTR1 or acute chelation with BCS increase network excitability in both hippocampal culture and intact retina. The observed changes to spontaneous neuronal activity in both systems suggest a general role for copper in modulating spontaneous activity in developing neural circuits and identify CTR1 as a molecular target for mediating this effect through maintenance of extracellular and intracellular

copper pools.

5.4 Concluding remarks

The utilization of metals for dynamic signaling purposes in the brain and other biological systems has largely focused on mobile fluxes of redox-inactive alkali and alkaline earth metals such as sodium, potassium, and Ca^{2+}, whereas redox-active metal transition metals have been viewed primarily as static metabolic cofactors. In this work we show that copper is an endogenous and dynamic mediator of neural circuits through spontaneous activity. The development of CF3, a unique fluorescent copper sensor with improved hydrophilicity, high selectivity and sensitivity to labile Cu^{+}, and ability to be used in one- or two-photon microscopy modes, along with a critical Ctrl-CF3 control dye that lacks a copper-responsive receptor, enables the direct identification of exchangeable copper pools in dissociated neuronal cultures as well as neural tissue that can be modulated by acute addition of a membrane-impermeable copper chelator. Two-photon Ca^{2+} imaging experiments have been employed to establish a fundamental new role for copper as physiological regulator of spontaneous activity. Specifically, we show that acute copper chelation in a dose-dependent manner in dissociated hippocampal culture and intact developing retina increases the cell participation and frequency of Ca^{2+} transients during spontaneous activity, and that this effect is reversible. Moreover, modulation of cellular copper status through genetic knockdown of the copper ion channel CTR1 leads to a similar increase in synchronization of Ca^{2+} transients, indicating it is involved in dynamic regulation of copper signaling.

Our results suggest that endogenous pools of copper that can be modulated in extracellular and/or intracellular spaces are used to regulate levels of spontaneous activity during neural circuit development through CTR1, which could include regulation of intracellular/extracellular copper concentrations, cell surface copper recycling, and/or loading of copper onto extracellular membrane receptors involved in Ca^{2+} uptake. Indeed, previous experiments suggest that copper influences synaptic transmission by modulation of a variety of targets, including NMDA receptors,16,17 $GABA_A$ receptors [Peters et al., 2011], and voltage-gated Ca^{2+} channels [Shcheglovitov et al., 2012, Gaier et al., 2013]. Additionally, a growing number of studies have established the importance of spontaneous activity in normal development of synapses and circuits [Moody and Bosma, 2005, Colonnese and Khazipov, 2010, Moore et al., 2011]. By identifying a role for endogenous copper in regulating spontaneous activity, a fundamental process in maintaining neural circuits in the brain, our work suggests that alterations in brain copper homeostasis in genetic disorders like Menkes and Wilson's diseases, as well as more complex neurodegenerative diseases such as Alzheimer's and Huntington's diseases and prion encephalopathies that are linked to copper mismanagement, can contribute to misregulation of cell-cell communication. Finally, these findings highlight the utility of CF3 and related molecular imaging probes to uncover unique and unexplored metal biology in living systems.and support a broader view for transition metals in cell signaling.

5.5 Experimental methods

Retinal preparation
P10-P12 C57BL/6 mice of either sex were deeply anesthetized with isoflurane and decapitated. Eyes were removed, and retinas were isolated in oxygenated artificial cerebrospinal fluid [ACSF; containing (in mM) 119.0 NaCl, 26.2 $NaHCO_3$, 11 glucose, 2.5 KCl, 1.0 K_2HPO_4, 2.5 $CaCl_2$, and 1.3 $MgCl_2$]. For Ca^{2+} and fluorescence resonance energy transfer (FRET) imaging, retinas were mounted GCL-up on filter paper (Millipore) and perfused continuously with oxygenated ACSF.

Imaging of dissociated hippocampal neuron cultures
For copper imaging, DIV 10-13 cultured hippocampal neurons were washed with HBSS, incubated with 2 μM CF3 or Ctrl-CF3 in HBSS for 20 min at 37 C, 5% CO2, and placed in fresh HBSS perfusion, or HBSS with 200 μM bathocuproine disulfonate disodium salt (BCS, Sigma). Images were taken on a custom-modified two-photon microscope (Fluoview 300, Olympus America) using a 60X objective (Olympus LUMPlanFl/IR ×60/0.90W) with excitation laser tuned to 900 nm. For confocal imaging, an Argon laser was used for excitation. In both cases emission was collected at wavelengths longer than 515 nm. ImageJ was used to threshold all images at a common pixel value for comparison between control and chelated conditions. To quantify comparison, the image was subdivided into multiple pixel regions, which were then averaged over for pairwise comparison between conditions.

For Ca^{2+} imaging, DIV 12-15 cultured hippocampal neurons were incubated with 5 μM Ca^{2+}-sensitive dye, Oregon Green BAPTA-1 AM (OGB) (Life Technologies) in HEPES buffered saline (HBS; in mM: 5 glucose, 120 NaCl, 10 HEPES, 2 $CaCl_2$, 2.5 KCl, 2 $MgCl_2$) for 30 min, washed with HBSS for 10 min. Images were acquired on a Leica confocal imaging system (CS SP) equipped with an argon gas ion laser and a Leica inverted microscope (DM IRBE) fitted with a Leica 63x objective (HCX PL Apo; NA, 1.32). OGB was excited at 488 nm, and the fluorescence signal was collected at 500-540 nm. Images were acquired every 1.45 s at 512 × 512 pixels. BCS was bath applied. Images were corrected for motion artifacts using the Turboreg ImageJ plugin. 5×5 pixel regions of interest were manually selected within all cells in the field of view using custom MATLAB scripts. Fluorescence signals were averaged within these regions over time. We quantified the correlation structure of spontaneous Ca^{2+} transients using the following approach. First, we identified cell events as the time points when the change in fluorescence exceeded 10% of the baseline fluorescence ($\Delta F/F > 10\%$). Second, we identified network events as the time points where more then 10% of cells exhibited events. Last we computed the fraction of cells that also exhibited above threshold transients in 1 second bins for a total duration of ±5 seconds (Figure 5.2b).

Retinal imaging
For two photon imaging of copper levels, retinas were bolus loaded either CF3 or a Ctrl-CF3, with excitation wavelength of 910 nm and emission was collected below 515 nm. For two-photon imaging of intracellular Ca^{2+} concentration, retinas were loaded with Oregon Green 488 BAPTA-1 AM using the multicell bolus loading technique [Stosiek et al., 2003]. Two-photon Ca^{2+} imaging of neurons in the GCL was performed using a custom-modified

two-photon microscope (Fluoview 300, Olympus America Inc.). XYZ scans were used to localize neurons in the GCL. Time series images were acquired at 1 Hz using a 60× objective (Olympus LUMPlanFI/IR 60×/0.90W) with the excitation laser tuned to 790 nm. aCSF containing 200 μM BCS or 15μM ATN-224 was bath applied on stage.

Images were corrected for motion artifacts using the Turboreg ImageJ plugin. 10x10 pixel regions of interest were manually selected within all cells in the field of view using custom MATLAB scripts. Fluorescence signals were averaged within these regions over time. Cell events were identified when the change in fluorescence exceeded 15% of the cells baseline fluorescence within 1 second. Cells were categorized as participating in a retinal wave if cell events correlated with neighboring cells.

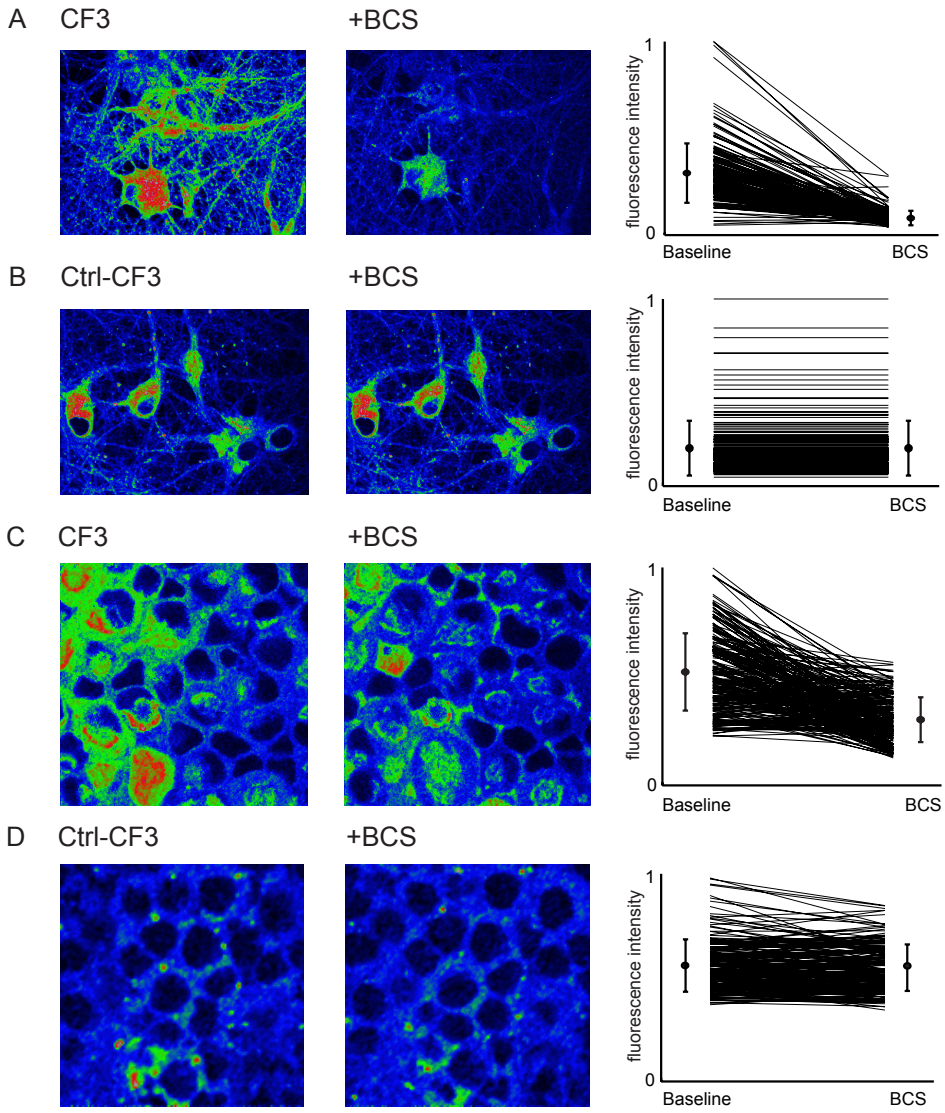

Figure 5.1: Live-cell molecular imaging with CF3 in dissociated hippocampal neurons and retinal tissue shows that acute BCS treatment alters intracellular labile Cu^{+} in two-photon mode. (A) Representative images are shown of hippocampal neurons were stained with 2 μM CF3 (CF3: baseline normalized mean = 0.32, sd = 0.15; after BCS: mean = 0.088, sd = 0.038; n = 192 15 μm squares) or (B) Ctrl-CF3 for 20 min with subsequent recording of baseline fluorescence followed by 30 min BCS perfusion (Ctrl-CF3: baseline normalized mean = 0.20, sd = 0.15; after BCS: mean = 0.20, sd = 0.15; n = 192 15 μm squares). Net changes in fluorescence brightness are quantified on the right with paired lines representing nonoverlapping 15 μM square regions of the field of view. Representative images of retinal neurons bolus loaded with (C) CF3 (CF3: baseline normalized mean = 0.49, sd = 0.16; after BCS: mean = 0.26, sd = 0.10; n = 256 15 μm squares) or (D) Ctrl-CF3 followed by 30 min BCS perfusion (Ctrl-CF3: baseline normalized mean = 0.57, sd = 0.13; after BCS: mean = 0.56, sd = 0.11; n = 256 15 μm squares). Net changes in fluorescence brightness are quantified on the right, with paired lines representing nonoverlapping 15 μm square regions of the field of view.

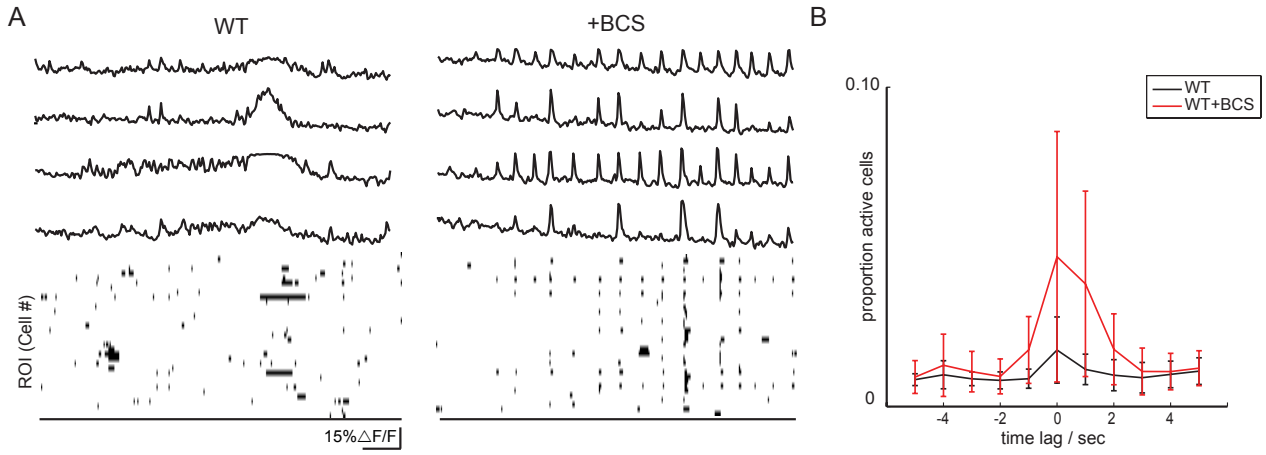

Figure 5.2: Copper chelation with BCS increases the correlated Ca^{2+} transients in dissociated hippocampal culture. (A) Sample $\Delta F/F$ traces from averaged regions from four different cells stained with Oregon Green BAPTA-1 AM (OGB). Each trace row corresponds to the same in cell in control solution first (left) followed by chelation with 200 μM BCS (right). Binary plots (bottom) show entire network activity, where a black point corresponds to a cell with a Ca^{2+} transient above threshold. (B) Mean and SD across cells of cross-correlation during times of high-synchronized firing (n = 3 cultures). When a time point was identified as having more than 10% of cells above threshold, the proportion of cells that were above threshold was calculated for 5 sec before and after. A flat line indicates uniform, random transients. Red corresponds to condition with acute 200 μM BCS wash-in.

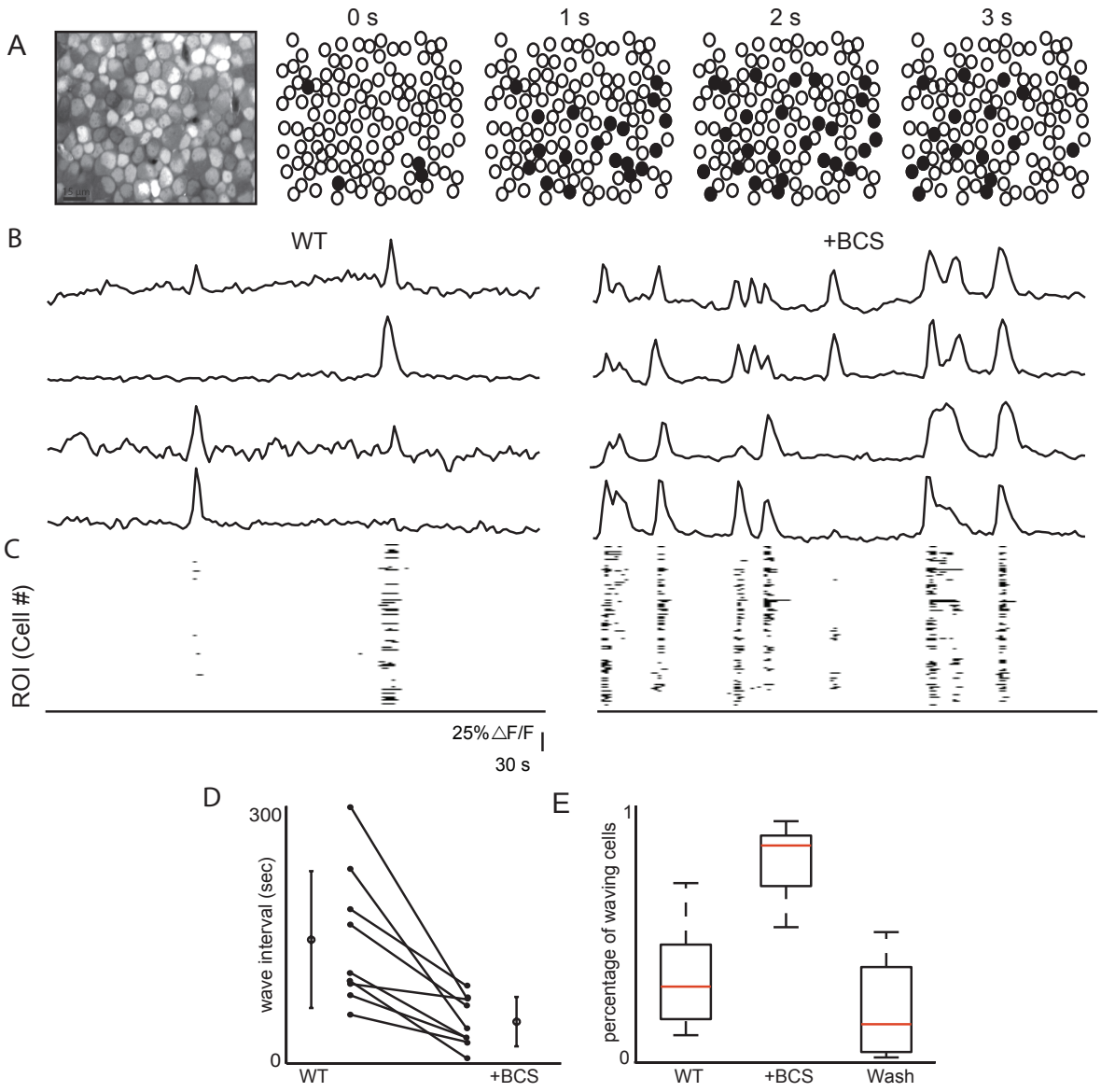

Figure 5.3: Copper chelation increases wave frequency and cell participation levels of correlated spontaneous activity in the developing retina. (A) Example of wave propagation in the ganglion cell layer (GCL) observed with two-photon Ca^{2+} imaging at a frame rat of 1 Hz. Leftmost image is in the retinal sample loaded with OGB. Circles are identified cells where black indicates cells with above-threshold $\Delta F/F$ in that frame. (B) Sample $\Delta F/F$ traces from averaged regions within four different cells. Each trace row corresponds to the same cell in control solution first (left) followed by chelation with 200 μM BCS (right). (C) Binary plots of neuronal Ca^{2+} transients exceeding threshold for all cells in the field of view. (D) Summary of effects of BCS on interevent interval where lines connect values of average wave interval for one retina in control versus chelation with BCS. Open circles are group means and SD. (E) Summary of effects of BCS on proportion of cells that are active during waves (n = 9 retinas, p¡0.001, Kruskal-Wallis test). Box boundaries indicate upper and lower quartiles, with the median plotted in red with whiskers extending to the most extreme values that are still considered not to be outliers.

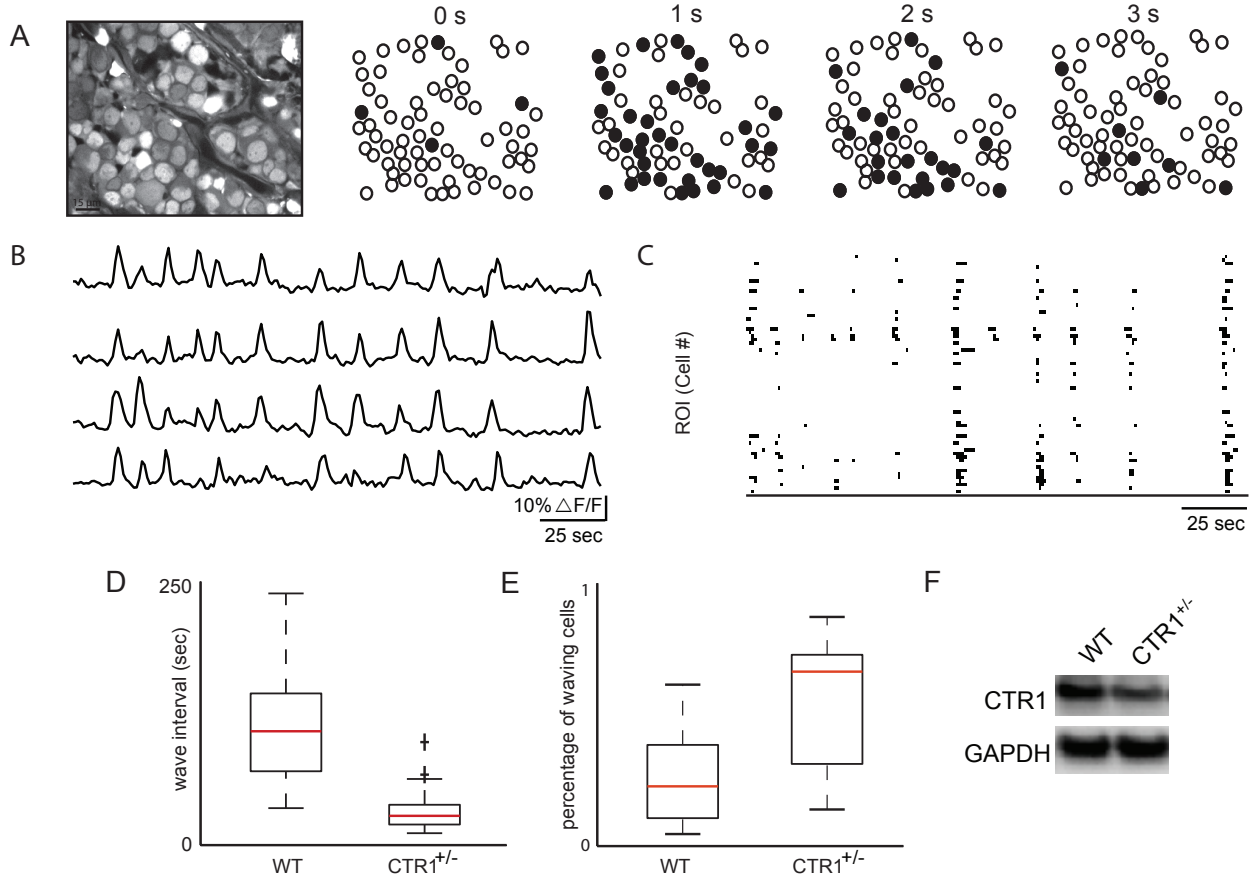

Figure 5.4: Partial knockdown of CTR1 in the retina increases wave frequency and cell participation of correlated spontaneous activity in the developing retina. (A) Example of wave propagation in the ganglion cell layer (GCL) observed with two-photon Ca^{2+} imaging at a frame rate of 1 Hz. Leftmost image is in the retinal sample loaded with OGB. Circles are identified cells where black indicates cells with $\Delta F/F$ greater than 15% in that frame. (B) Sample $\Delta F/F$ traces from averaged regions within four different cells. Each trace row represents a different cell. (C) Binary plots of neuronal Ca^{2+} transients greater than 15% $\Delta F/F$ for all cells in the field of view. (D) Summary of differences between WT and $CTR1^{+/-}$ retina on interevent interval (WT: n = 33 waves; $CTR1^{+/-}$: n = 129 waves). (E) Summary of differences between WT and $CTR1^{+/-}$ retina on proportion of cells that are active during waves (WT: n = 18 retinas; $CTR1^{+/-}$: n = 16 retinas). Box boundaries indicate upper and lower quartiles, with the median plotted in red with whiskers extending to the most extreme values that are still considered not to be outliers. (F) Representative western blot of CTR1 expression in WT and $CTR1^{+/-}$ developing retina. GAPDH was used as a loading control.

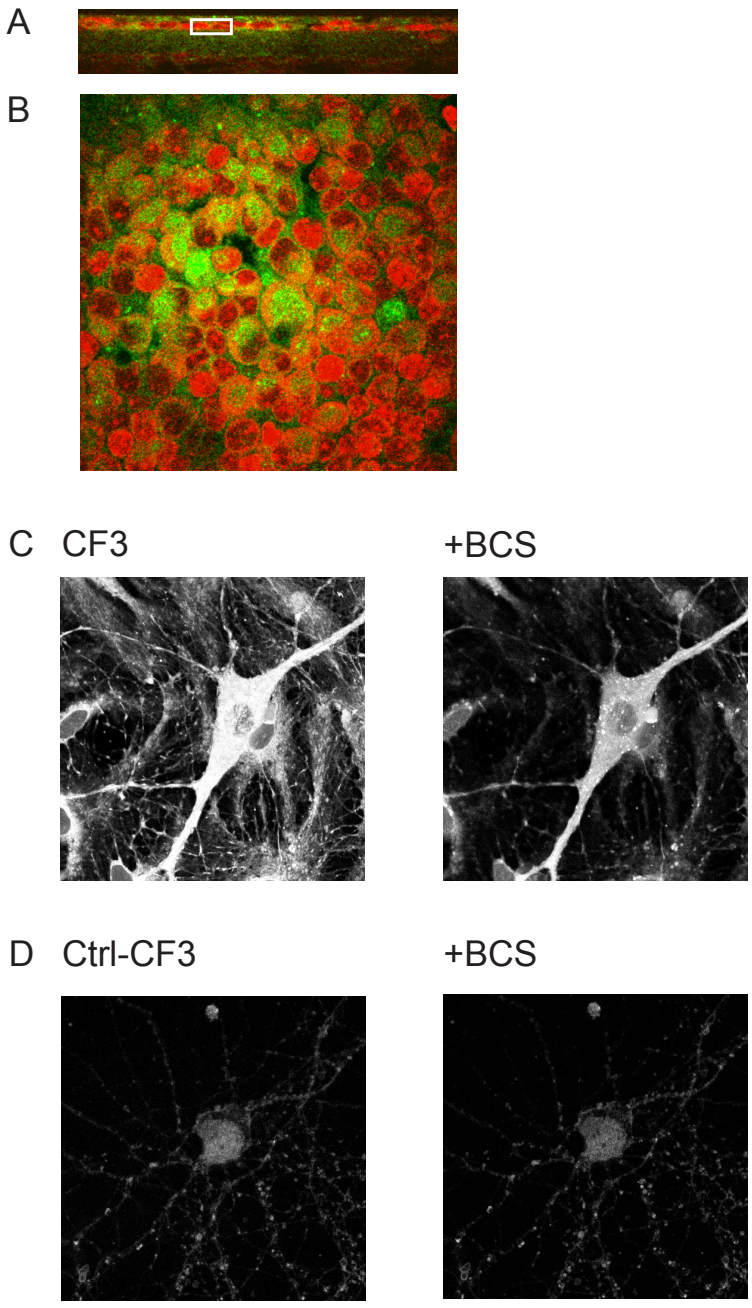

Figure 5.5: Partial knockdown of CTR1 in the retina increases wave frequency and cell participation of correlated spontaneous activity in the developing retina. (A) CF3 co-loaded with nucleic acid dye Syto-17, orthogonal projection of two-photon Z-stacks shows dye penetration through to the inner nuclear layer. White box indicates depth at which *(B)* was imaged. (B) CF3 co-loaded with nucleic acid dye Syto-17 (0.4 μM), ganglion cell layer, showing that CF3 is present in the cytosol as well as in the extracellular space. (C) Live-cell molecular imaging with CF3 in dissociated hippocampal neurons shows that acute BCS treatment alters intracellular labile Cu^{+} in one-photon mode. Representative images are shown of hippocampal neurons were loaded with 2 μM CF3 or (D) Ctrl-CF3 for 20 min with subsequent recording of baseline fluorescence followed by 30 min BCS perfusion (n = 3 cultures).

Bibliography

James B Ackman, Timothy J Burbridge, and Michael C Crair. Retinal waves coordinate patterned activity throughout the developing visual system. *Nature*, 490(7419):219–225, October 2012. ISSN 1476-4687. doi: 10.1038/nature11529. PMID: 23060192 PMCID: PMC3962269.

Paul A Adlard, Robert A Cherny, David I Finkelstein, Elisabeth Gautier, Elysia Robb, Mikhalina Cortes, Irene Volitakis, Xiang Liu, Jeffrey P Smith, Keyla Perez, Katrina Laughton, Qiao-Xin Li, Susan A Charman, Joseph A Nicolazzo, Simon Wilkins, Karolina Deleva, Toni Lynch, Gaik Kok, Craig W Ritchie, Rudolph E Tanzi, Roberto Cappai, Colin L Masters, Kevin J Barnham, and Ashley I Bush. Rapid restoration of cognition in alzheimer's transgenic mice with 8-hydroxy quinoline analogs is associated with decreased interstitial abeta. *Neuron*, 59(1):43–55, July 2008. ISSN 1097-4199. doi: 10.1016/j.neuron.2008.06.018. PMID: 18614028.

Alejandro Akrouh and Daniel Kerschensteiner. Intersecting circuits generate precisely patterned retinal waves. *Neuron*, 79(2):322–334, July 2013. ISSN 1097-4199. doi: 10.1016/j.neuron.2013.05.012. PMID: 23830830 PMCID: PMC3737599.

Bruce Alberts, Alexander Johnson, Julian Lewis, Martin Raff, Keith Roberts, and Peter Walter. Molecular biology of the cell, 2002. URL `http://www.ncbi.nlm.nih.gov/books/NBK21054/`.

Camille Allne, Adriano Cattani, James B Ackman, Paolo Bonifazi, Laurent Aniksztejn, Yehezkel Ben-Ari, and Rosa Cossart. Sequential generation of two distinct synapse-driven network patterns in developing neocortex. *J. Neurosci.*, 28(48):12851–12863, November 2008. ISSN 1529-2401. doi: 10.1523/JNEUROSCI.3733-08.2008. PMID: 19036979.

Itaru Arai, Masashi Tanaka, and Masao Tachibana. Active roles of electrically coupled bipolar cell network in the adult retina. *J. Neurosci.*, 30(27):9260–9270, July 2010. ISSN 1529-2401. doi: 10.1523/JNEUROSCI.1590-10.2010. PMID: 20610761.

G B Awatramani and M M Slaughter. Intensity-dependent, rapid activation of presynaptic metabotropic glutamate receptors at a central synapse. *J. Neurosci.*, 21(2):741–749, January 2001. ISSN 1529-2401. PMID: 11160453.

A Bansal, J H Singer, B J Hwang, W Xu, A Beaudet, and M B Feller. Mice lacking specific nicotinic acetylcholine receptor subunits exhibit dramatically altered spontaneous activity patterns and reveal a limited role for retinal waves in forming ON and OFF circuits in the inner retina. *J. Neurosci.*, 20(20):7672–7681, October 2000. ISSN 1529-2401. PMID: 11027228.

Kevin J Barnham, Colin L Masters, and Ashley I Bush. Neurodegenerative diseases and oxidative stress. *Nat Rev Drug Discov*, 3(3):205–214, March 2004. ISSN 1474-1776. doi: 10.1038/nrd1330. PMID: 15031734.

J S Beckman, A G Estvez, J P Crow, and L Barbeito. Superoxide dismutase and the death of motoneurons in ALS. *Trends Neurosci.*, 24(11 Suppl):S15–20, November 2001. ISSN 0166-2236. PMID: 11881740.

N Belluardo, G Mud, A Trovato-Salinaro, S Le Gurun, A Charollais, V Serre-Beinier, G Amato, J A Haefliger, P Meda, and D F Condorelli. Expression of connexin36 in the adult and developing rat brain. *Brain Res.*, 865(1):121–138, May 2000. ISSN 0006-8993. PMID: 10814742.

Aaron G Blankenship and Marla B Feller. Mechanisms underlying spontaneous patterned activity in developing neural circuits. *Nat. Rev. Neurosci.*, 11(1):18–29, January 2010. ISSN 1471-0048. doi: 10.1038/nrn2759. PMID: 19953103 PMCID: PMC2902252.

Aaron G Blankenship, Kevin J Ford, Juliette Johnson, Rebecca P Seal, Robert H Edwards, David R Copenhagen, and Marla B Feller. Synaptic and extrasynaptic factors governing glutamatergic retinal waves. *Neuron*, 62(2):230–241, April 2009. ISSN 1097-4199. doi: 10.1016/j.neuron.2009.03.015. PMID: 19409268 PMCID: PMC2807181.

Aaron G. Blankenship, Aaron M. Hamby, Alana Firl, Shri Vyas, Stephan Maxeiner, Klaus Willecke, and Marla B. Feller. The role of neuronal connexins 36 and 45 in shaping spontaneous firing patterns in the developing retina. *J Neurosci*, 31(27):9998–10008, July 2011. ISSN 0270-6474. doi: 10.1523/JNEUROSCI.5640-10.2011. URL `http://www.ncbi.nlm.nih.gov/pmc/articles/PMC3142875/`. PMID: 21734291 PMCID: PMC3142875.

Stewart A Bloomfield and Bela Völgyi. The diverse functional roles and regulation of neuronal gap junctions in the retina. *Nat. Rev. Neurosci.*, 10(7):495–506, July 2009. ISSN 1471-0048. doi: 10.1038/nrn2636. PMID: 19491906 PMCID: PMC3381350.

P Bonifazi, M Goldin, M A Picardo, I Jorquera, A Cattani, G Bianconi, A Represa, Y Ben-Ari, and R Cossart. GABAergic hub neurons orchestrate synchrony in developing hippocampal networks. *Science*, 326(5958):1419–1424, December 2009. ISSN 1095-9203. doi: 10.1126/science.1175509. PMID: 19965761.

Joanna Borowska, Stuart Trenholm, and Gautam B Awatramani. An intrinsic neural oscillator in the degenerating mouse retina. *J. Neurosci.*, 31(13):5000–5012, March 2011. ISSN 1529-2401. doi: 10.1523/JNEUROSCI.5800-10.2011. PMID: 21451038.

George J Brewer. Copper excess, zinc deficiency, and cognition loss in alzheimer's disease. *Biofactors*, 38(2):107–113, April 2012. ISSN 1872-8081. doi: 10.1002/biof.1005. PMID: 22438177.

Kevin L. Briggman and Thomas Euler. Bulk electroporation and population calcium imaging in the adult mammalian retina. *Journal of Neurophysiology*, 105(5):2601–2609, May 2011. ISSN 0022-3077, 1522-1598. doi: 10.1152/jn.00722.2010. URL `http://jn.physiology.org/content/105/5/2601`.

D R Brown, K Qin, J W Herms, A Madlung, J Manson, R Strome, P E Fraser, T Kruck, A von Bohlen, W Schulz-Schaeffer, A Giese, D Westaway, and H Kretzschmar. The cellular prion protein binds copper in vivo. *Nature*, 390(6661):684–687, December 1997. ISSN 0028-0836. doi: 10.1038/37783. PMID: 9414160.

Ed Bullmore and Olaf Sporns. Complex brain networks: graph theoretical analysis of structural and functional systems. *Nat. Rev. Neurosci.*, 10(3):186–198, March 2009. ISSN 1471-0048. doi: 10.1038/nrn2575. PMID: 19190637.

Shawn C. Burdette and Stephen J. Lippard. Meeting of the minds: Metalloneurochemistry. *PNAS*, 100(7):3605–3610, April 2003. ISSN 0027-8424, 1091-6490. doi: 10.1073/pnas.0637711100. URL `http://www.pnas.org/content/100/7/3605`. PMID: 12655069.

A I Bush. Metals and neuroscience. *Curr Opin Chem Biol*, 4(2):184–191, April 2000. ISSN 1367-5931. PMID: 10742195.

Ashley I Bush. Drug development based on the metals hypothesis of alzheimer's disease. *J. Alzheimers Dis.*, 15(2):223–240, October 2008. ISSN 1387-2877. PMID: 18953111.

D A Butts, M B Feller, C J Shatz, and D S Rokhsar. Retinal waves are governed by collective network properties. *J. Neurosci.*, 19(9):3580–3593, May 1999. ISSN 0270-6474. PMID: 10212317.

J. Camakaris, I. Voskoboinik, and J. F. Mercer. Molecular mechanisms of copper homeostasis. *Biochemical and Biophysical Research Communications*, 261(2): 225–232, August 1999. ISSN 0006-291X. doi: 10.1006/bbrc.1999.1073. URL `http://www.sciencedirect.com/science/article/pii/S0006291X99910732`.

M Catsicas, V Bonness, D Becker, and P Mobbs. Spontaneous ca2+ transients and their transmission in the developing chick retina. *Curr. Biol.*, 8(5):283–286, February 1998. ISSN 0960-9822. PMID: 9501073.

Mark S. Cembrowski, Stephen M. Logan, Miao Tian, Li Jia, Wei Li, William L. Kath, Hermann Riecke, and Joshua H. Singer. The mechanisms of repetitive spike generation in an axonless retinal interneuron. *Cell Rep*, 1(2):155–166, February 2012. ISSN 2211-1247. doi: 10.1016/j.celrep.2011.12.006. URL `http://www.ncbi.nlm.nih.gov/pmc/articles/PMC3406326/`. PMID: 22832164 PMCID: PMC3406326.

Chu Chen. ZD7288 inhibits postsynaptic glutamate receptor-mediated responses at hippocampal perforant pathgranule cell synapses. *European Journal of Neuroscience*, 19(3): 643–649, February 2004. ISSN 1460-9568. doi: 10.1111/j.0953-816X.2003.03174.x. URL `http://onlinelibrary.wiley.com/doi/10.1111/j.0953-816X.2003.03174.x/abstract`.

Shan Chen and Jeffrey S Diamond. Synaptically released glutamate activates extrasynaptic NMDA receptors on cells in the ganglion cell layer of rat retina. *J. Neurosci.*, 22(6): 2165–2173, March 2002. ISSN 1529-2401. PMID: 11896156.

Aaron Clauset, Cosma Rohilla Shalizi, and M. E. J. Newman. Power-law distributions in empirical data. *SIAM Review*, 51(4):661–703, November 2009. ISSN 0036-1445, 1095-7200. doi: 10.1137/070710111. URL `http://arxiv.org/abs/0706.1062`. arXiv:0706.1062 [cond-mat, physics:physics, stat].

Hollis Cline. Sperry and hebb: oil and vinegar? *Trends Neurosci.*, 26(12):655–661, December 2003. ISSN 0166-2236. doi: 10.1016/j.tins.2003.10.005. PMID: 14624849.

Matthew T Colonnese and Rustem Khazipov. "Slow activity transients" in infant rat visual cortex: a spreading synchronous oscillation patterned by retinal waves. *J. Neurosci.*, 30 (12):4325–4337, March 2010. ISSN 1529-2401. doi: 10.1523/JNEUROSCI.4995-09.2010. PMID: 20335468 PMCID: PMC3467103.

Barry W Connors and Michael A Long. Electrical synapses in the mammalian brain. *Annu. Rev. Neurosci.*, 27:393–418, 2004. ISSN 0147-006X. doi: 10.1146/annurev.neuro.26.041002.131128. PMID: 15217338.

Jeremy E Cook and David L Becker. Gap-junction proteins in retinal development: new roles for the "nexus". *Physiology (Bethesda)*, 24:219–230, August 2009. ISSN 1548-9213. doi: 10.1152/physiol.00007.2009. PMID: 19675353.

Julie L Coombs, Deborah Van Der List, and Leo M Chalupa. Morphological properties of mouse retinal ganglion cells during postnatal development. *J. Comp. Neurol.*, 503(6): 803–814, August 2007. ISSN 0021-9967. doi: 10.1002/cne.21429. PMID: 17570502.

R R Crichton and J L Pierre. Old iron, young copper: from mars to venus. *Biometals*, 14 (2):99–112, June 2001. ISSN 0966-0844. PMID: 11508852.

Scott J Cruikshank, Matthew Hopperstad, Meg Younger, Barry W Connors, David C Spray, and Miduturu Srinivas. Potent block of cx36 and cx50 gap junction channels by mefloquine. *Proc. Natl. Acad. Sci. U.S.A.*, 101(33):12364–12369, August 2004. ISSN 0027-8424. doi: 10.1073/pnas.0402044101. PMID: 15297615 PMCID: PMC514481.

N Cuenca, E Fernndez, M Garca, and J De Juan. Dendrites of rod dominant ON-bipolar cells are coupled by gap junctions in carp retina. *Neurosci. Lett.*, 162(1-2):34–38, November 1993. ISSN 0304-3940. PMID: 8121632.

M R Deans and D L Paul. Mouse horizontal cells do not express connexin26 or connexin36. *Cell Commun. Adhes.*, 8(4-6):361–366, 2001. ISSN 1541-9061. PMID: 12064619 PMCID: PMC2834531.

M R Deans, J R Gibson, C Sellitto, B W Connors, and D L Paul. Synchronous activity of inhibitory networks in neocortex requires electrical synapses containing connexin36. *Neuron*, 31(3):477–485, August 2001. ISSN 0896-6273. PMID: 11516403.

Michael R Deans, Bela Völgyi, Daniel A Goodenough, Stewart A Bloomfield, and David L Paul. Connexin36 is essential for transmission of rod-mediated visual signals in the mammalian retina. *Neuron*, 36(4):703–712, November 2002. ISSN 0896-6273. PMID: 12441058 PMCID: PMC2834592.

Karin Dedek, Konrad Schultz, Mario Pieper, Petra Dirks, Stephan Maxeiner, Klaus Willecke, Reto Weiler, and Ulrike Janssen-Bienhold. Localization of heterotypic gap junctions composed of connexin45 and connexin36 in the rod pathway of the mouse retina. *Eur. J. Neurosci.*, 24(6):1675–1686, September 2006. ISSN 0953-816X. doi: 10.1111/j.1460-9568.2006.05052.x. PMID: 17004931.

Karin Dedek, Tobias Breuninger, Luis Prez de Sevilla Müller, Stephan Maxeiner, Konrad Schultz, Ulrike Janssen-Bienhold, Klaus Willecke, Thomas Euler, and Reto Weiler. A novel type of interplexiform amacrine cell in the mouse retina. *Eur. J. Neurosci.*, 30(2):217–228, July 2009. ISSN 1460-9568. doi: 10.1111/j.1460-9568.2009.06808.x. PMID: 19614986.

Luca Della Santina, Ilaria Piano, Lorenzo Cangiano, Antonella Caputo, Andreas Ludwig, Luigi Cervetto, and Claudia Gargini. Processing of retinal signals in normal and HCN deficient mice. *PLoS ONE*, 7(1):e29812, 2012. ISSN 1932-6203. doi: 10.1371/journal.pone.0029812. PMID: 22279546 PMCID: PMC3261154.

Michael Demarque, Alfonso Represa, Hlne Becq, Ilgam Khalilov, Yehezkel Ben-Ari, and Laurent Aniksztejn. Paracrine intercellular communication by a ca2+- and SNARE-independent release of GABA and glutamate prior to synapse formation. *Neuron*, 36 (6):1051–1061, December 2002. ISSN 0896-6273. PMID: 12495621.

Jonathan B Demb and Joshua H Singer. Intrinsic properties and functional circuitry of the AII amacrine cell. *Vis. Neurosci.*, 29(1):51–60, January 2012. ISSN 1469-8714. doi: 10.1017/S0952523811000368. PMID: 22310372 PMCID: PMC3561778.

R Dermietzel, M Kremer, G Paputsoglu, A Stang, I M Skerrett, D Gomes, M Srinivas, U Janssen-Bienhold, R Weiler, B J Nicholson, R Bruzzone, and D C Spray. Molecular and functional diversity of neural connexins in the retina. *J. Neurosci.*, 20(22):8331–8343, November 2000. ISSN 1529-2401. PMID: 11069940.

Karen Deuschle, Sakiko Okumoto, Marcus Fehr, Loren L Looger, Leonid Kozhukh, and Wolf B Frommer. Construction and optimization of a family of genetically encoded metabolite sensors by semirational protein engineering. *Protein Sci.*, 14(9):2304–2314, September 2005. ISSN 0961-8368. doi: 10.1110/ps.051508105. PMID: 16131659 PMCID: PMC2253473.

Bryan C Dickinson and Christopher J Chang. Chemistry and biology of reactive oxygen species in signaling or stress responses. *Nat Chem Biol*, 7(8): 504–511, July 2011. ISSN 1552-4450. doi: 10.1038/nchembio.607. URL `http://www.ncbi.nlm.nih.gov/pmc/articles/PMC3390228/`. PMID: 21769097 PMCID: PMC3390228.

Sheel C. Dodani, Dylan W. Domaille, Christine I. Nam, Evan W. Miller, Lydia A. Finney, Stefan Vogt, and Christopher J. Chang. Calcium-dependent copper redistributions in neuronal cells revealed by a fluorescent copper sensor and x-ray fluorescence microscopy. *PNAS*, 108(15):5980–5985, April 2011. ISSN 0027-8424, 1091-6490. doi: 10.1073/pnas.1009932108. URL `http://www.pnas.org/content/108/15/5980`. PMID: 21444780.

Xufang Duan, Eric Block, Zhen Li, Timothy Connelly, Jian Zhang, Zhimin Huang, Xubo Su, Yi Pan, Lifang Wu, Qiuyi Chi, Siji Thomas, Shaozhong Zhang, Minghong Ma, Hiroaki Matsunami, Guo-Qiang Chen, and Hanyi Zhuang. Crucial role of copper in detection of metal-coordinating odorants. *PNAS*, 109(9):3492–3497, February 2012. ISSN 0027-8424, 1091-6490. doi: 10.1073/pnas.1111297109. URL `http://www.pnas.org/content/109/9/3492`. PMID: 22328155.

Chris Dulla, Hiroaki Tani, Sakiko Okumoto, Wolf B Frommer, Rich J Reimer, and John R Huguenard. Imaging of glutamate in brain slices using FRET sensors. *J. Neurosci. Methods*, 168(2):306–319, March 2008. ISSN 0165-0270. doi: 10.1016/j.jneumeth.2007.10.017. PMID: 18160134 PMCID: PMC2267481.

Galina Dvoriantchikova, Dmitry Ivanov, Yuri Panchin, and Valery I Shestopalov. Expression of pannexin family of proteins in the retina. *FEBS Lett.*, 580(9):2178–2182, April 2006. ISSN 0014-5793. doi: 10.1016/j.febslet.2006.03.026. PMID: 16616526.

Stephen J Eglen, Jay Demas, and Rachel O L Wong. Mapping by waves. patterned spontaneous activity regulates retinotopic map refinement. *Neuron*, 40(6):1053–1055, December 2003. ISSN 0896-6273. PMID: 14687538.

Justin Elstrott and Marla B Feller. Direction-selective ganglion cells show symmetric participation in retinal waves during development. *J. Neurosci.*, 30(33):11197–11201, August 2010. ISSN 1529-2401. doi: 10.1523/JNEUROSCI.2302-10.2010. PMID: 20720127 PMCID: PMC2928560.

A Feigenspan, B Teubner, K Willecke, and R Weiler. Expression of neuronal connexin36 in AII amacrine cells of the mammalian retina. *J. Neurosci.*, 21(1):230–239, January 2001. ISSN 1529-2401. PMID: 11150340.

Andreas Feigenspan, Ulrike Janssen-Bienhold, Sheriar Hormuzdi, Hannah Monyer, Joachim Degen, Goran Shl, Klaus Willecke, Josef Ammermller, and Reto Weiler. Expression of connexin36 in cone pedicles and OFF-cone bipolar cells of the mouse retina. *J. Neurosci.*, 24(13):3325–3334, March 2004. ISSN 1529-2401. doi: 10.1523/JNEUROSCI.5598-03.2004. PMID: 15056712.

David A Feldheim and Dennis D M O'Leary. Visual map development: bidirectional signaling, bifunctional guidance molecules, and competition. *Cold Spring Harb Perspect Biol*, 2 (11):a001768, November 2010. ISSN 1943-0264. doi: 10.1101/cshperspect.a001768. PMID: 20880989 PMCID: PMC2964178.

Sarah Feldt, Paolo Bonifazi, and Rosa Cossart. Dissecting functional connectivity of neuronal microcircuits: experimental and theoretical insights. *Trends Neurosci.*, 34(5):225–236, May 2011. ISSN 1878-108X. doi: 10.1016/j.tins.2011.02.007. PMID: 21459463.

M B Feller, D P Wellis, D Stellwagen, F S Werblin, and C J Shatz. Requirement for cholinergic synaptic transmission in the propagation of spontaneous retinal waves. *Science*, 272(5265):1182–1187, May 1996. ISSN 0036-8075. PMID: 8638165.

Alana Firl, Georgeann S. Sack, Zachary L. Newman, Hiroaki Tani, and Marla B. Feller. Extrasynaptic glutamate and inhibitory neurotransmission modulate ganglion cell participation during glutamatergic retinal waves. *J Neurophysiol*, 109 (7):1969–1978, April 2013. ISSN 0022-3077. doi: 10.1152/jn.00039.2013. URL `http://www.ncbi.nlm.nih.gov/pmc/articles/PMC3628007/`. PMID: 23343894 PMCID: PMC3628007.

Sally I Firth, Chih-Tien Wang, and Marla B Feller. Retinal waves: mechanisms and function in visual system development. *Cell Calcium*, 37(5):425–432, May 2005. ISSN 0143-4160. doi: 10.1016/j.ceca.2005.01.010. PMID: 15820390.

K F Fischer, P D Lukasiewicz, and R O Wong. Age-dependent and cell class-specific modulation of retinal ganglion cell bursting activity by GABA. *J. Neurosci.*, 18(10):3767–3778, May 1998. ISSN 0270-6474. PMID: 9570807.

Kevin J Ford and Marla B Feller. Assembly and disassembly of a retinal cholinergic network. *Vis. Neurosci.*, 29(1):61–71, January 2012. ISSN 1469-8714. doi: 10.1017/S0952523811000216. PMID: 21787461 PMCID: PMC3982217.

Kevin J Ford, Aude L Flix, and Marla B Feller. Cellular mechanisms underlying spatiotemporal features of cholinergic retinal waves. *J. Neurosci.*, 32(3):850–863, January 2012. ISSN 1529-2401. doi: 10.1523/JNEUROSCI.5309-12.2012. PMID: 22262883 PMCID: PMC3311224.

Jonathan H Fox, Jibrin A Kama, Gregory Lieberman, Raman Chopra, Kate Dorsey, Vanita Chopra, Irene Volitakis, Robert A Cherny, Ashley I Bush, and Steven Hersch. Mechanisms of copper ion mediated huntington's disease progression. *PLoS ONE*, 2(3):e334, 2007. ISSN 1932-6203. doi: 10.1371/journal.pone.0000334. PMID: 17396163 PMCID: PMC1828629.

E D Gaier, B A Eipper, and R E Mains. Copper signaling in the mammalian nervous system: synaptic effects. *J. Neurosci. Res.*, 91(1):2–19, January 2013. ISSN 1097-4547. doi: 10.1002/jnr.23143. PMID: 23115049 PMCID: PMC3926505.

O Garaschuk, J Linn, J Eilers, and A Konnerth. Large-scale oscillatory calcium waves in the immature cortex. *Nat. Neurosci.*, 3(5):452–459, May 2000. ISSN 1097-6256. doi: 10.1038/74823. PMID: 10769384.

Urs Gerber. Metabotropic glutamate receptors in vertebrate retina. *Doc Ophthalmol*, 106 (1):83–87, January 2003. ISSN 0012-4486. PMID: 12675489.

Keith B Godfrey, Stephen J Eglen, and Nicholas V Swindale. A multi-component model of the developing retinocollicular pathway incorporating axonal and synaptic growth. *PLoS Comput. Biol.*, 5(12):e1000600, December 2009. ISSN 1553-7358. doi: 10.1371/journal.pcbi.1000600. PMID: 20011124 PMCID: PMC2782179.

Shiaoching Gong, Chen Zheng, Martin L Doughty, Kasia Losos, Nicholas Didkovsky, Uta B Schambra, Norma J Nowak, Alexandra Joyner, Gabrielle Leblanc, Mary E Hatten, and Nathaniel Heintz. A gene expression atlas of the central nervous system based on bacterial artificial chromosomes. *Nature*, 425(6961):917–925, October 2003. ISSN 1476-4687. doi: 10.1038/nature02033. PMID: 14586460.

C S Goodman and C J Shatz. Developmental mechanisms that generate precise patterns of neuronal connectivity. *Cell*, 72 Suppl:77–98, January 1993. ISSN 0092-8674. PMID: 8428376.

G W Gordon, G Berry, X H Liang, B Levine, and B Herman. Quantitative fluorescence resonance energy transfer measurements using fluorescence microscopy. *Biophys. J.*, 74 (5):2702–2713, May 1998. ISSN 0006-3495. doi: 10.1016/S0006-3495(98)77976-7. PMID: 9591694 PMCID: PMC1299610.

M E Götz, G Künig, P Riederer, and M B Youdim. Oxidative stress: free radical production in neural degeneration. *Pharmacol. Ther.*, 63(1):37–122, 1994. ISSN 0163-7258. PMID: 7972344.

William Guido. Refinement of the retinogeniculate pathway. *J. Physiol. (Lond.)*, 586(Pt 18): 4357–4362, September 2008. ISSN 1469-7793. doi: 10.1113/jphysiol.2008.157115. PMID: 18556365 PMCID: PMC2614014.

M Güldenagel, G Söhl, A Plum, O Traub, B Teubner, R Weiler, and K Willecke. Expression patterns of connexin genes in mouse retina. *J. Comp. Neurol.*, 425(2):193–201, September 2000. ISSN 0021-9967. PMID: 10954839.

Kathryn L. Haas and Katherine J. Franz. Application of metal coordination chemistry to explore and manipulate cell biology. *Chem Rev*, 109(10): 4921–4960, October 2009. ISSN 0009-2665. doi: 10.1021/cr900134a. URL `http://www.ncbi.nlm.nih.gov/pmc/articles/PMC2761982/`. PMID: 19715312 PMCID: PMC2761982.

Yi Han and Stephen C Massey. Electrical synapses in retinal ON cone bipolar cells: subtype-specific expression of connexins. *Proc. Natl. Acad. Sci. U.S.A.*, 102(37):13313–13318, September 2005. ISSN 0027-8424. doi: 10.1073/pnas.0505067102. PMID: 16150718 PMCID: PMC1201596.

Kristi A Hansen, Christine L Torborg, Justin Elstrott, and Marla B Feller. Expression and function of the neuronal gap junction protein connexin 36 in developing mammalian retina. *J. Comp. Neurol.*, 493(2):309–320, December 2005. ISSN 0021-9967. doi: 10.1002/cne.20759. PMID: 16255034.

E G Harks, A D de Roos, P H Peters, L H de Haan, A Brouwer, D L Ypey, E J van Zoelen, and A P Theuvenet. Fenamates: a novel class of reversible gap junction blockers. *J. Pharmacol. Exp. Ther.*, 298(3):1033–1041, September 2001. ISSN 0022-3565. PMID: 11504800.

D E Hartter and A Barnea. Evidence for release of copper in the brain: depolarization-induced release of newly taken-up 67copper. *Synapse*, 2(4):412–415, 1988. ISSN 0887-4476. doi: 10.1002/syn.890020408. PMID: 3187909.

Jun Hasegawa, Takehisa Obara, Kohichi Tanaka, and Masao Tachibana. High-density presynaptic transporters are required for glutamate removal from the first visual synapse. *Neuron*, 50(1):63–74, April 2006. ISSN 0896-6273. doi: 10.1016/j.neuron.2006.02.022. PMID: 16600856.

DO Hebb. *The Organization of Behavior*. Wiley, New York, 1949.

Matthias H Hennig, Christopher Adams, David Willshaw, and Evelyne Sernagor. Early-stage waves in the retinal network emerge close to a critical state transition between local and global functional connectivity. *J. Neurosci.*, 29(4):1077–1086, January 2009. ISSN 1529-2401. doi: 10.1523/JNEUROSCI.4880-08.2009. PMID: 19176816.

M H Higgs, C Romano, and P D Lukasiewicz. Presynaptic effects of group III metabotropic glutamate receptors on excitatory synaptic transmission in the retina. *Neuroscience*, 115 (1):163–172, 2002. ISSN 0306-4522. PMID: 12401331.

Sonja Hombach, Ulrike Janssen-Bienhold, Goran Söhl, Timm Schubert, Heinrich Büssow, Thomas Ott, Reto Weiler, and Klaus Willecke. Functional expression of connexin57 in horizontal cells of the mouse retina. *Eur. J. Neurosci.*, 19(10):2633–2640, May 2004. ISSN 0953-816X. doi: 10.1111/j.0953-816X.2004.03360.x. PMID: 15147297.

Geoffrey C. Horwitz, Andrea Lelli, Gwenaelle S. G. Geleoc, and Jeffrey R. Holt. HCN channels are not required for mechanotransduction in sensory hair cells of the mouse inner ear. *PLoS One*, 5(1), January 2010. ISSN 1932-6203. doi: 10.1371/journal.pone.0008627. URL `http://www.ncbi.nlm.nih.gov/pmc/articles/PMC2797612/`. PMID: 20062532 PMCID: PMC2797612.

He Huang, Hui Li, and Shi Gang He. Identification of connexin 50 and 57 mRNA in a-type horizontal cells of the rabbit retina. *Cell Res.*, 15(3):207–211, March 2005. ISSN 1001-0602. doi: 10.1038/sj.cr.7290288. PMID: 15780184.

Andrew D Huberman, Marla B Feller, and Barbara Chapman. Mechanisms underlying development of visual maps and receptive fields. *Annu. Rev. Neurosci.*, 31:479–509, 2008. ISSN 0147-006X. doi: 10.1146/annurev.neuro.31.060407.125533. PMID: 18558864 PMCID: PMC2655105.

D L Huffman and T V O'Halloran. Function, structure, and mechanism of intracellular copper trafficking proteins. *Annu. Rev. Biochem.*, 70:677–701, 2001. ISSN 0066-4154. doi: 10.1146/annurev.biochem.70.1.677. PMID: 11395420.

Christelle Hureau and Peter Faller. Aß-mediated ROS production by cu ions: structural insights, mechanisms and relevance to alzheimer's disease. *Biochimie*, 91(10):1212–1217, October 2009. ISSN 1638-6183. doi: 10.1016/j.biochi.2009.03.013. PMID: 19332103.

Dumitru A Iacobas, Marcia Urban-Maldonado, Sanda Iacobas, Eliana Scemes, and David C Spray. Array analysis of gene expression in connexin-43 null astrocytes. *Physiol. Genomics*, 15(3):177–190, November 2003. ISSN 1531-2267. doi: 10.1152/physiolgenomics.00062.2003. PMID: 12928503 PMCID: PMC2651830.

Dumitru A Iacobas, Sanda Iacobas, and David C Spray. Connexin-dependent transcellular transcriptomic networks in mouse brain. *Prog. Biophys. Mol. Biol.*, 94(1-2):169–185, June 2007. ISSN 0079-6107. doi: 10.1016/j.pbiomolbio.2007.03.015. PMID: 17507080.

Eugene M Izhikevich. Which model to use for cortical spiking neurons? *IEEE Trans Neural Netw*, 15(5):1063–1070, September 2004. ISSN 1045-9227. doi: 10.1109/TNN.2004.832719. PMID: 15484883.

R A Jacoby and D W Marshak. Synaptic connections of DB3 diffuse bipolar cell axons in macaque retina. *J. Comp. Neurol.*, 416(1):19–29, January 2000. ISSN 0021-9967. PMID: 10578100 PMCID: PMC3341735.

Stephen G Kaler. ATP7A-related copper transport diseases-emerging concepts and future trends. *Nat Rev Neurol*, 7(1):15–29, January 2011. ISSN 1759-4766. doi: 10.1038/nrneurol.2010.180. PMID: 21221114.

Kimiko Katoh, Yoshihiro Omori, Akishi Onishi, Shigeru Sato, Mineo Kondo, and Takahisa Furukawa. Blimp1 suppresses chx10 expression in differentiating retinal photoreceptor precursors to ensure proper photoreceptor development. *J. Neurosci.*, 30(19):6515–6526, May 2010. ISSN 1529-2401. doi: 10.1523/JNEUROSCI.0771-10.2010. PMID: 20463215.

L C Katz and C J Shatz. Synaptic activity and the construction of cortical circuits. *Science*, 274(5290):1133–1138, November 1996. ISSN 0036-8075. PMID: 8895456.

Daniel Kerschensteiner. Spontaneous network activity and synaptic development. *Neuroscientist*, November 2013. ISSN 1089-4098. doi: 10.1177/1073858413510044. PMID: 24280071.

Daniel Kerschensteiner and Rachel O L Wong. A precisely timed asynchronous pattern of ON and OFF retinal ganglion cell activity during propagation of retinal waves. *Neuron*, 58(6):851–858, June 2008. ISSN 1097-4199. doi: 10.1016/j.neuron.2008.04.025. PMID: 18579076 PMCID: PMC2553397.

Daniel Kerschensteiner, Josh L Morgan, Edward D Parker, Renate M Lewis, and Rachel O L Wong. Neurotransmission selectively regulates synapse formation in parallel circuits in vivo. *Nature*, 460(7258):1016–1020, August 2009. ISSN 1476-4687. doi: 10.1038/nature08236. PMID: 19693082 PMCID: PMC2746695.

A H Kihara, V Paschon, P S Akamine, K C Saito, M Leonelli, J X Jiang, D E Hamassaki, and L R G Britto. Differential expression of connexins during histogenesis of the chick retina. *Dev Neurobiol*, 68(11):1287–1302, September 2008. ISSN 1932-8451. doi: 10.1002/dneu.20652. PMID: 18506822.

Alexandre Hiroaki Kihara, Leandro Mantovani de Castro, Mônica Aparecida Belmonte, Chao Yun Irene Yan, Anselmo Sigari Moriscot, and Dânia Emi Hamassaki. Expression of connexins 36, 43, and 45 during postnatal development of the mouse retina. *J. Neurobiol.*, 66(13):1397–1410, November 2006. ISSN 0022-3034. doi: 10.1002/neu.20299. PMID: 17029293.

Byung-Eun Kim, Tracy Nevitt, and Dennis J Thiele. Mechanisms for copper acquisition, distribution and regulation. *Nat. Chem. Biol.*, 4(3):176–185, March 2008. ISSN 1552-4469. doi: 10.1038/nchembio.72. PMID: 18277979.

In-Jung Kim, Yifeng Zhang, Markus Meister, and Joshua R Sanes. Laminar restriction of retinal ganglion cell dendrites and axons: subtype-specific developmental patterns revealed with transgenic markers. *J. Neurosci.*, 30(4):1452–1462, January 2010. ISSN 1529-2401. doi: 10.1523/JNEUROSCI.4779-09.2010. PMID: 20107072 PMCID: PMC2822471.

Lowry A Kirkby, Georgeann S Sack, Alana Firl, and Marla B Feller. A role for correlated spontaneous activity in the assembly of neural circuits. *Neuron*, 80(5):1129–1144, December 2013. ISSN 1097-4199. doi: 10.1016/j.neuron.2013.10.030. PMID: 24314725.

Helga Kolb and E. V. Famigilietti. Rod and cone pathways in the inner plexiform layer of cat retina. *Science*, 186(4158):47–49, October 1974. ISSN 0036-8075, 1095-9203. doi: 10.1126/science.186.4158.47. URL `http://www.sciencemag.org/content/186/4158/47`. PMID: 4417736.

J Lee, J R Prohaska, and D J Thiele. Essential role for mammalian copper transporter ctr1 in copper homeostasis and embryonic development. *Proc. Natl. Acad. Sci. U.S.A.*, 98(12): 6842–6847, June 2001. ISSN 0027-8424. doi: 10.1073/pnas.111058698. PMID: 11391005 PMCID: PMC34440.

Bin Lin, Tatjana C Jakobs, and Richard H Masland. Different functional types of bipolar cells use different gap-junctional proteins. *J. Neurosci.*, 25(28):6696–6701, July 2005. ISSN 1529-2401. doi: 10.1523/JNEUROSCI.1894-05.2005. PMID: 16014731.

Michael A Long, Michael R Deans, David L Paul, and Barry W Connors. Rhythmicity without synchrony in the electrically uncoupled inferior olive. *J. Neurosci.*, 22(24):10898–10905, December 2002. ISSN 1529-2401. PMID: 12486184 PMCID: PMC2834587.

Svetlana Lutsenko, Natalie L Barnes, Mee Y Bartee, and Oleg Y Dmitriev. Function and regulation of human copper-transporting ATPases. *Physiol. Rev.*, 87(3):1011–1046, July 2007. ISSN 0031-9333. doi: 10.1152/physrev.00004.2006. PMID: 17615395.

Svetlana Lutsenko, Ashima Bhattacharjee, and Ann L Hubbard. Copper handling machinery of the brain. *Metallomics*, 2(9):596–608, September 2010. ISSN 1756-591X. doi: 10.1039/c0mt00006j. PMID: 21072351.

Jean-Bernard Manent, Michal Demarque, Isabel Jorquera, Christophe Pellegrino, Yehezkel Ben-Ari, Laurent Aniksztejn, and Alfonso Represa. A noncanonical release of GABA and glutamate modulates neuronal migration. *J. Neurosci.*, 25(19):4755–4765, May 2005. ISSN 1529-2401. doi: 10.1523/JNEUROSCI.0553-05.2005. PMID: 15888651.

David J Margolis, Andrew J Gartland, Joshua H Singer, and Peter B Detwiler. Network oscillations drive correlated spiking of ON and OFF ganglion cells in the rd1 mouse model of retinal degeneration. *PLoS ONE*, 9(1):e86253, 2014. ISSN 1932-6203. doi: 10.1371/journal.pone.0086253. PMID: 24489706 PMCID: PMC3904909.

Olivier Marre, Dario Amodei, Nikhil Deshmukh, Kolia Sadeghi, Frederick Soo, Timothy E. Holy, and Michael J. Berry. Mapping a complete neural population in the retina. *J. Neurosci.*, 32(43):14859–14873, October 2012. ISSN 0270-6474, 1529-2401. doi: 10.1523/JNEUROSCI.0723-12.2012. URL http://www.jneurosci.org/content/32/43/14859. PMID: 23100409.

Richard H Masland. The neuronal organization of the retina. *Neuron*, 76(2):266–280, October 2012. ISSN 1097-4199. doi: 10.1016/j.neuron.2012.10.002. PMID: 23083731 PMCID: PMC3714606.

Stephen C Massey, Jennifer J O'Brien, E Brady Trexler, Wei Li, Joyce W Keung, Stephen L Mills, and John O'Brien. Multiple neuronal connexins in the mammalian retina. *Cell Commun. Adhes.*, 10(4-6):425–430, December 2003. ISSN 1541-9061. PMID: 14681052.

Ryota Matsuo, Suguru Kobayashi, Satoshi Watanabe, Shigeyuki Namiki, Sho Iinuma, Hirokazu Sakamoto, Kenzo Hirose, and Etsuro Ito. Glutamatergic neurotransmission in the procerebrum (olfactory center) of a terrestrial mollusk. *J. Neurosci. Res.*, 87(13):3011–3023, October 2009. ISSN 1097-4547. doi: 10.1002/jnr.22130. PMID: 19472222.

Stephan Maxeiner, Karin Dedek, Ulrike Janssen-Bienhold, Josef Ammermüller, Hendrik Brune, Taryn Kirsch, Mario Pieper, Joachim Degen, Olaf Krüger, Klaus Willecke, and Reto Weiler. Deletion of connexin45 in mouse retinal neurons disrupts the rod/cone signaling pathway between AII amacrine and ON cone bipolar cells and leads to impaired visual transmission. *J. Neurosci.*, 25(3):566–576, January 2005. ISSN 1529-2401. doi: 10.1523/JNEUROSCI.3232-04.2005. PMID: 15659592.

Alberto Mazzoni, Frdric D. Broccard, Elizabeth Garcia-Perez, Paolo Bonifazi, Maria Elisabetta Ruaro, and Vincent Torre. On the dynamics of the spontaneous activity in neuronal networks. *PLoS ONE*, 2(5):e439, May 2007. doi: 10.1371/journal.pone.0000439. URL http://dx.plos.org/10.1371/journal.pone.0000439.

Todd McLaughlin, Christine L Torborg, Marla B Feller, and Dennis D M O'Leary. Retinotopic map refinement requires spontaneous retinal waves during a brief critical period of development. *Neuron*, 40(6):1147–1160, December 2003. ISSN 0896-6273. PMID: 14687549.

M Meister, R O Wong, D A Baylor, and C J Shatz. Synchronous bursts of action potentials in ganglion cells of the developing mammalian retina. *Science*, 252(5008):939–943, May 1991. ISSN 0036-8075. PMID: 2035024.

Glenn L. Millhauser. Copper binding in the prion protein. *Acc Chem Res*, 37 (2):79–85, February 2004. ISSN 0001-4842. doi: 10.1021/ar0301678. URL http://www.ncbi.nlm.nih.gov/pmc/articles/PMC2907897/. PMID: 14967054 PMCID: PMC2907897.

William J Moody and Martha M Bosma. Ion channel development, spontaneous activity, and activity-dependent development in nerve and muscle cells. *Physiol. Rev.*, 85(3):883–941, July 2005. ISSN 0031-9333. doi: 10.1152/physrev.00017.2004. PMID: 15987798.

Anna R Moore, Wen-Liang Zhou, Igor Jakovcevski, Nada Zecevic, and Srdjan D Antic. Spontaneous electrical activity in the human fetal cortex in vitro. *J. Neurosci.*, 31(7): 2391–2398, February 2011. ISSN 1529-2401. doi: 10.1523/JNEUROSCI.3886-10.2011. PMID: 21325506 PMCID: PMC3564513.

Josh L Morgan, Anuradha Dhingra, Noga Vardi, and Rachel O L Wong. Axons and dendrites originate from neuroepithelial-like processes of retinal bipolar cells. *Nat. Neurosci.*, 9(1): 85–92, January 2006. ISSN 1097-6256. doi: 10.1038/nn1615. PMID: 16341211.

Eric M Morrow, C-M Amy Chen, and Constance L Cepko. Temporal order of bipolar cell genesis in the neural retina. *Neural Dev*, 3:2, 2008. ISSN 1749-8104. doi: 10.1186/1749-8104-3-2. PMID: 18215319 PMCID: PMC2248187.

Luis Perez de Sevilla Müller, Karin Dedek, Ulrike Janssen-Bienhold, Arndt Meyer, Maria M Kreuzberg, Susanne Lorenz, Klaus Willecke, and Reto Weiler. Expression and modulation of connexin 30.2, a novel gap junction protein in the mouse retina. *Vis. Neurosci.*, 27(3-4): 91–101, July 2010. ISSN 1469-8714. doi: 10.1017/S0952523810000131. PMID: 20537217.

Shigeyuki Namiki, Hirokazu Sakamoto, Sho Iinuma, Masamitsu Iino, and Kenzo Hirose. Optical glutamate sensor for spatiotemporal analysis of synaptic transmission. *Eur. J. Neurosci.*, 25(8):2249–2259, April 2007. ISSN 0953-816X. doi: 10.1111/j.1460-9568.2007.05511.x. PMID: 17445223.

E A Newman. Propagation of intercellular calcium waves in retinal astrocytes and müller cells. *J. Neurosci.*, 21(7):2215–2223, April 2001. ISSN 1529-2401. PMID: 11264297 PMCID: PMC2409971.

Eric A Newman. Calcium increases in retinal glial cells evoked by light-induced neuronal activity. *J. Neurosci.*, 25(23):5502–5510, June 2005. ISSN 1529-2401. doi: 10.1523/JNEUROSCI.1354-05.2005. PMID: 15944378 PMCID: PMC1405916.

Michel Nguyen, Anne Robert, Alix Sournia-Saquet, Laure Vendier, and Bernard Meunier. Characterization of new specific copper chelators as potential drugs for the treatment of alzheimer's disease. *Chemistry*, May 2014. ISSN 1521-3765. doi: 10.1002/chem.201402143. PMID: 24797103.

Jennifer J O'Brien, Wei Li, Feng Pan, Joyce Keung, John O'Brien, and Stephen C Massey. Coupling between a-type horizontal cells is mediated by connexin 50 gap junctions in the rabbit retina. *J. Neurosci.*, 26(45):11624–11636, November 2006. ISSN 1529-2401. doi: 10.1523/JNEUROSCI.2296-06.2006. PMID: 17093084.

Nicholas Oesch and Jeffrey Diamond. A night vision neuron gets a day job. *Nat Neurosci*, 12(10):1209–1211, October 2009. ISSN 1097-6256. doi: 10.1038/nn1009-1209. URL `http://www.nature.com/neuro/journal/v12/n10/full/nn1009-1209.html`.

Yohei Okubo, Hiroshi Sekiya, Shigeyuki Namiki, Hirokazu Sakamoto, Sho Iinuma, Miwako Yamasaki, Masahiko Watanabe, Kenzo Hirose, and Masamitsu Iino. Imaging extrasynaptic glutamate dynamics in the brain. *Proc. Natl. Acad. Sci. U.S.A.*, 107(14):6526–6531, April 2010. ISSN 1091-6490. doi: 10.1073/pnas.0913154107. PMID: 20308566 PMCID: PMC2851965.

Sakiko Okumoto, Loren L Looger, Kristina D Micheva, Richard J Reimer, Stephen J Smith, and Wolf B Frommer. Detection of glutamate release from neurons by genetically encoded surface-displayed FRET nanosensors. *Proc. Natl. Acad. Sci. U.S.A.*, 102(24):8740–8745, June 2005. ISSN 0027-8424. doi: 10.1073/pnas.0503274102. PMID: 15939876 PMCID: PMC1143584.

Feng Pan, Stephen L Mills, and Stephen C Massey. Screening of gap junction antagonists on dye coupling in the rabbit retina. *Vis. Neurosci.*, 24(4):609–618, August 2007. ISSN 0952-5238. doi: 10.1017/S0952523807070472. PMID: 17711600 PMCID: PMC2213422.

Feng Pan, David L Paul, Stewart A Bloomfield, and Bela Völgyi. Connexin36 is required for gap junctional coupling of most ganglion cell subtypes in the mouse retina. *J. Comp. Neurol.*, 518(6):911–927, March 2010. ISSN 1096-9861. doi: 10.1002/cne.22254. PMID: 20058323 PMCID: PMC2860380.

Kirkwood E Personius, Qiang Chang, George Z Mentis, Michael J O'Donovan, and Rita J Balice-Gordon. Reduced gap junctional coupling leads to uncorrelated motor neuron firing and precocious neuromuscular synapse elimination. *Proc. Natl. Acad. Sci. U.S.A.*, 104(28): 11808–11813, July 2007. ISSN 0027-8424. doi: 10.1073/pnas.0703357104. PMID: 17609378 PMCID: PMC1913899.

Christian Peters, Braulio Muoz, Fernando J Seplveda, Juan Urrutia, Mauricio Quiroz, Sandra Luza, Giancarlo V De Ferrari, Luis G Aguayo, and Carlos Opazo. Biphasic effects of copper on neurotransmission in rat hippocampal neurons. *J. Neurochem.*, 119(1):78–88, October 2011. ISSN 1471-4159. doi: 10.1111/j.1471-4159.2011.07417.x. PMID: 21824141.

Emily L Que, Dylan W Domaille, and Christopher J Chang. Metals in neurobiology: probing their chemistry and biology with molecular imaging. *Chem. Rev.*, 108(5):1517–1549, May 2008. ISSN 1520-6890. doi: 10.1021/cr078203u. PMID: 18426241.

Arundhati Ray, Georg Zoidl, Svenja Weickert, Petra Wahle, and Rolf Dermietzel. Site-specific and developmental expression of pannexin1 in the mouse nervous system. *Eur. J. Neurosci.*, 21(12):3277–3290, June 2005. ISSN 0953-816X. doi: 10.1111/j.1460-9568.2005.04139.x. PMID: 16026466.

Nigel J Robinson and Dennis R Winge. Copper metallochaperones. *Annu. Rev. Biochem.*, 79:537–562, 2010. ISSN 1545-4509. doi: 10.1146/annurev-biochem-030409-143539. PMID: 20205585 PMCID: PMC3986808.

B Roerig and M B Feller. Neurotransmitters and gap junctions in developing neural circuits. *Brain Res. Brain Res. Rev.*, 32(1):86–114, April 2000. PMID: 10751659.

Matthew J M Rowan, Harris Ripps, and Wen Shen. Fast glutamate uptake via EAAT2 shapes the cone-mediated light offset response in bipolar cells. *J. Physiol. (Lond.)*, 588(Pt 20):3943–3956, October 2010. ISSN 1469-7793. doi: 10.1113/jphysiol.2010.191437. PMID: 20807794 PMCID: PMC3000584.

J. L. Sánchez-Alonso, J. V. Halliwell, and A. Colino. ZD 7288 inhibits t-type calcium current in rat hippocampal pyramidal cells. *Neuroscience Letters*, 439(3): 275–280, July 2008. ISSN 0304-3940. doi: 10.1016/j.neulet.2008.05.016. URL `http://www.sciencedirect.com/science/article/pii/S0304394008006423`.

Masha G Savelieff, Sanghyun Lee, Yuzhong Liu, and Mi Hee Lim. Untangling amyloid-, tau, and metals in alzheimer's disease. *ACS Chem. Biol.*, 8(5):856–865, May 2013. ISSN 1554-8937. doi: 10.1021/cb400080f. PMID: 23506614.

Eliana Scemes, Sylvia O Suadicani, Gerhard Dahl, and David C Spray. Connexin and pannexin mediated cell-cell communication. *Neuron Glia Biol.*, 3(3):199–208, August 2007. ISSN 1741-0533. doi: 10.1017/S1740925X08000069. PMID: 18634611 PMCID: PMC2588549.

Michelle L Schlief, Ann Marie Craig, and Jonathan D Gitlin. NMDA receptor activation mediates copper homeostasis in hippocampal neurons. *J. Neurosci.*, 25(1):239–246, January 2005. ISSN 1529-2401. doi: 10.1523/JNEUROSCI.3699-04.2005. PMID: 15634787.

Michelle L Schlief, Tim West, Ann Marie Craig, David M Holtzman, and Jonathan D Gitlin. Role of the menkes copper-transporting ATPase in NMDA receptor-mediated neuronal toxicity. *Proc. Natl. Acad. Sci. U.S.A.*, 103(40):14919–14924, October 2006. ISSN 0027-8424. doi: 10.1073/pnas.0605390103. PMID: 17003121 PMCID: PMC1578502.

Timm Schubert, Joachim Degen, Klaus Willecke, Sheriar G Hormuzdi, Hannah Monyer, and Reto Weiler. Connexin36 mediates gap junctional coupling of alpha-ganglion cells in mouse retina. *J. Comp. Neurol.*, 485(3):191–201, May 2005. ISSN 0021-9967. doi: 10.1002/cne.20510. PMID: 15791644.

Ronen Segev, Joe Goodhouse, Jason Puchalla, and 2nd Berry, Michael J. Recording spikes from a large fraction of the ganglion cells in a retinal patch. *Nat. Neurosci.*, 7(10):1154–1161, October 2004. ISSN 1097-6256. doi: 10.1038/nn1323. PMID: 15452581.

E Sernagor, S J Eglen, and M J O'Donovan. Differential effects of acetylcholine and glutamate blockade on the spatiotemporal dynamics of retinal waves. *J. Neurosci.*, 20(2):RC56, January 2000. ISSN 1529-2401. PMID: 10632622.

Aleksandr Shcheglovitov, Iuliia Vitko, Roman M Lazarenko, Peihan Orestes, Slobodan M Todorovic, and Edward Perez-Reyes. Molecular and biophysical basis of glutamate and trace metal modulation of voltage-gated ca(v)2.3 calcium channels. *J. Gen. Physiol.*, 139 (3):219–234, March 2012. ISSN 1540-7748. doi: 10.1085/jgp.201110699. PMID: 22371363 PMCID: PMC3289959.

Shwu-Jiuan Sheu, Youn-Shen Bee, and Chih-Hsien Chen. Resveratrol and large-conductance calcium-activated potassium channels in the protection of human retinal pigment epithelial cells. *J Ocul Pharmacol Ther*, 24(6):551–555, December 2008. ISSN 1557-7732. doi: 10.1089/jop.2008.0013. PMID: 19049310.

Sandra Siegert, Brigitte Gross Scherf, Karina Del Punta, Nick Didkovsky, Nathaniel Heintz, and Botond Roska. Genetic address book for retinal cell types. *Nat. Neurosci.*, 12(9): 1197–1204, September 2009. ISSN 1546-1726. doi: 10.1038/nn.2370. PMID: 19648912.

Owen M. Siggs, Justin T. Cruite, Xin Du, Sophie Rutschmann, Eliezer Masliah, Bruce Beutler, and Michael B. A. Oldstone. Disruption of copper homeostasis due to a mutation of atp7a delays the onset of prion disease. *Proc Natl Acad Sci U S A*, 109(34): 13733–13738, August 2012. ISSN 0027-8424. doi: 10.1073/pnas.1211499109. URL `http://www.ncbi.nlm.nih.gov/pmc/articles/PMC3427069/`. PMID: 22869751 PMCID: PMC3427069.

J H Singer, R R Mirotznik, and M B Feller. Potentiation of l-type calcium channels reveals nonsynaptic mechanisms that correlate spontaneous activity in the developing mammalian retina. *J. Neurosci.*, 21(21):8514–8522, November 2001. ISSN 1529-2401. PMID: 11606640.

Itender Singh, Abhay P. Sagare, Mireia Coma, David Perlmutter, Robert Gelein, Robert D. Bell, Richard J. Deane, Elaine Zhong, Margaret Parisi, Joseph Ciszewski, R. Tristan Kasper, and Rashid Deane. Low levels of copper disrupt brain amyloid-? homeostasis by altering its production and clearance. *Proc Natl Acad Sci U S A*, 110(36): 14771–14776, September 2013. ISSN 0027-8424. doi: 10.1073/pnas.1302212110. URL `http://www.ncbi.nlm.nih.gov/pmc/articles/PMC3767519/`. PMID: 23959870 PMCID: PMC3767519.

M M Slaughter and R F Miller. 2-amino-4-phosphonobutyric acid: a new pharmacological tool for retina research. *Science*, 211(4478):182–185, January 1981. ISSN 0036-8075. PMID: 6255566.

G Söhl, M Güldenagel, O Traub, and K Willecke. Connexin expression in the retina. *Brain Res. Brain Res. Rev.*, 32(1):138–145, April 2000. PMID: 10751663.

Goran Söhl, Stephan Maxeiner, and Klaus Willecke. Expression and functions of neuronal gap junctions. *Nat. Rev. Neurosci.*, 6(3):191–200, March 2005. ISSN 1471-003X. doi: 10.1038/nrn1627. PMID: 15738956.

Florentina Soto, Xiaofeng Ma, Jacob L Cecil, Bradly Q Vo, Susan M Culican, and Daniel Kerschensteiner. Spontaneous activity promotes synapse formation in a cell-type-dependent manner in the developing retina. *J. Neurosci.*, 32(16):5426–5439, April 2012. ISSN 1529-2401. doi: 10.1523/JNEUROSCI.0194-12.2012. PMID: 22514306 PMCID: PMC3353326.

D Larry Sparks and Bernard G Schreurs. Trace amounts of copper in water induce beta-amyloid plaques and learning deficits in a rabbit model of alzheimer's disease. *Proc. Natl. Acad. Sci. U.S.A.*, 100(19):11065–11069, September 2003. ISSN 0027-8424. doi: 10.1073/pnas.1832769100. PMID: 12920183 PMCID: PMC196927.

David C Spray and Dumitru A Iacobas. Organizational principles of the connexin-related brain transcriptome. *J. Membr. Biol.*, 218(1-3):39–47, August 2007. ISSN 0022-2631. doi: 10.1007/s00232-007-9049-5. PMID: 17657523.

Rosanna Squitti, Tjaard Hoogenraad, George Brewer, Ashley I Bush, and Renato Polimanti. Copper status in alzheimer's disease and other neurodegenerative disorders 2013. *Int J Alzheimers Dis*, 2013:838274, 2013. ISSN 2090-8024. doi: 10.1155/2013/838274. PMID: 24455406 PMCID: PMC3880705.

Rebecca C Stacy, Jay Demas, Robert W Burgess, Joshua R Sanes, and Rachel O L Wong. Disruption and recovery of patterned retinal activity in the absence of acetylcholine. *J. Neurosci.*, 25(41):9347–9357, October 2005. ISSN 1529-2401. doi: 10.1523/JNEUROSCI.1800-05.2005. PMID: 16221843.

Ben K Stafford, Alexander Sher, Alan M Litke, and David A Feldheim. Spatial-temporal patterns of retinal waves underlying activity-dependent refinement of retinofugal projections. *Neuron*, 64(2):200–212, October 2009. ISSN 1097-4199. doi: 10.1016/j.neuron.2009.09.021. PMID: 19874788 PMCID: PMC2771121.

Steven F Stasheff. Emergence of sustained spontaneous hyperactivity and temporary preservation of OFF responses in ganglion cells of the retinal degeneration (rd1) mouse. *J. Neurophysiol.*, 99(3):1408–1421, March 2008. ISSN 0022-3077. doi: 10.1152/jn.00144.2007. PMID: 18216234.

Christoph Stosiek, Olga Garaschuk, Knut Holthoff, and Arthur Konnerth. In vivo two-photon calcium imaging of neuronal networks. *Proc. Natl. Acad. Sci. U.S.A.*, 100(12): 7319–7324, June 2003. ISSN 0027-8424. doi: 10.1073/pnas.1232232100. PMID: 12777621 PMCID: PMC165873.

Megan R Sullivan, Axel Nimmerjahn, Dmitry V Sarkisov, Fritjof Helmchen, and Samuel S-H Wang. In vivo calcium imaging of circuit activity in cerebellar cortex. *J. Neurophysiol.*,

94(2):1636–1644, August 2005. ISSN 0022-3077. doi: 10.1152/jn.01013.2004. PMID: 16079125.

Mohsin Md Syed, Seunghoon Lee, Shigang He, and Z Jimmy Zhou. Spontaneous waves in the ventricular zone of developing mammalian retina. *J. Neurophysiol.*, 91(5):1999–2009, May 2004a. ISSN 0022-3077. doi: 10.1152/jn.01129.2003. PMID: 14681336.

Mohsin Md Syed, Seunghoon Lee, Jijian Zheng, and Z Jimmy Zhou. Stage-dependent dynamics and modulation of spontaneous waves in the developing rabbit retina. *J. Physiol. (Lond.)*, 560(Pt 2):533–549, October 2004b. ISSN 0022-3751. doi: 10.1113/jphysiol.2004.066597. PMID: 15308679 PMCID: PMC1665265.

Brett A Szmajda and Steven H Devries. Glutamate spillover between mammalian cone photoreceptors. *J. Neurosci.*, 31(38):13431–13441, September 2011. ISSN 1529-2401. doi: 10.1523/JNEUROSCI.2105-11.2011. PMID: 21940436 PMCID: PMC3212989.

Yukari Takeda, Sean M Ward, Kenton M Sanders, and Sang Don Koh. Effects of the gap junction blocker glycyrrhetinic acid on gastrointestinal smooth muscle cells. *Am. J. Physiol. Gastrointest. Liver Physiol.*, 288(4):G832–841, April 2005. ISSN 0193-1857. doi: 10.1152/ajpgi.00389.2004. PMID: 15528254.

Hiroaki Tani, Chris G Dulla, John R Huguenard, and Richard J Reimer. Glutamine is required for persistent epileptiform activity in the disinhibited neocortical brain slice. *J. Neurosci.*, 30(4):1288–1300, January 2010. ISSN 1529-2401. doi: 10.1523/JNEUROSCI.0106-09.2010. PMID: 20107056 PMCID: PMC2821093.

Christine L Torborg and Marla B Feller. Spontaneous patterned retinal activity and the refinement of retinal projections. *Prog. Neurobiol.*, 76(4):213–235, July 2005. ISSN 0301-0082. doi: 10.1016/j.pneurobio.2005.09.002. PMID: 16280194.

Christine L Torborg, Kristi A Hansen, and Marla B Feller. High frequency, synchronized bursting drives eye-specific segregation of retinogeniculate projections. *Nat. Neurosci.*, 8 (1):72–78, January 2005. ISSN 1097-6256. doi: 10.1038/nn1376. PMID: 15608630 PMCID: PMC1463890.

Kenneth R Tovar, Brady J Maher, and Gary L Westbrook. Direct actions of carbenoxolone on synaptic transmission and neuronal membrane properties. *J. Neurophysiol.*, 102(2): 974–978, August 2009. ISSN 0022-3077. doi: 10.1152/jn.00060.2009. PMID: 19535488 PMCID: PMC2724329.

Stuart Trenholm, Joanna Borowska, Jiawei Zhang, Alex Hoggarth, Kyle Johnson, Steven Barnes, Timothy J Lewis, and Gautam B Awatramani. Intrinsic oscillatory activity arising within the electrically coupled AII amacrine-ON cone bipolar cell network is driven by voltage-gated na+ channels. *J. Physiol. (Lond.)*, 590(Pt 10):2501–2517, May 2012. ISSN 1469-7793. doi: 10.1113/jphysiol.2011.225060. PMID: 22393249 PMCID: PMC3424767.

Jason W Triplett and David A Feldheim. Eph and ephrin signaling in the formation of topographic maps. *Semin. Cell Dev. Biol.*, 23(1):7–15, February 2012. ISSN 1096-3634. doi: 10.1016/j.semcdb.2011.10.026. PMID: 22044886 PMCID: PMC3288406.

Joan Selverstone Valentine and P John Hart. Misfolded CuZnSOD and amyotrophic lateral sclerosis. *Proc. Natl. Acad. Sci. U.S.A.*, 100(7):3617–3622, April 2003. ISSN 0027-8424. doi: 10.1073/pnas.0730423100. PMID: 12655070 PMCID: PMC152971.

Jacco van Rheenen, Michiel Langeslag, and Kees Jalink. Correcting confocal acquisition to optimize imaging of fluorescence resonance energy transfer by sensitized emission. *Biophys. J.*, 86(4):2517–2529, April 2004. ISSN 0006-3495. doi: 10.1016/S0006-3495(04)74307-6. PMID: 15041688 PMCID: PMC1304099.

Margaret Lin Veruki and Espen Hartveit. Electrical synapses mediate signal transmission in the rod pathway of the mammalian retina. *J. Neurosci.*, 22(24):10558–10566, December 2002. ISSN 0270-6474, 1529-2401. URL `http://www.jneurosci.org/content/22/24/10558`. PMID: 12486148.

Margaret Lin Veruki and Espen Hartveit. Meclofenamic acid blocks electrical synapses of retinal AII amacrine and on-cone bipolar cells. *J. Neurophysiol.*, 101(5):2339–2347, May 2009. ISSN 0022-3077. doi: 10.1152/jn.00112.2009. PMID: 19279153.

Margaret Lin Veruki, Svein Harald Mrkve, and Espen Hartveit. Activation of a presynaptic glutamate transporter regulates synaptic transmission through electrical signaling. *Nat. Neurosci.*, 9(11):1388–1396, November 2006. ISSN 1097-6256. doi: 10.1038/nn1793. PMID: 17041592.

John P Vessey, Melanie R Lalonde, Hossein A Mizan, Nicole C Welch, Melanie E M Kelly, and Steven Barnes. Carbenoxolone inhibition of voltage-gated ca channels and synaptic transmission in the retina. *J. Neurophysiol.*, 92(2):1252–1256, August 2004. ISSN 0022-3077. doi: 10.1152/jn.00148.2004. PMID: 15028741.

Bela Völgyi, Joseph Abrams, David L Paul, and Stewart A Bloomfield. Morphology and tracer coupling pattern of alpha ganglion cells in the mouse retina. *J. Comp. Neurol.*, 492 (1):66–77, November 2005. ISSN 0021-9967. doi: 10.1002/cne.20700. PMID: 16175559 PMCID: PMC2834591.

C Wahl-Schott and M Biel. HCN channels: structure, cellular regulation and physiological function. *Cell. Mol. Life Sci.*, 66(3):470–494, February 2009. ISSN 1420-9071. doi: 10.1007/s00018-008-8525-0. PMID: 18953682.

Chih-Tien Wang, Aaron G Blankenship, Anastasia Anishchenko, Justin Elstrott, Michael Fikhman, Shigetada Nakanishi, and Marla B Feller. GABA(A) receptor-mediated signaling alters the structure of spontaneous activity in the developing retina. *J. Neurosci.*, 27 (34):9130–9140, August 2007. ISSN 1529-2401. doi: 10.1523/JNEUROSCI.1293-07.2007. PMID: 17715349 PMCID: PMC2933517.

M Weliky and L C Katz. Correlational structure of spontaneous neuronal activity in the developing lateral geniculate nucleus in vivo. *Science*, 285(5427):599–604, July 1999. ISSN 0036-8075. PMID: 10417392.

Frank S Werblin. Six different roles for crossover inhibition in the retina: correcting the nonlinearities of synaptic transmission. *Vis. Neurosci.*, 27(1-2):1–8, March 2010. ISSN 1469-8714. doi: 10.1017/S0952523810000076. PMID: 20392301 PMCID: PMC2990954.

Klaus Willecke, Jürgen Eiberger, Joachim Degen, Dominik Eckardt, Alessandro Romualdi, Martin Güldenagel, Urban Deutsch, and Goran Söhl. Structural and functional diversity of connexin genes in the mouse and human genome. *Biol. Chem.*, 383(5):725–737, May 2002. ISSN 1431-6730. doi: 10.1515/BC.2002.076. PMID: 12108537.

R O Wong, M Meister, and C J Shatz. Transient period of correlated bursting activity during development of the mammalian retina. *Neuron*, 11(5):923–938, November 1993. ISSN 0896-6273. PMID: 8240814.

R O Wong, A Chernjavsky, S J Smith, and C J Shatz. Early functional neural networks in the developing retina. *Nature*, 374(6524):716–718, April 1995. ISSN 0028-0836. doi: 10.1038/374716a0. PMID: 7715725.

W T Wong, J R Sanes, and R O Wong. Developmentally regulated spontaneous activity in the embryonic chick retina. *J. Neurosci.*, 18(21):8839–8852, November 1998. ISSN 0270-6474. PMID: 9786990.

W T Wong, K L Myhr, E D Miller, and R O Wong. Developmental changes in the neurotransmitter regulation of correlated spontaneous retinal activity. *J. Neurosci.*, 20(1): 351–360, January 2000. ISSN 1529-2401. PMID: 10627612.

S N Wu, C R Jan, and H T Chiang. Fenamates stimulate BKCa channel osteoblast-like MG-63 cells activity in the human. *J. Investig. Med.*, 49(6):522–533, November 2001. ISSN 1081-5589. PMID: 11730088.

Guiran Xiao, Qiangwang Fan, Xiaoxi Wang, and Bing Zhou. Huntington disease arises from a combinatory toxicity of polyglutamine and copper binding. *Proc. Natl. Acad. Sci. U.S.A.*, 110(37):14995–15000, September 2013. ISSN 1091-6490. doi: 10.1073/pnas.1308535110. PMID: 23980182 PMCID: PMC3773747.

Hong-ping Xu, Hui Chen, Qian Ding, Zheng-Hua Xie, Ling Chen, Ling Diao, Ping Wang, Lin Gan, Michael C Crair, and Ning Tian. The immune protein CD3zeta is required for normal development of neural circuits in the retina. *Neuron*, 65(4):503–515, February 2010. ISSN 1097-4199. doi: 10.1016/j.neuron.2010.01.035. PMID: 20188655 PMCID: PMC3037728.

Haitao You, Shigeki Tsutsui, Shahid Hameed, Thomas J. Kannanayakal, Lina Chen, Peng Xia, Jordan D. T. Engbers, Stuart A. Lipton, Peter K. Stys, and Gerald W. Zamponi. Aßneurotoxicity depends on interactions between copper ions, prion

protein, and n-methyl-d-aspartate receptors. *Proc Natl Acad Sci U S A*, 109(5): 1737–1742, January 2012. ISSN 0027-8424. doi: 10.1073/pnas.1110789109. URL `http://www.ncbi.nlm.nih.gov/pmc/articles/PMC3277185/`. PMID: 22307640 PMCID: PMC3277185.

Z J Zhou. Direct participation of starburst amacrine cells in spontaneous rhythmic activities in the developing mammalian retina. *J. Neurosci.*, 18(11):4155–4165, June 1998. ISSN 0270-6474. PMID: 9592095.

Z J Zhou. The function of the cholinergic system in the developing mammalian retina. *Prog. Brain Res.*, 131:599–613, 2001. ISSN 0079-6123. PMID: 11420974.

Z J Zhou and D Zhao. Coordinated transitions in neurotransmitter systems for the initiation and propagation of spontaneous retinal waves. *J. Neurosci.*, 20(17):6570–6577, September 2000. ISSN 0270-6474. PMID: 10964962.